The Thesis Committee for Ahmad Alfakher
Certifies that this is the approved version of the following Thesis:

Carbon Dioxide Mobility and Sweep Alteration Using Surface-Coated Silica Nanoparticles

APPROVED BY
SUPERVISING COMMITTEE:

David DiCarlo, Supervisor

Larry W. Lake

Carbon Dioxide Mobility and Sweep Alteration Using Surface-Coated Silica Nanoparticles

by

Ahmad Alfakher

Thesis

Presented to the Faculty of the Graduate School of

The University of Texas at Austin

in Partial Fulfillment

of the Requirements

for the Degree of

Master of Science in Engineering

The University of Texas at Austin

August 2019

Dedication

To my wife, for always believing in me and making me a better person. To my son, for all the joy he brings into my life. To my mom and dad, for always being there for me and without whom I wouldn't be where I am today. To my mother-in-law and father-in-law, for their continuous support and encouragement.

Acknowledgements

I would like to first thank Dr. David DiCarlo for his support and guidance. His insight was instrumental in completing this work. Dr. Larry W. Lake's comments and input greatly improved this work.

My colleague Lauren Churchwell provided invaluable instruction and tips on experimental setup and troubleshooting.

Colleagues Hasan Khan, Xiao Luo, Xiongyu Jasper Chen, Zach Murphy, Prasanna Iyer, Anuradha Radhakrishnan, Shehab Alzobaidi, David Fukuyama, and Nat Hsu contributed valuable feedback on experimental procedures, material handling, and data analysis.

I would also like to thank the staff at the Hildebrand Department of Petroleum and Geosystems Engineering, especially Glen Baum, Gary Miscoe, Daryl Nygaard, Barbara Messmore, and Amy Stewart.

Finally, I would like to acknowledge my sponsor Saudi Aramco for giving me this opportunity.

Abstract

Carbon Dioxide Mobility and Sweep Alteration Using Surface-Coated Silica Nanoparticles

Ahmad Alfakher, M.S.E.

The University of Texas at Austin, 2019

Supervisor: David DiCarlo

Solvent flooding is a well-established method of enhanced oil recovery (EOR), CO_2 being the solvent most often used. CO_2 has also been injected into saline aquifers as a method of storage in an application of Carbon Capture and Storage (CCS). Both applications suffer from poor sweep efficiency. Creating in-situ CO_2 foam has previously been shown to improve the sweep efficiency of CO_2 floods.

This study tested the use of surface-coated silica nanoparticles as an in-situ CO_2 foaming agent. In each experiment, the pressure drop was measured in five separate sections in the core, as well as along the whole core. In addition, the saturation in the core was measured periodically using a CT scanner. The experiments consisted of vertical core floods where liquid CO_2 displaced brine from the top to the bottom of the core, comparing the results in cases where surface-coated silica nanoparticles were suspended in the brine to cases with no nanoparticles.

Pressure drop readings were analyzed to exclude capillary effects and calculate relevant flow parameters, such as CO_2 mobility. In these experiments, the mobility of CO_2 was on average 89% less in floods with nanoparticles compared to floods with no nanoparticles. This reduction in mobility was found to be long-lasting. Breakthrough occurred 45% later in foamed CO_2, and the final CO_2 saturation was also 45% greater than with un-foamed CO_2.

The new measurements and mobility calculations in this study show how nanoparticles stabilize the CO_2 front. They can also be used to upscale the behavior observed from the core-scale to the reservoir scale.

Table of Contents

List of Tables

List of Figures

List of Illustrations

Chapter 1: Introduction

1.1: Application of CO_2 Injection to Enhanced Oil Recovery (EOR)

Primary and secondary methods of oil production yield a wildly varying range of ultimate recoveries, with a recovery of one-third the oil originally present being a rough average. The remaining two-thirds thus becomes a target for other methods and technologies. A group of such methods is enhanced oil recovery, which rely on injecting foreign materials into a reservoir for the purpose of recovering additional oil. Categories of EOR include chemical flooding, solvent flooding and thermal processes. CO_2 flooding is an example of a solvent EOR method, CO_2 being the most commonly used solvent. CO_2 flooding and can increase the recovery by up to 15 percent (Lake, Johns, Rossen, & Pope, 2014).

1.2: Application of CO_2 Injection to Carbon Capture and Storage (CCS)

The emissions of greenhouse gases have been steadily increasing since 1970, with emissions from hydrocarbon combustion accounting for almost 80% of the increase. Emissions are expected to increase further because of a growing global population and increased economic activity, resulting in adverse effects on the climate. Mitigating these effects and reducing emissions requires a combination of methods including increased efficiencies, increased use of low emission energy sources, in addition to carbon capture and storage (IPCC, 2014).

The geologic storage of CO_2 by injection into a brine aquifer is the only method of carbon storage that has been implemented on a commercial scale. CO_2 can be trapped in brine aquifers by multiple methods, two of which will be discussed here.

The first is structural trapping, which relies on the presence of a competent seal above the brine aquifer as well as a trapping structure. In hydrocarbon reservoirs, the presence of a hydrocarbon accumulation itself is the proof of the seal's competency. In the lack of a hydrocarbon accumulation, such as the case in saline aquifers, it is difficult to assess the integrity or presence of a seal. In addition, the CO_2 that accumulates at high saturations in a structural trap would have a high mobility. Therefore, the risk of CO_2 leaking using this method is high.

The second is residual trapping, which depends on the CO_2 being trapped by capillary forces as a residual saturation inside the rock. This method has a lower chance of leaking, as the mobility of trapped CO_2 is virtually non-existent. However, its disadvantage is its reliance on the typically low CO_2 sweep efficiency (Rackley, 2017).

One of the problems facing expanded use of CO_2 EOR is CO_2 availability. Only a quarter of the CO_2 used for EOR is sourced from plants, while the remainder three quarters is sourced from natural underground accumulations. In EOR applications, CO_2 is permanently stored in the reservoir as it displaces oil. It is therefore an effective method of carbon storage that also generates revenue that could offset the cost of carbon capture. When the field is to be abandoned, excess CO_2 can either be stored in the reservoir itself or in a deeper saline aquifer (Hill, Hovorka, & Melzer, 2013).

1.3: CO_2 FLOODING FUNDAMENTALS

One of the most important parameters in fluid displacement is the end-point mobility ratio. Starting from Darcy's law:

$$Q=-\frac{k}{\mu}\cdot\frac{1}{A}\cdot\frac{dP}{dx}$$

Where Q is the volumetric flowrate, k is the rock permeability, μ is the fluid viscosity, A is the cross-sectional area, and dP/dx is the pressure drop. The fluid mobility is defined as:

$$\lambda_i = k\cdot\frac{k_{ri}}{\mu_i}$$

Where k_{ri} is the relative permeability to phase i and is a function of fluid saturation as shown in Figure 1.

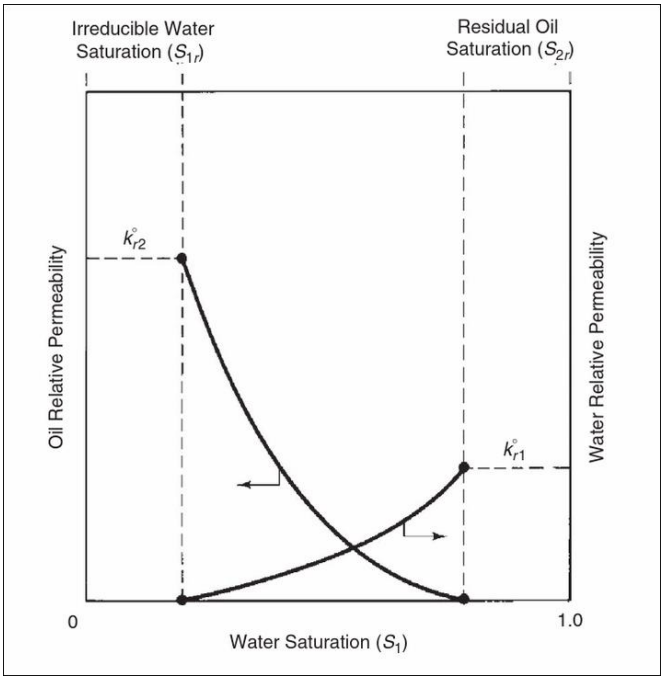

Figure 1: Typical relative permeability curve (Lake, Johns, Rossen, & Pope, 2014)

The end-point fluid mobility is the fluid mobility evaluated at the end-point of the relative permeability curve for that fluid, and is defined as:

$$\lambda_i^o = \mathrm{k} \cdot \frac{\mathrm{k}_{ri}^o}{\mu_i}$$

The end-point mobility ratio is defined as the end-point mobility of the displacing fluid divided by the end-point mobility of the resident fluid:

$$\mathrm{M}^o = \frac{\lambda_1^o}{\lambda_2^o} = \frac{k_{r1}^o / \mu_1}{k_{r2}^o / \mu_2}$$

A mobility ratio greater than 1 indicates that the displacing fluid is more mobile than the resident fluid, which favors a non-stable flood and leads to viscous fingering. A mobility ratio less than 1 indicates that the displacing fluid is less mobile than the resident fluid, which favors a stable flood and inhibits viscous fingering. As the mobility of CO_2 is much greater than that of brine, because of its low viscosity, CO_2 floods suffer from viscous fingering and consequently low sweep efficiencies as illustrated in Figure 2. The figure shows an unstable flood front moving from an injector at the bottom-left corner to a producer at the top-right corner. A significant portion of the area represented in the figure is not swept by the injected fluid. This is an issue in cases where CO_2 is displacing brine, oil or both. CO_2 injection tends to suffer from channeling and viscous fingering because of its high mobility.

Another important aspect affecting sweep efficiency is buoyancy effects caused by density differences. CO_2 is a supercritical fluid at reservoir conditions that, more than many other solvents, behaves like a liquid as it has a relatively high density. Therefore, it

will not tend to separate by gravity from oils especially if they are light. Gravity segregation remains a problem when injecting into a brine-saturated formation, or an oil-bearing formation with a high saturation of water. The gravity number is the ratio of gravity to viscous forces and is used to evaluate the extent to which fluids will move because of buoyancy effects (Lake, Johns, Rossen, & Pope, 2014):

$$N_g^o = \frac{k k_{r2}^o \Delta\rho g}{\mu_2 u}$$

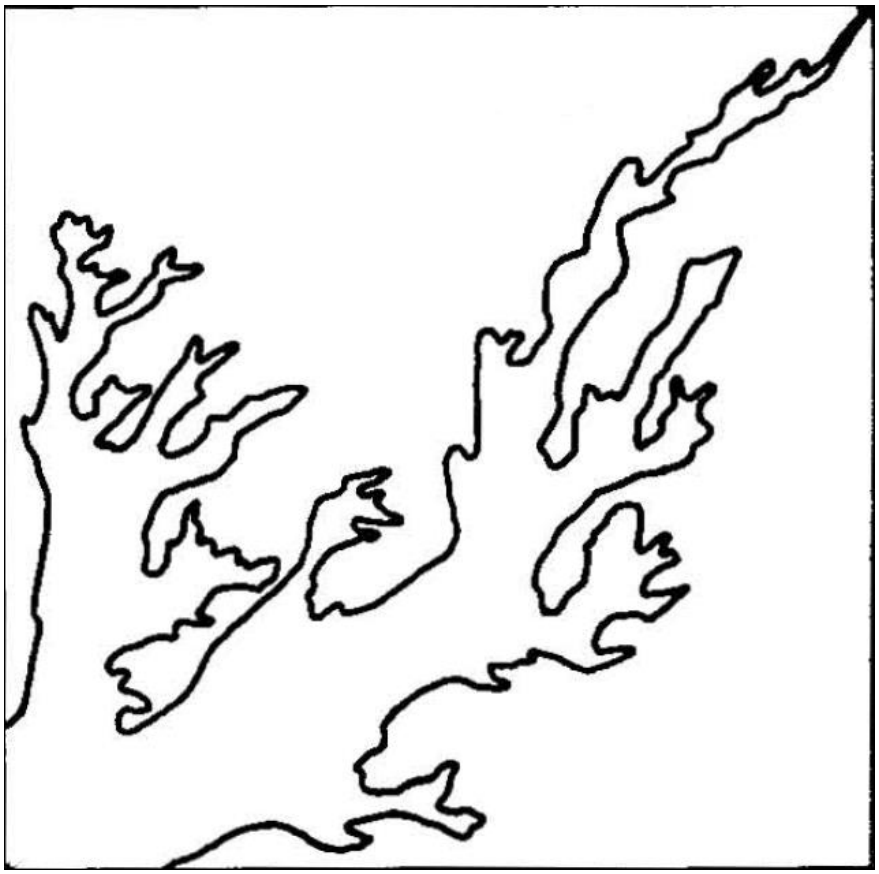

Figure 2: Viscous fingering in miscible displacement (Habermann, 1960)

1.4: CO_2 FOAM

Multiple injection strategies have been devised and tested to overcome the challenges and disadvantages of CO_2 flooding. These include creating a foam or alternating the injection between CO_2 and another liquid (Shan & Rossen, 2004).

Foam stabilization using solid particles and no surfactants has previously been studied and demonstrated (Aveyard, Binks, & Clint, 2002), and ex-situ CO_2 foam has previously been generated and observed with the use of surfactants, nanoparticles or both as stabilizing agents (Emrani & Nasr-El-Din, 2015). As in-situ CO_2 foam generation cannot be directly observed in porous media, it has been inferred from effects expected from and associated with foams and emulsions (Aminzadeh, et al., 2012).

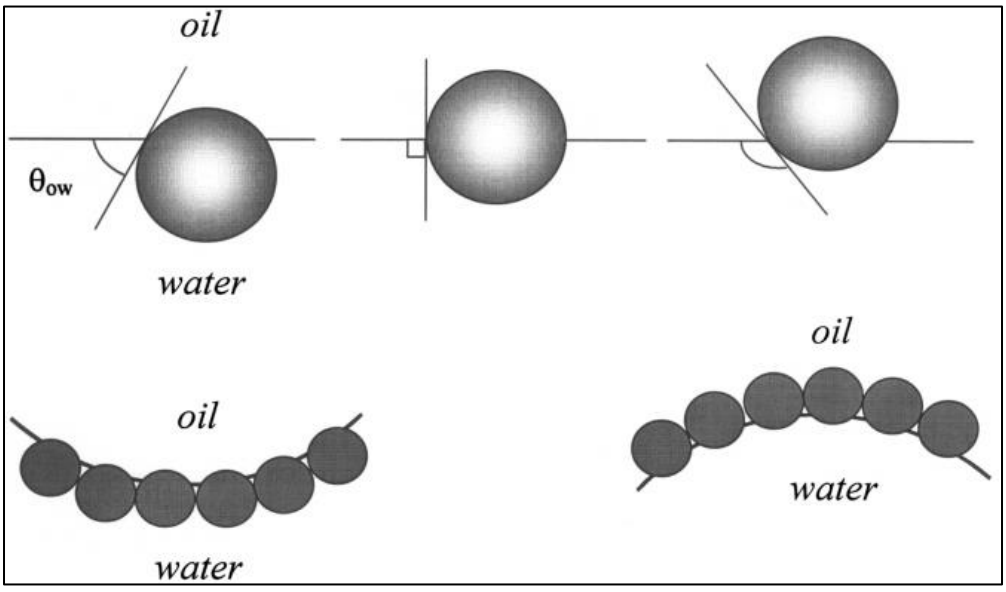

Figure 3: Emulsion type dependency on particle wettability (Aveyard, Binks, & Clint, 2002)

Before surfactants or nanoparticles can stabilize liquid CO_2 droplets into a CO_2/brine foam or emulsion, the CO_2 needs to be dispersed in the water as discontinuous droplets, which the stabilizing agent then acts on. The method by which CO_2 changes from a continuous phase to disconnected bubbles or droplets in a water-wet medium is called Roof snap-off, and results from the capillary forces associated with forcing the CO_2 through the constrictions of a pore throat (Roof, 1970).

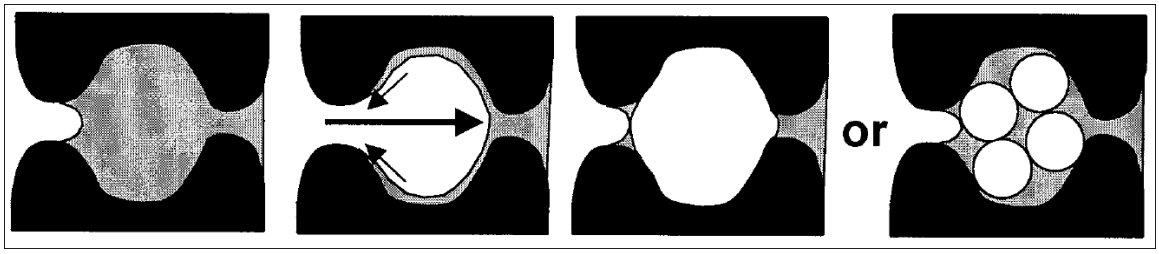

Figure 4: Roof snap-off in foam generation (Rossen W. R., 2003)

The application and importance of Roof snap-off on the creation of in-situ foam has been demonstrated both thorough modeling by Rossen et al. (Rossen W. R., 1999) and Deng et al. (Deng, Cardenas, & Bennett, 2013), and in experiments by Gauglitz et al. (Gauglitz, Friedmann, Kam, & Rossen, 2002). One method of preventing those bubbles from coalescing and thus creating CO_2 foam is through injecting it into a core saturated with a surfactant solution, which has been shown to greatly reduce the CO_2 mobility for multiple pore volumes of injection after breakthrough (Kovscek, Patzek, & Radke, 1993). CO_2 foams stabilized by surfactants are however not stable in harsh reservoir conditions of high temperature and salinity (Rossen W. R., 1996).

1.5: USE OF NANOPARTICLES IN CO_2 FLOODING

Flooding a core initially saturated with nanoparticle brine with liquid CO_2 has been shown to increase sweep efficiency using CT scans (Aminzadeh, et al., 2012). Foaming CO_2 has been shown to decrease its mobility by causing a significant portion of the gas to be stationary or trapped (Tang & Kovscek, 2004). Others have shown that saturating a core with nanoparticle brine improves the sweep of CO_2 in buoyancy-driven flow (Senthilnathan, 2017), in water-wet as well as oil-wet pores (Alghamdi, 2015), and increased CO_2 trapping was studied in both drainage and subsequent imbibition (Wung, 2015).

Chapter 2: Experimental Equipment, Setup and Procedures

2.1: Experimental Equipment

The cores used for all three experiments are Berea sandstone that are each 0.071 meters (2.8 inches) in diameter and 0.61 meters (24 inches) in length. The core holder is an aluminum Hassler type Phoenix Instruments UTPT-HY. The core holder has multiple stainless-steel pressure taps that allow for recording pressure drops along multiple sections of the core. In these experiments, the core was divided to five sections along which the pressure drop was measured. This is in addition to measuring the pressure drop along the entire core. This is illustrated in Figure 5.

The core is wrapped with heat-shrink Teflon tubing from Geophysical Supply Company that is 0.076 meters (3 inches) in diameter. The Teflon tubing is shrunk on the core using a Steinel HL 1810 S professional heat gun.

Experimental fluids including sodium chloride brine, nanoparticle sodium chloride brine, and liquid CO_2 are kept in 1.5-liter stainless steel piston accumulators manufactured by Phoenix Instruments. Two Teledyne ISCO 100DM syringe pumps are used in continuous flow mode to pump water to the accumulators. The vacuum pump used is a Marvac Scientific Manufacturing Company model B3.

Fisher Scientific sodium chloride that is 99% pure is used to prepare brines. Brine used for core 1 was 5% sodium chloride by weight. Brine used for cores 2 and 3 was 2% sodium chloride by weight. The surface-coated silica nanoparticles used in the experiments are provided by Nissan Chemical America Corporation. The nanoparticles

used for the core 1 are EOR 5XS-V2, mixed to a solution of 5% nanoparticles and 5% sodium chloride by weight. The nanoparticles used for cores 2 and 3 are EOR 5XS-V4.2, mixed to a solution of 2% nanoparticles and 2% sodium chloride by weight. Both stock nanoparticle solutions are 20% nanoparticles.

Pressure in the core is regulated at the outlet using a Core Laboratories BP 100-T-SS back pressure regulator (BPR). The diaphragm used in the BPR is A-1422-GFT graphite-impregnated Teflon, as Viton rubber diaphragms would be damaged by CO_2. Pressure drops are measured using six Emerson Rosemount 3051S pressure transducers. The transducers are connected to the core in the order show in Figure 5.

To obtain saturation data, the core holder was placed in a vertical positioning system (VPS) which moved the core vertically through an X-ray computed tomography (CT) scanner. The scanner is a Picker medical scanner (model PQ 6000), that is outfitted for petrophysical use by Universal Systems (model HD-350). As stainless steel would interfere with the CT scanner readings, the core holder used is made of aluminum. Additionally, poly-ether-ether-ketone (PEEK) polymer tubing is used for connections to the core holder instead of stainless-steel tubing. The flexibility of PEEK tubing is also required for the core holder movement.

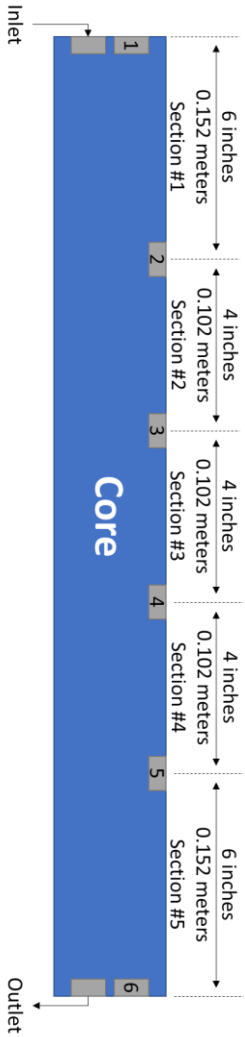

Figure 5: Pressure tap locations in core cross section sketch

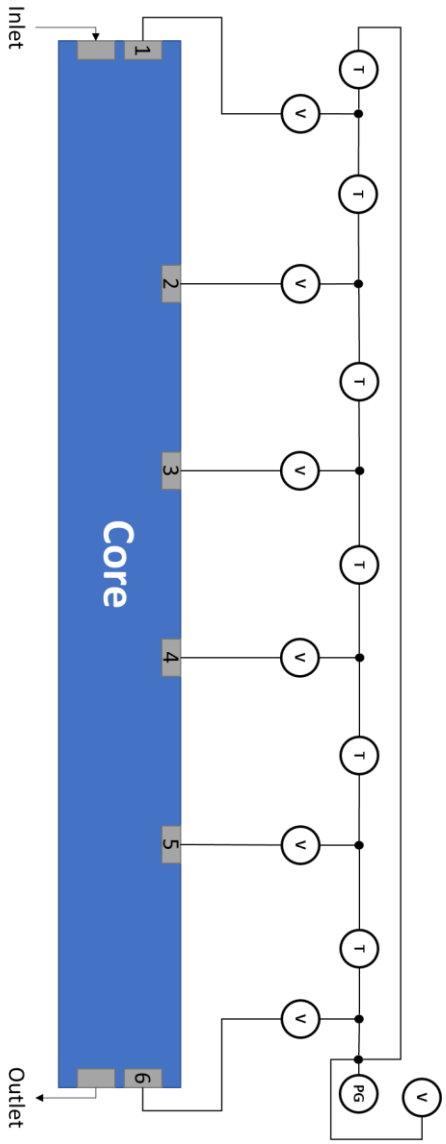

Figure 6: Transducer & core holder port diagram

2.2: EXPERIMENTAL SETUP

The core is first dried in an oven at 348 Kelvin (75 degrees Celsius) for 12 hours. Then, a layer of Teflon tubing is shrunk around the core. Four layers of aluminum foil are then wrapped on the Teflon layer. A second layer of Teflon is then shrunk on the aluminum foil layers.

The inner layer of Teflon acts as a water barrier to prevent brine from damaging the layers of aluminum foil. The four layers of aluminum foil act as a CO_2 barrier to prevent it from damaging the rubber sleeve inside the core holder. The outer Teflon layer holds the aluminum foil layers in place, and acts as a physical barrier to prevent them from being damaged while the core is inserted into the core holder.

The core is inserted into the core holder and secured from both ends. A drill is used to drill through the Teflon and aluminum layers through each pressure tap. This allows pressure communication at the pressure tap locations so pressure drops can be measured. Water is used to apply a confining pressure of 10.34 megapascals (1,500 psi).

The core is then connected to the tubing lines needed for the experiment. Each transducer has two ports and reads the difference in pressure between these two ports. The connections in these experiments are done as in Table 1. The numbers 1 through 6 in Table 1 refer to the locations in Figure 4. Note that each pressure tap is shared by two transducers. The core is vacuumed to -98 kilopascals (-29 inches of Mercury) for 3 hours. Brine is then pumped to the vacuumed core until it is saturated and is at experimental pressure of 6.89 megapascals (1,000 psi).

Transducer	Port A	Port B
Whole Core	1	6
Section #1	1	2
Section #2	2	3
Section #3	3	4
Section #4	4	5
Section #5	5	6

Table 1: Transducer and pressure tap connection order

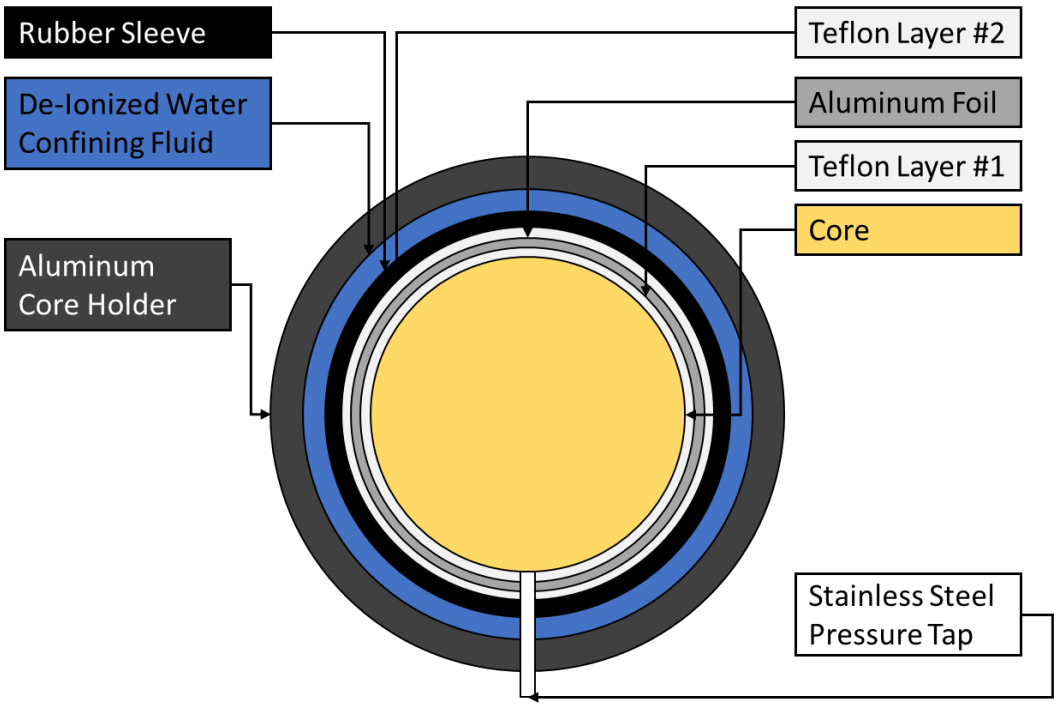

Figure 7: Core cross-section after applying confining pressure

2.3: EXPERIMENTAL PROCEDURES

One pore volume of brine is pumped to flush the core and measure permeability.

The first CO_2 flood is then conducted to acquire a baseline. Liquid CO_2 is pumped to the core to displace brine. After the CO_2 flood is complete, CO_2 is vented out of the core until it is completely depressurized. When the core is at atmospheric pressure, brine is pumped to the core until it breaks through. The outlet is then closed, and the core is pressurized to experimental pressure. One pore volume of brine is then pumped through the core to flush any remaining CO_2 that might have dissolved into the brine. Pressure drops are recorded, and permeability measured, ensuring no change from the first brine flood.

A second CO_2 flood is then conducted and compared to the previous flood to show repeatability. The same procedure is then followed to desaturate the core of CO_2 and saturate again with brine. Prior to the nanoparticle brine flood, the core is saturated with nanoparticle brine by pumping at least one pore volume of nanoparticle brine through the core.

The CT scanner is used to take 59 slices that are each 10 millimeters thick. Although the length of the core would require 61 slices of 10-millimeter length, the first and last slices are unusable because of interference from the core holder endcap. Slices that contain a pressure tap or confining pressure port are also unusable because of interference form the pressure taps or confining pressure ports which are stainless steel. Therefore, saturation data will contain gaps in those locations. A sketch of the experimental setup is presented in Figure 8.

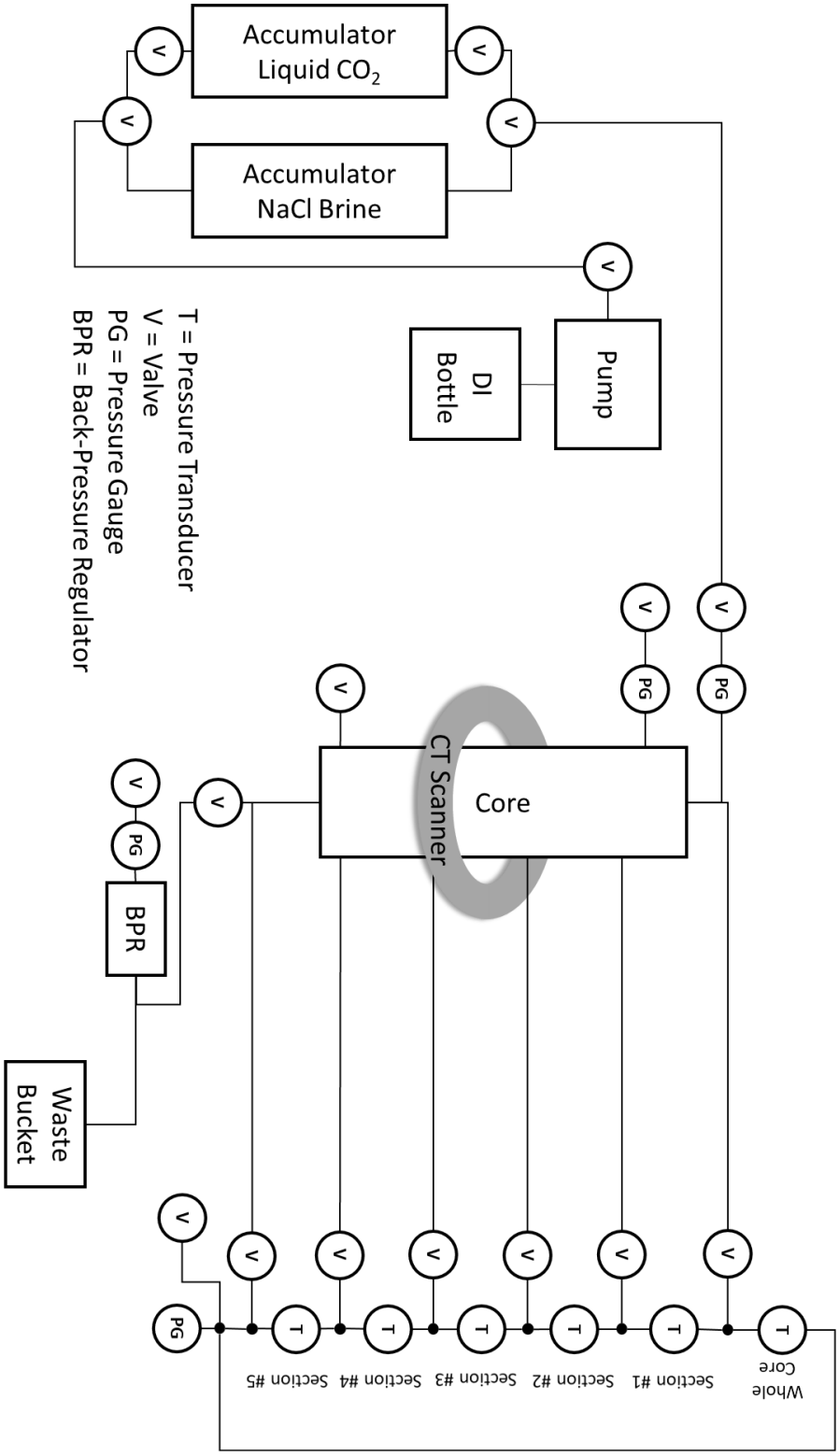

Figure 8: Experimental setup

Chapter 3: Experimental Results

3.1: Brine Floods

A brine flood was conducted prior to each CO_2 flood. In the case of CO_2 floods with nanoparticles, the brine flood was conducted with nanoparticle brine. These brine floods serve the purpose of purging the core of CO_2 from the previous flood, and as a check that permeability has not been altered from the previous flood. In the case of nanoparticle brine floods, it also serves the purpose of measuring nanoparticle brine viscosity, which in all cases has been measured to be the same as the brine viscosity without nanoparticles. Table 2, Table 3, and Table 4 summarize the data from the brine floods prior to each CO_2 flood. It is important to note that the permeability in each core is constant between floods. This shows the effectiveness of the method used in removing all CO_2 from the core between CO_2 floods, and bringing the core back to initial conditions. It is also worth noting that the brine floods that contain nanoparticles exhibit the same pressure drops as the brine floods that do not contain nanoparticles. This shows that nanoparticles have no effect on brine mobility.

Core #		1		
Flood #		1	2	3
Flowrate	mL/min	0.5		
Porosity		0.20		
Nanoparticles	Y/N	N	N	Y
Pressure Drop (psi)	Whole	1.62	1.65	1.59
	#1	0.44	0.47	0.41
	#2	0.32	0.27	0.39
	#3	0.23	0.31	0.16
	#4	0.24	0.21	0.28
	#5	0.41	0.38	0.40
Total Mobility ($x10^{-12}$ m^2/Pa-s)	Whole	114	113	117
	#1	105	98	114
	#2	98	116	80
	#3	137	98	191
	#4	130	146	110
	#5	113	123	117
Permeability (mD)	Whole	121	120	124
	#1	112	104	122
	#2	104	124	85
	#3	146	105	203
	#4	138	155	117
	#5	120	131	124

Table 2: Core #1 brine flood summary

Core #		2			
Flood #		1	2	3	4
Flowrate	mL/min	1.0			
Porosity		0.25			
Nanoparticles	Y/N	N	N	N	Y
Pressure Drop (psi)	Whole	1.30	1.31	1.28	1.27
	#1	0.29	0.31	0.33	0.35
	#2	0.20	0.19	0.21	0.23
	#3	0.17	0.20	0.18	0.19
	#4	0.25	0.23	0.22	0.20
	#5	0.32	0.34	0.30	0.28
Total Mobility ($x10^{-12}$ m^2/Pa-s)	Whole	286	282	290	291
	#1	321	297	280	263
	#2	313	318	298	271
	#3	357	308	352	326
	#4	248	266	283	306
	#5	288	272	310	334
Permeability (mD)	Whole	305	300	309	310
	#1	342	316	298	280
	#2	333	339	317	288
	#3	379	328	374	347
	#4	263	283	301	326
	#5	306	289	329	356

Table 3: Core #2 brine flood summary

Core #		3			
Flood #		1	2	3	4
Flowrate	mL/min	1.0			
Porosity		0.24			
Nanoparticles	Y/N	N	N	Y	N
Pressure Drop (psi)	Whole	1.30	1.30	1.29	1.29
	#1	0.33	0.30	0.30	0.31
	#2	0.16	0.19	0.19	0.19
	#3	0.17	0.17	0.16	0.16
	#4	0.18	0.24	0.19	0.19
	#5	0.39	0.38	0.37	0.36
Total Mobility ($x10^{-12}$ m^2/Pa-s)	Whole	285	286	288	288
	#1	282	312	313	299
	#2	382	330	326	325
	#3	361	374	390	375
	#4	348	256	326	331
	#5	238	246	248	256
Permeability (mD)	Whole	303	304	307	307
	#1	300	332	333	318
	#2	406	351	347	345
	#3	384	398	415	399
	#4	371	273	347	352
	#5	253	262	264	272

Table 4: Core #3 brine flood summary

3.2: CO_2 Floods Without Nanoparticles

Multiple CO_2 floods were conducted on each core without the use of nanoparticles to establish a baseline the nanoparticle floods can be compared to.

3.2.1: Saturation Profile

The following graph shows CO_2 saturation on the vertical axis versus position along the core on the horizontal axis for a CO_2 flood without nanoparticles. Each line is taken at a different dimensionless time (pore volumes pumped). The front moves from lower to greater slice number.

It can be seen in the graph that the flood front moves as a shock where the CO_2 saturation changes from zero to 0.24 in the span of 10 slices (0.1 meters or 0.16 of the core's length), and that the shock is followed by a rarefaction wave. Unlike a typical Buckley-Leverett solution to an immiscible displacement where the inlet saturation is constant, the saturation at the inlet in these experiments is found to be increasing with time. An edge effect can also be seen at the outlet of the core, where saturations are slightly greater than would be expected from the trend. Breakthrough occurred when the shock reached the outlet, which from the graph is between 0.31 and 0.36 pore volumes pumped.

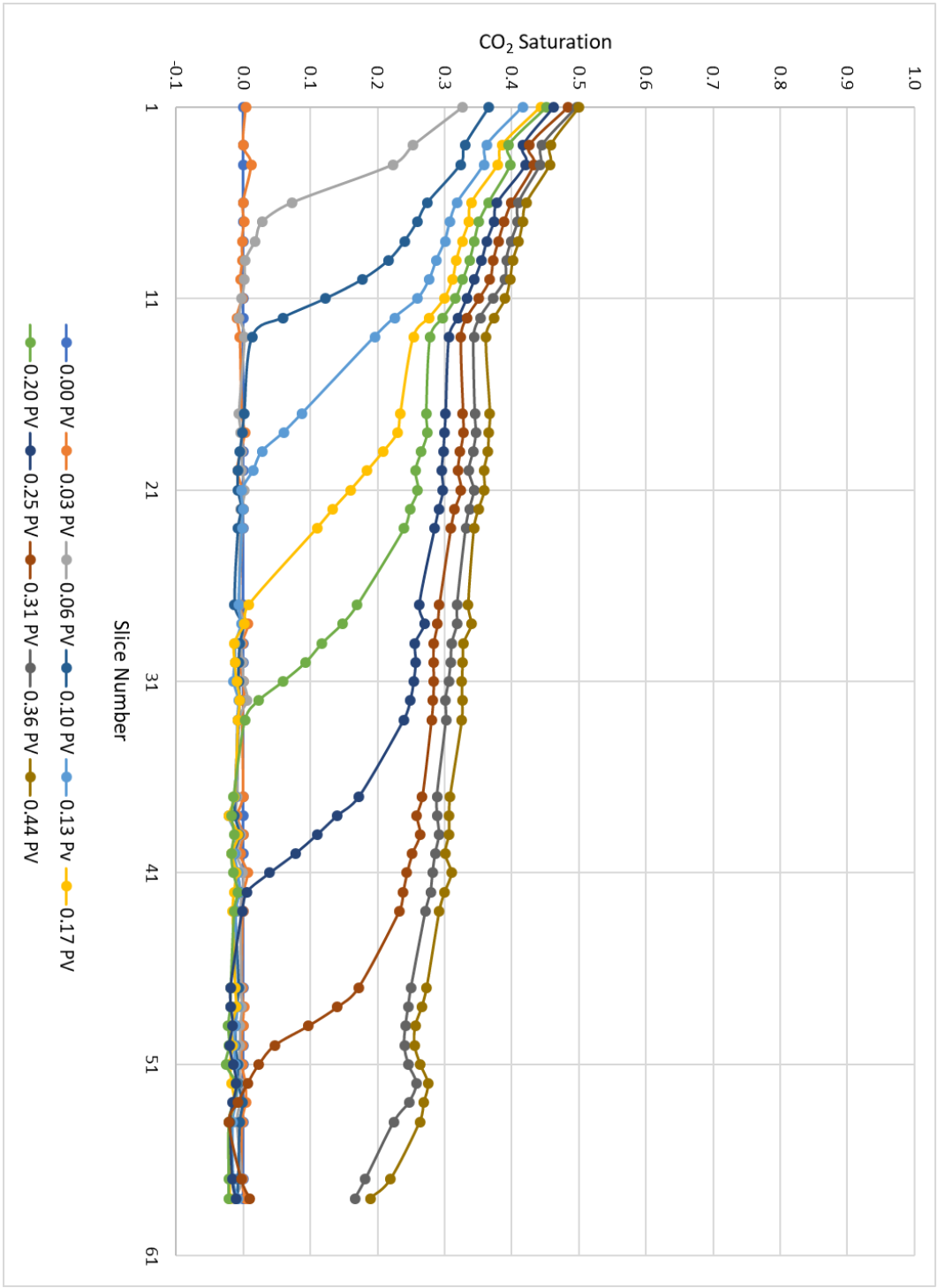

Figure 9: Core #3 flood #2 saturation profiles without nanoparticles

3.2.2: Pressure Drop Profile

Figure 10 shows pressure drops on the vertical axis versus dimensionless time (pore volumes pumped) on the horizontal axis for a CO_2 flood without nanoparticles. Each color represents the pressure drop readings from one of the transducers. As shown in Figure 8.

There are clear jumps in the data caused by capillary pressure. It is important to understand when and how these pressure jumps occur, so that the analysis is done properly on the data. The following is an explanation of how capillary pressure affects pressure transducer readings, which will be followed by data analysis in the next chapter. These pressure jumps occur when the CO_2 front reaches a pressure tap location which results in the pressure transducer reading through the CO_2 phase on one end and through the brine in the other. This causes the pressure drop readings to not only represent the viscous pressure drop, but to also include capillary pressure. Because of the fingering nature of CO_2 displacement, the CO_2 will not necessarily reach the location of each pressure tap as it advances through. When this occurs and the CO_2 flood passes through a pressure tap without saturating the exact area of the pressure tap, the jump will be absent from that transducer. Additionally, when the CO_2 front reaches a pressure tap having skipped the one before it, a negative pressure drop is recorded as seen in Figure 10.

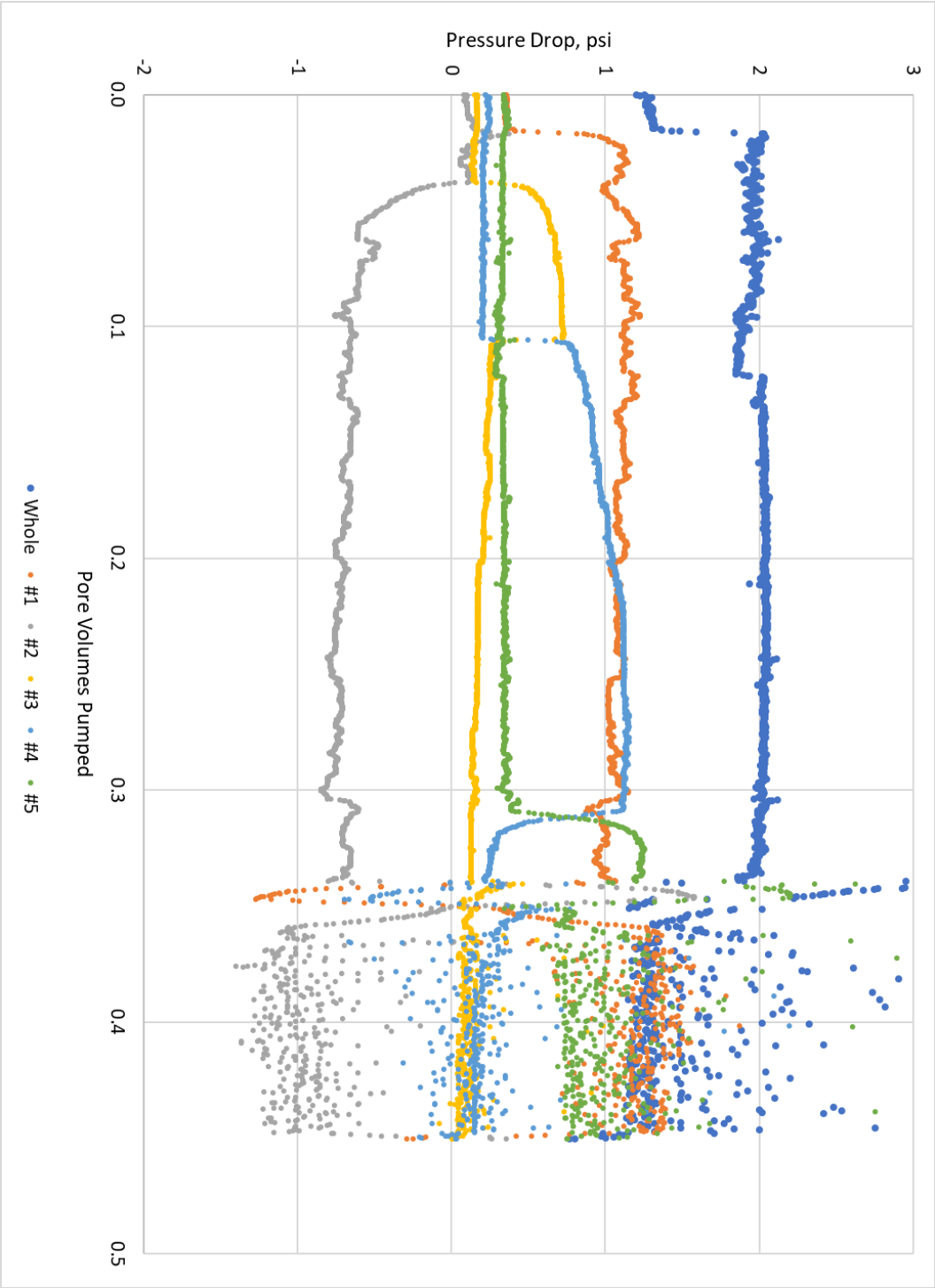

Figure 10: Core #3 flood #2 pressure drops without nanoparticles

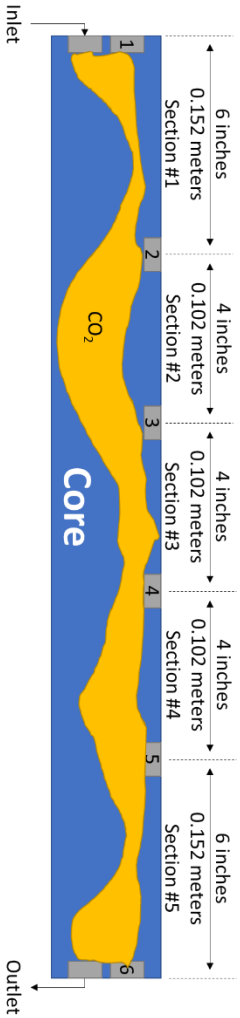

Figure 11: Sketch of CO_2 front reaching all pressure tap locations

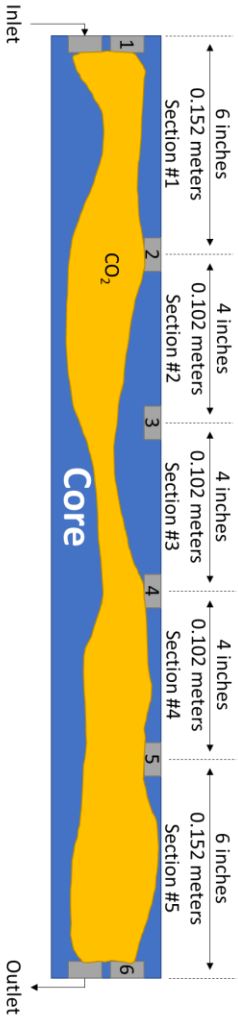

Figure 12: Sketch of CO_2 front skipping pressure tap #3 location

When CO_2 starts exiting the core through the BPR at breakthrough, it pushes through one side of the BPR diaphragm while still a liquid at 6.89 megapascals (1,000 psi) and instantaneously becomes a gas at atmospheric pressure on the other side. The phase change, accompanied with the rapid gas expansion from the large pressure decrease, results in pressure pulses that travel all the way to the inside of the core. For that reason, a large amount of noise is introduced to the pressure drop measurements

taken by the pressure transducers starting at breakthrough. This marked increase in pressure difference measurement noise can be used as an indication of breakthrough. In Figure 10, breakthrough can be inferred to be at 0.34 pore volumes from the marked increase in pressure difference noise, which is consistent with the time at which the CO_2 front in the CT saturation data in Figure 9 reaches the outlet.

At 0.01 pore volumes in Figure 10, a sudden increase is observed in the readings from the whole core transducer and the transducer for section #1. This is an indication that the line at the inlet to the core, which these two transducers share, is now reading through the CO_2 phase. Both transducers are still however reading through the brine phase through their respective second ends.

At 0.04 pore volumes, a sudden increase is observed in the reading from the transducer for section #3 coupled with a sudden decrease in the reading from the transducer for section #2 and a lack of an associated drop of the reading from the transducer for section #1. This is an indication that the CO_2 front has passed through the first pressure tap without that tap switching to reading through the CO_2 phase, explaining why the readings for section #1 never decrease to normal values. The CO_2 front then reaches the second pressure tap, which switches to reading through the CO_2 phase. Therefore, the transducer for section #2 now reads through the CO_2 phase only at the downstream end, resulting in a negative measurement of capillary pressure and the resulting sudden decrease in pressure readings. This is coupled with a sudden increase in the readings from section #3, as it shares the second pressure tap with the section #2 transducer. But while the second pressure tap is at the downstream end for the section #2

transducer, it's at the upstream end for section #3 transducer, resulting in a positive capillary pressure reading.

At 0.11 pore volumes, there is a sudden increase in the pressure drop reading of the section #3 transducer and a corresponding increase in the section #4 transducer. This is an indication that CO_2 has reached the location of the third pressure tap, which the section #3 and section #4 transducers share from the downstream and upstream sides respectively.

At 0.31 pore volumes, a similar sudden pressure drop decrease and pressure drop increase is observed in the section #4 and section #5 transducer readings respectively. This is an indication that the fourth pressure tap is now reading pressure through the CO_2 phase.

Although the pressure reading for section #1 never returns to normal readings, it is not an indication that the CO_2 front has not reached the section of the core that contains that pressure tap. The reading in section #1 indeed does not decrease even after breakthrough. Similarly, the jump in a transducer's reading is not an indication that the CO_2 front has just reached that location. For the sudden pressure drop reading jump to occur, CO_2 must reach the location of the pressure tap in the core which does not necessarily correspond to the location of the CO_2 front.

Figure 13 illustrates this point further. In the figure, the crossover between the section #4 transducer and the section #5 transducer occur after breakthrough, at which point the CO_2 front has clearly moved past the location of the fourth pressure tap. This is

an indication that the exact location of the fourth pressure tap inside the core was not saturated with CO_2 even when the CO_2 front has broken through at the outlet.

Figure 13 is an example of the pressure taps reading through the CO_2 phase in succession, without one being skipped over. This results in the pressure crossovers occurring in order, and the absence of negative pressure drop jumps caused by negative readings of capillary pressure. The difference between the initial pressure drop reading and that after the jump is a measurement of capillary pressure in that section. The ratio of the initial pressure drop reading and that after the front has passed is a measure of both brine/CO_2 viscosity difference and CO_2 relative permeability.

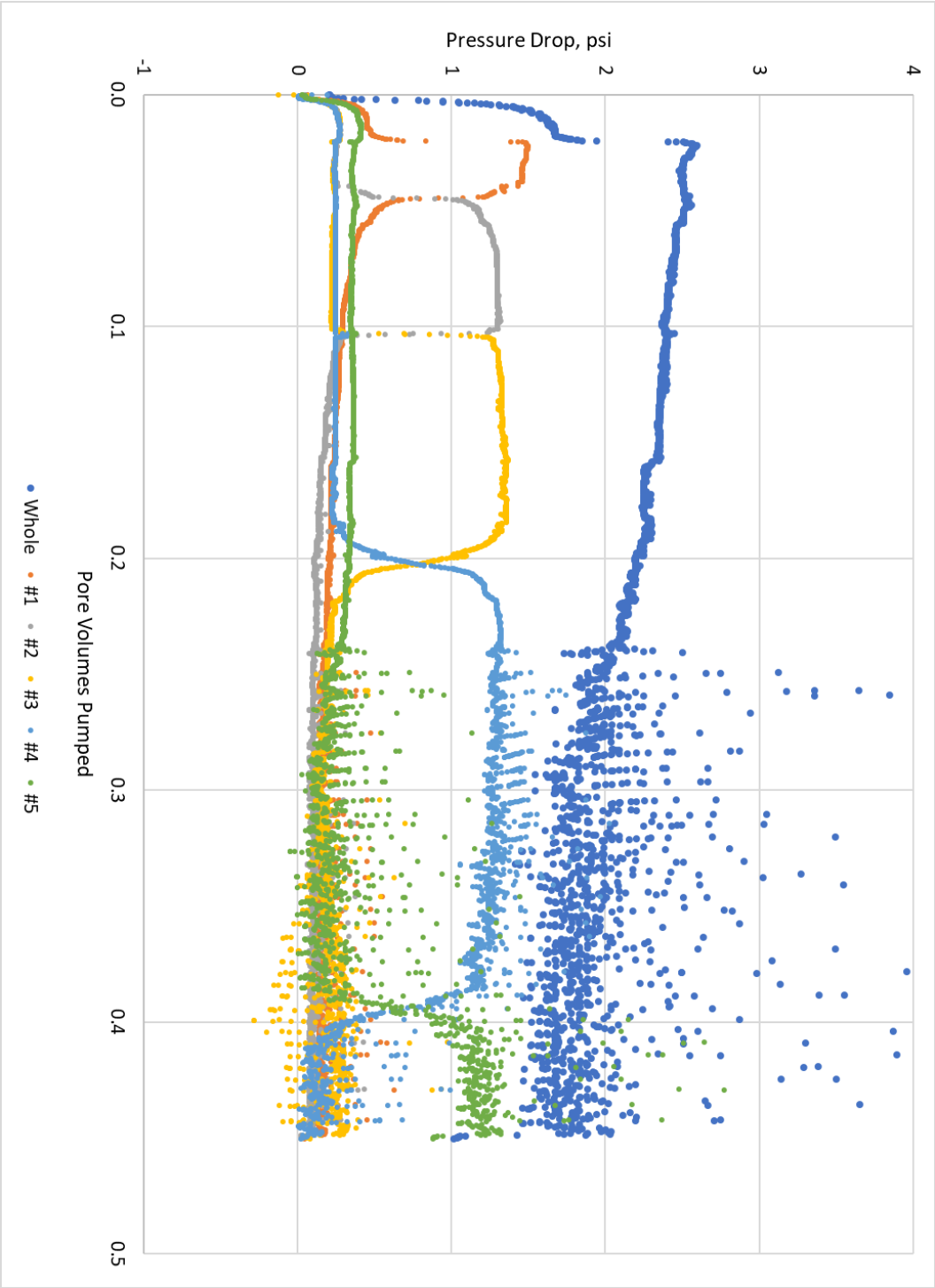

Figure 13: Core #1 flood #2 pressure drops without nanoparticles

3.3: CO_2 Floods With Nanoparticles

One CO_2 flood in each core is conducted with the core initially saturated with nanoparticle brine.

3.3.1: Saturation Profile

Figure 14 shows CO_2 saturation on the vertical axis versus position along the core on the horizontal axis for a CO_2 flood with nanoparticles. Each line is taken at a different dimensionless time (pore volumes pumped). The front moves from the inlet to the outlet; from lower to greater slice number.

It can be seen in the graph that the CO_2 front has a sharper shock in the presence of nanoparticles and goes to a greater saturation. The saturation change in the shock is from zero to 0.46, as opposed to 0.26 in the flood without nanoparticles. The shock's saturation change also occurs in the span of 5 slices (0.05 meters or 0.08 of the core's length), which is half the value in the flood with no nanoparticles. Rarefaction is also present with nanoparticles, as the saturation behind the shock increases from 0.46 to 0.76. Breakthrough can be inferred from the location and movement of the shock in dimensionless time, which from the graph is between 0.46 and 0.51 pore volumes pumped. Therefore, breakthrough was delayed by 0.1 to 0.2 pore volumes, or 28% to 56%. Similar to the previous flood, the CO_2 saturation at the inlet also increases with time in this flood.

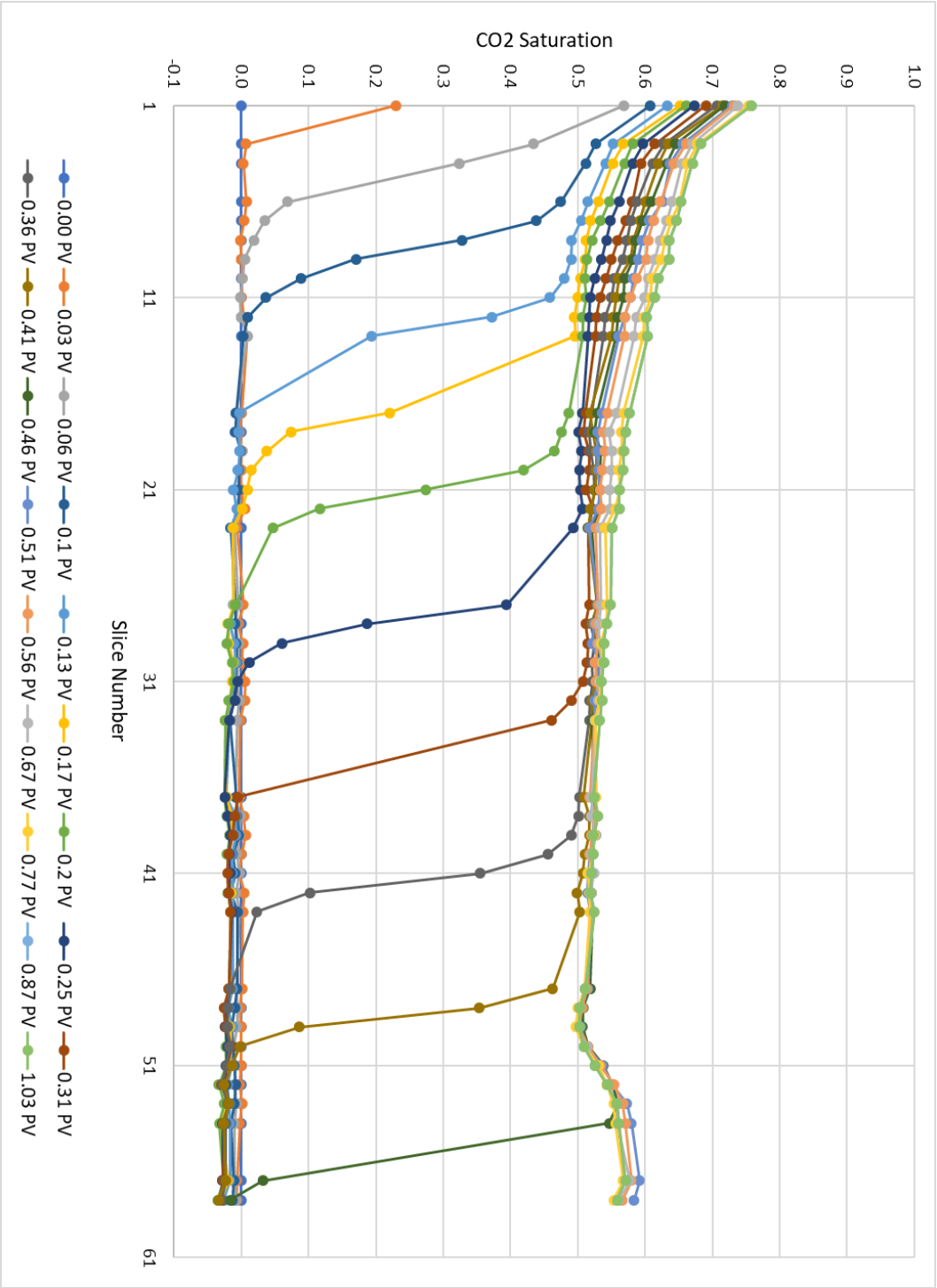

Figure 14: Core #3 flood #3 saturation profiles with nanoparticles

3.3.2: Pressure Drop Profile

Figure 15 shows pressure drops on the vertical axis versus dimensionless time (pore volumes pumped) on the horizontal axis for a CO_2 flood with nanoparticles.

The first difference to take note of is the difference in magnitude and behavior of the pressure drops. The pressure drop for the whole core without nanoparticles in Figure 10 increased to 2.04 psi with the capillary pressure effect and remained constant at that value. Similarly, the whole core pressure drop in Figure 13 increased to 2.49 psi with the capillary pressure effect and started decreasing afterwards. The whole core pressure drop in Figure 15 similarly increases to 2.02 psi with the capillary pressure effect, but unlike the floods without nanoparticles it keeps increasing to 5.83 psi. Inferring the breakthrough time from the pressure data noise also shows that breakthrough was delayed to 0.50 pore volumes as opposed to 0.34 pore volumes in Figure 10.

The presence of nanoparticles suppresses the effect of capillary pressure on pressure drop readings. This is apparent in Figure 16, where the increase in pressure drop caused by capillary pressure is only seen in readings from the whole core and section #1 transducers but is absent in the readings from other transducers. This is inferred to be caused by the creation of CO_2/brine in-situ foam, making the CO_2 phase discontinuous

When the CO_2 front reaches one of the pressure taps in this example, the pressure drop starts increasing gradually. Pressure drop reading increases caused by capillary pressure are observed to be sudden in floods without nanoparticles, and this is therefore taken to be caused by the increased viscosity of CO_2 foam, and not because of capillary pressure. Table 5, Table 6, and Table 7 summarize the data from the CO_2 floods.

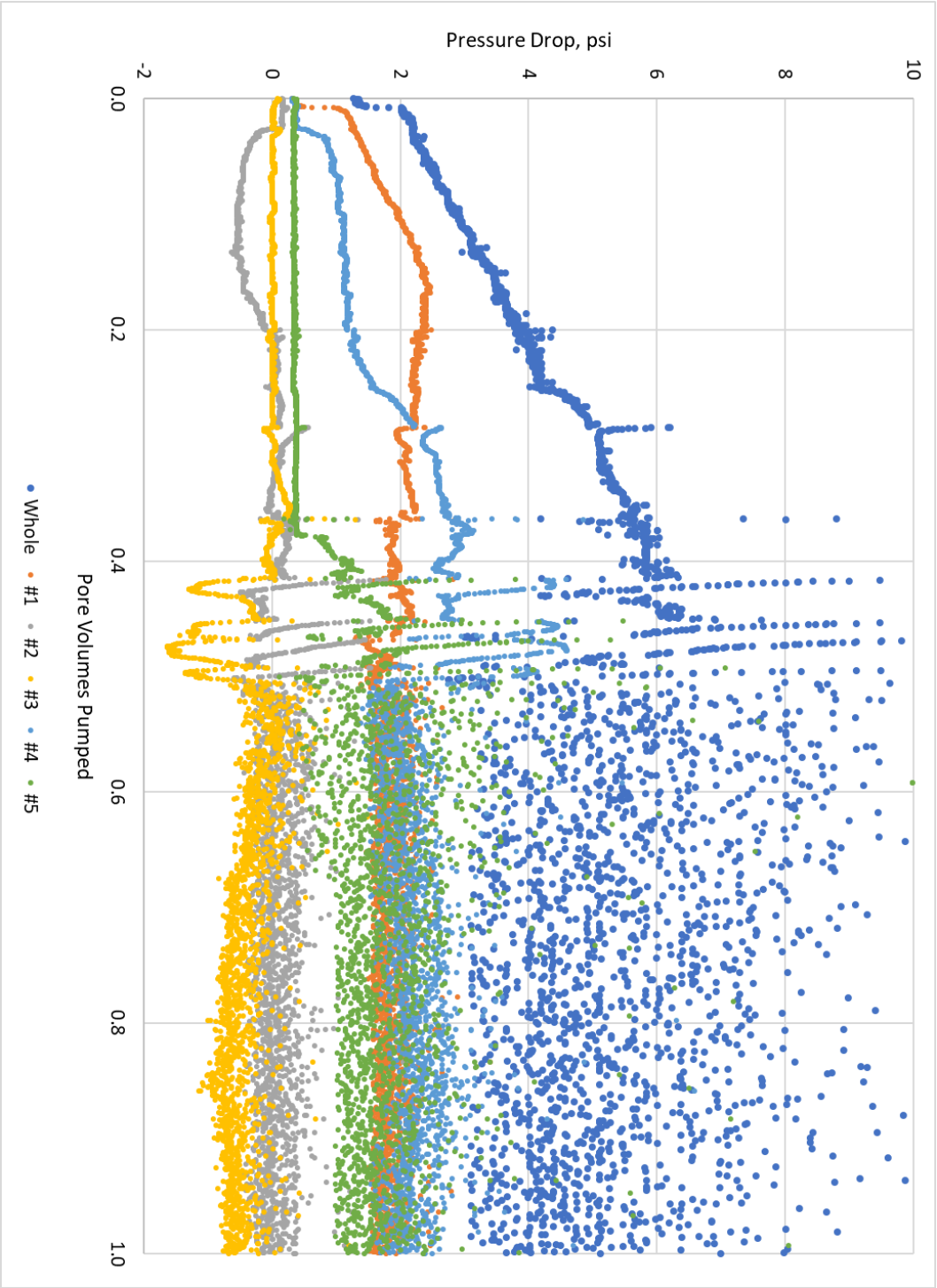

Figure 15: Core #3 flood #3 pressure drops with nanoparticles

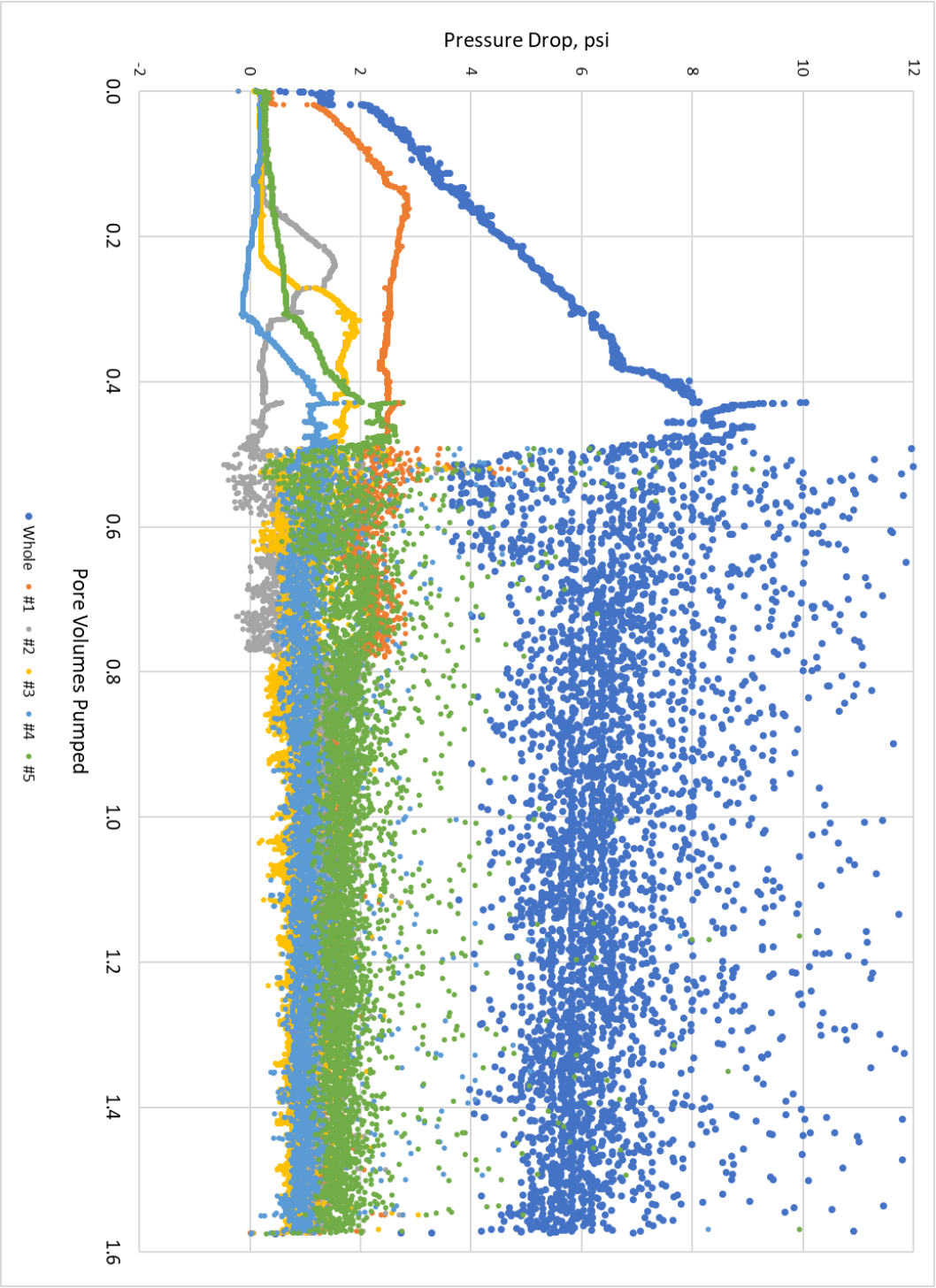

Figure 16: Core #2 flood #4 pressure drops with nanoparticles

Core #		1		
Flood #		1	2	3
Flowrate	mL/min	0.5		
Pore Volumes at Breakthrough		0.25	0.24	0.36
Nanoparticles	Y/N	N	N	Y
Pressure Drop Before Front (psi)	Whole	1.77	1.68	1.72
	#1	0.56	0.19	0.45
	#2	0.26	0.24	0.20
	#3	0.24	0.24	0.33
	#4	0.22	0.24	0.00
	#5	0.32	0.36	0.60
Pressure Drop During Front (psi)	Whole	2.60	2.49	10.45
	#1	1.55	1.46	4.64
	#2	0.95	1.30	1.98
	#3	1.31	1.33	2.18
	#4	1.32	1.32	1.65
	#5	1.22	1.15	1.62
Pressure Drop After Front (psi)	Whole	1.46		
	#1	0.29	0.27	
	#2	0.13	0.12	
	#3	0.18	0.11	
	#4	0.14	0.09	
	#5			

Table 5: Core #1 CO_2 flood summary

Core #		2			
Flood #		1	2	3	4
Flowrate	mL/min	1.0			
Pore Volumes at Breakthrough		0.34	0.33	0.32	0.47
Nanoparticles	Y/N	N	N	N	Y
Pressure Drop Before Front (psi)	Whole	1.22	1.31	1.28	1.28
	#1	0.31	0.35	0.33	0.36
	#2	0.21	0.23	0.15	0.13
	#3	0.16	0.17	0.20	0.21
	#4	0.20	0.21	0.21	0.19
	#5	0.30	0.34	0.25	0.27
Pressure Drop During Front (psi)	Whole	1.95	2.04	2.00	8.35
	#1	1.02	1.08	1.04	2.80
	#2	0.94	1.04	-0.71	1.51
	#3	0.35	-0.55	-0.54	1.84
	#4	0.99	1.02	1.12	1.32
	#5	0.76	1.15	1.02	2.62
Pressure Drop After Front (psi)	Whole	1.03	1.11	1.45	5.79
	#1	0.08	0.16		1.07
	#2	0.10	0.09		0.85
	#3	0.10	0.09	0.20	0.75
	#4	0.10		0.10	1.06
	#5				0.99

Table 6: Core #2 CO_2 flood summary

Core #		3			
Flood #		1	2	3	4
Flowrate	mL/min	1.0			
Pore Volumes at Breakthrough		0.35	0.34	0.50	0.35
Nanoparticles	Y/N	N	N	Y	N
Pressure Drop Before Front (psi)	Whole	1.12	1.31	1.30	1.13
	#1	0.14	0.35	0.38	0.30
	#2	0.17	0.13	0.11	0.13
	#3	0.17	0.17	0.11	0.16
	#4	0.17	0.20	0.38	0.17
	#5	0.34	0.35	0.38	0.28
Pressure Drop During Front (psi)	Whole	1.83	2.03	5.83	2.01
	#1	0.91	1.11	2.35	1.01
	#2	0.59	-0.60		-0.62
	#3	0.55	0.73		0.59
	#4	0.70	1.12	2.86	
	#5	1.02	1.22	1.54	1.18
Pressure Drop After Front (psi)	Whole	0.92	1.25	4.22	1.30
	#1	0.08		1.77	0.20
	#2	0.07			0.14
	#3	0.08	0.09		
	#4	0.06	0.15	2.11	
	#5				

Table 7: Core #3 CO_2 flood summary

3.4: CO_2 Flood Post-Flush

After the nanoparticle CO_2 flood, the core was flushed with 4.4 pore volumes of brine with no nanoparticles before conducting the next CO_2 flood.

3.4.1: Saturation Profile

The results in this flood are similar to the flood without nanoparticles. The flood front moves as a shock where the CO_2 saturation changes from zero to 0.3 in the length of 10 slices (0.1 meters or 0.16 of the core's length), and the shock is followed by a rarefaction wave. Breakthrough occurred when the shock reached the outlet, which from the graph is briefly after 0.36 pore volumes pumped.

3.4.2: Pressure Drop Profile

The pressure data in this flood are also similar to those of floods without nanoparticles. This is further indication that the nanoparticles have not adsorbed onto the rock and were flushed by flooding the core with brine.

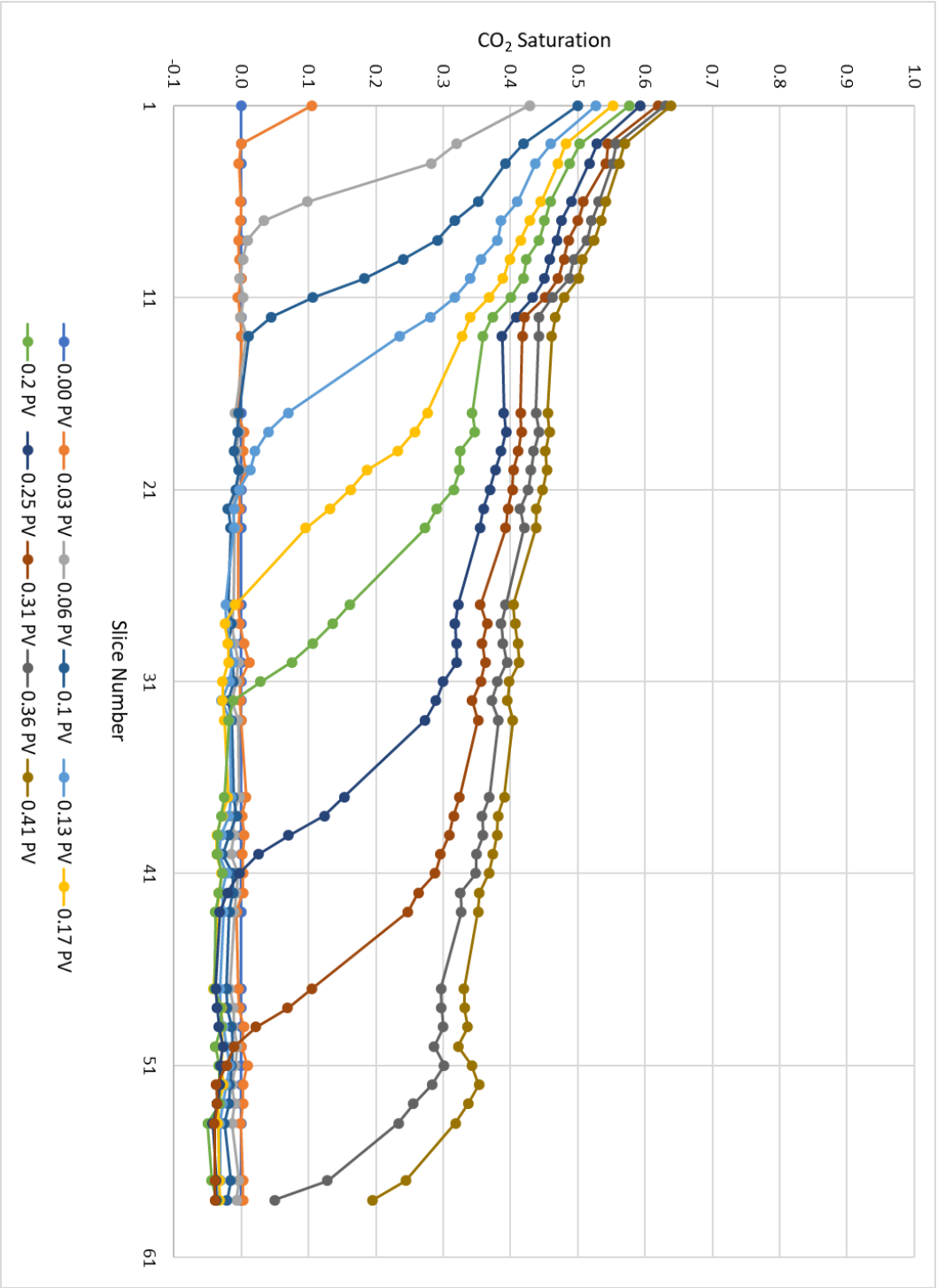

Figure 17: Core #3 flood #4 saturation profiles post brine flush

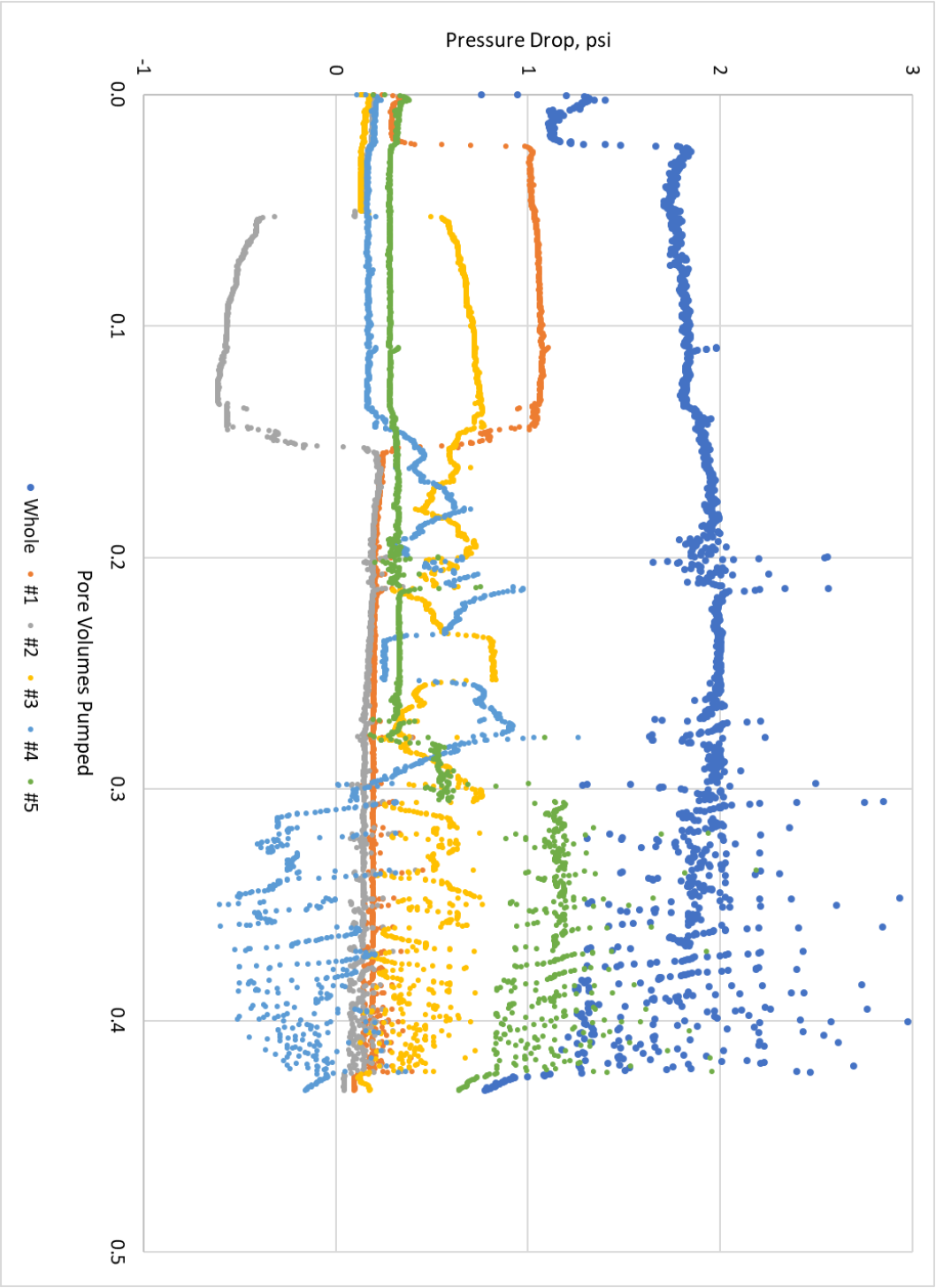

Figure 18: Core #3 flood #4 pressure drops post brine flush

Chapter 4: Discussion

4.1: SUMMARY

Saturating the core with nanoparticle brine before flooding it with CO_2 was observed to cause the following effects:

- Pressure drops in the nanoparticle case were a multiple of 5-10 greater than those in the no-nanoparticle case. Additionally, the pressure drop in the nanoparticle case increased as the core became more saturated with CO_2. This can be seen in Figure 19.
- The mobility of CO_2 was reduced by ten times on average compared to CO_2 without the use of nanoparticles, as summarized in Table 11.
- The pressure drops increased sequentially in each section of the core in the nanoparticle case, as seen in Figure 16. The increase was gradual, indicating it was being caused by viscous effects and not capillary effects, as illustrated in chapter 3.2.2.
- At the same flowrate, the CO_2 front moved slower through the core in the nanoparticle case, as illustrated in Figure 20.
- The final CO_2 saturation in the core was greater by 45% in the nanoparticle case, as seen in Figure 21 and Figure 24.
- Breakthrough in the nanoparticle case was delayed by 45%, as summarized in Table 5, Table 6, and Table 7.

- The pressure drops in the nanoparticle case remain two to ten times greater than those in no-nanoparticle cases, even after the core is flooded with 1.0 to 1.5 pore volumes of CO_2, as illustrated in Figure 22.
- The pressure drops also remain elevated in individual core sections over the entire flood. Considering that section #1 represents 25% of the pore volume, a flood of 1.0 to 1.5 core pore volumes equates to a flood of 4.0 to 6.0 pore volumes in section #1. Figure 23 shows that nanoparticle-case pressure drops are 2-10 times greater in that section at the end of the flood.

The greater CO_2 saturation achieved in the nanoparticle case compared to the base case, the slower breakthrough time, and the increased overall core pressure drop is consistent with results from multiple previous studies, as highlighted and referenced in chapter 1.5 of this thesis. These effects have been interpreted to indicate the formation of an in-situ CO_2/brine foam or emulsion stabilized by nanoparticles during the flood. Moreover, the effluent from the core in the nanoparticle case was observed to be foam-like as shown in Picture 1.

The new measurement of pressure drops across separate segments of the core adds some insight and further evidence to the foam or emulsion hypothesis; foams have much lower mobilities and greater pressure drops than separate fluid phases, as is observed. This lower mobility helps stabilize the CO_2 flood and thus results in a greater CO_2 saturation and improved brine displacement.

One of the major questions investigated by these experiments, besides measuring the mobility decrease, is whether that mobility decrease changes with time. More

particularly, the investigation into whether the increase in CO_2 saturation at the inlet would cause the CO_2 foam to break. In these experiments, it is observed that the CO2 foam does not break for the entire duration of the flood, which in section #1 is after flooding with 4 to 6 pore volumes and reaching an average CO_2 saturation of 0.65.

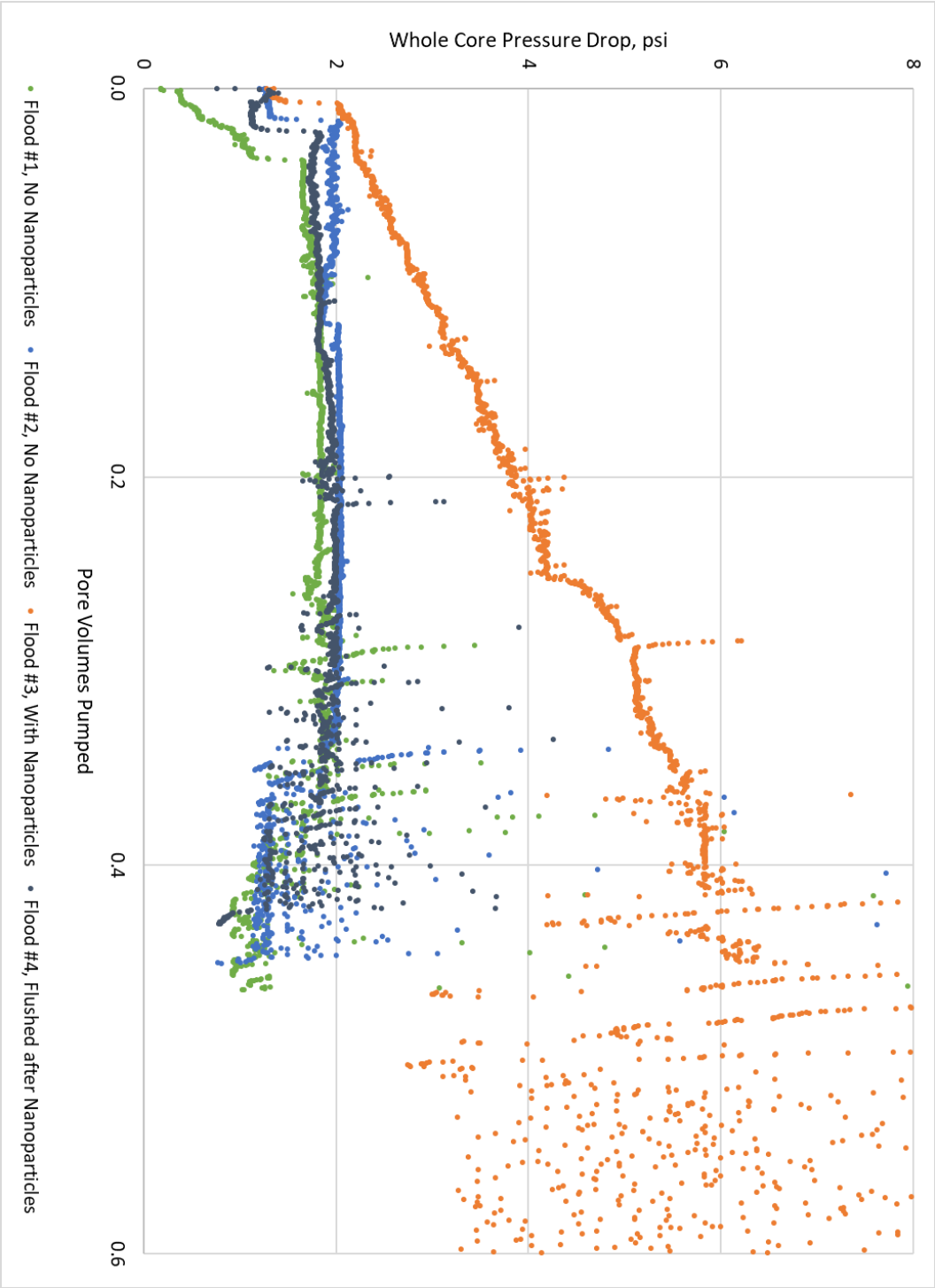

Figure 19: Whole core pressure drop comparison of CO_2 floods with and without nanoparticles in core #2

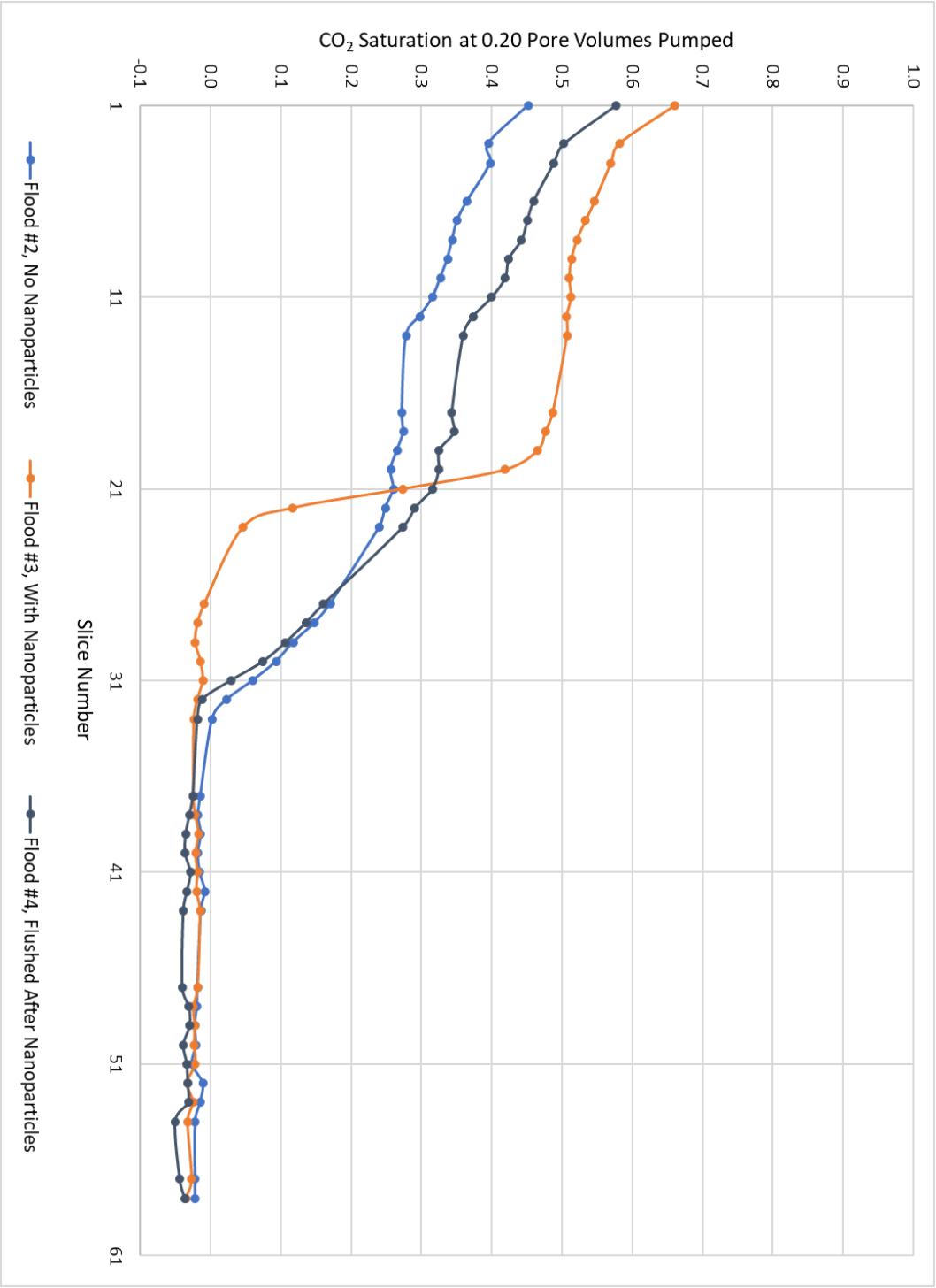

Figure 20: Comparison of CO_2 saturation profile at 0.20 pore volumes pumped of CO_2 floods with and without nanoparticles

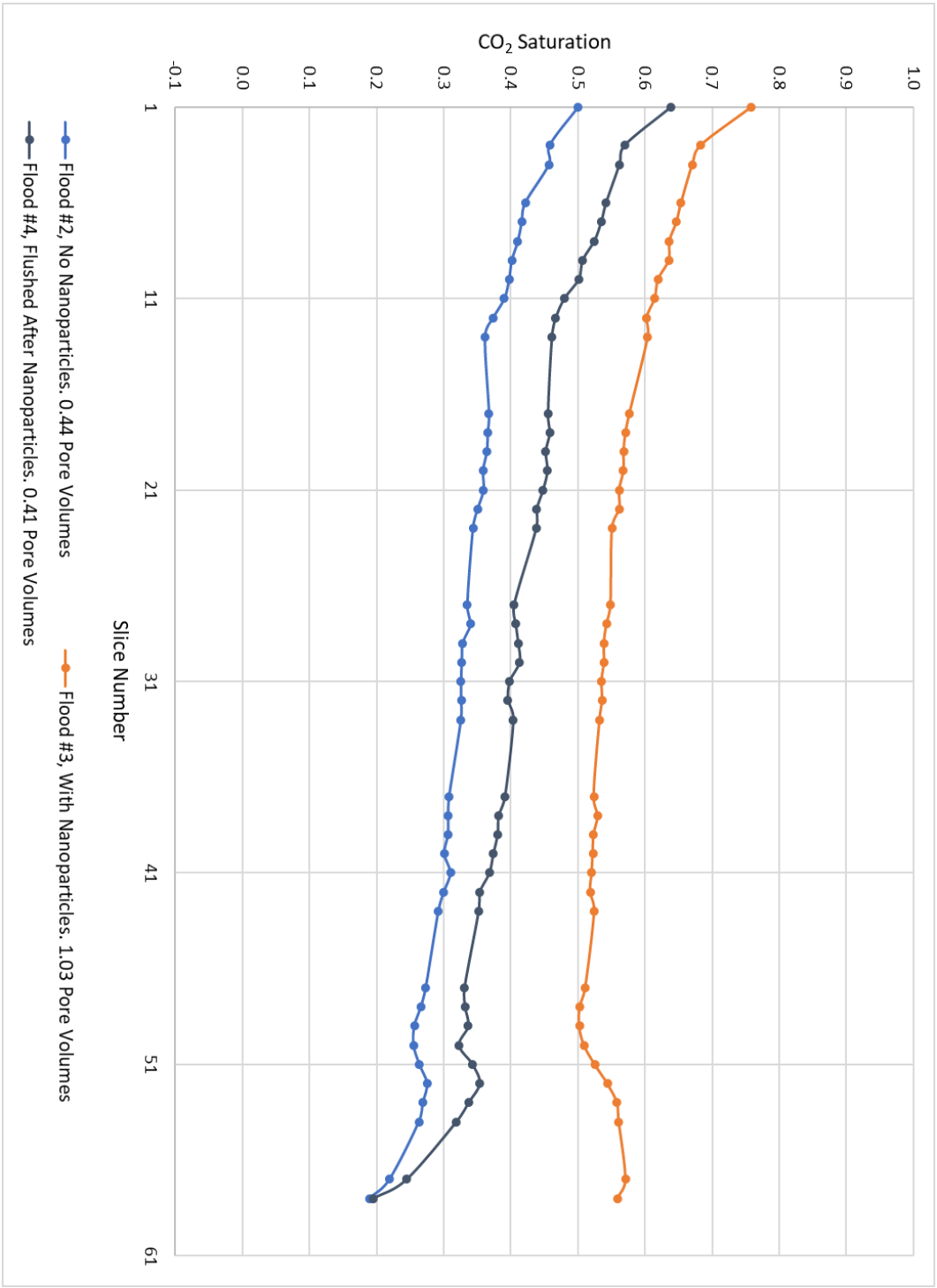

Figure 21: Final CO_2 saturation profile comparison of CO_2 floods with and without nanoparticles

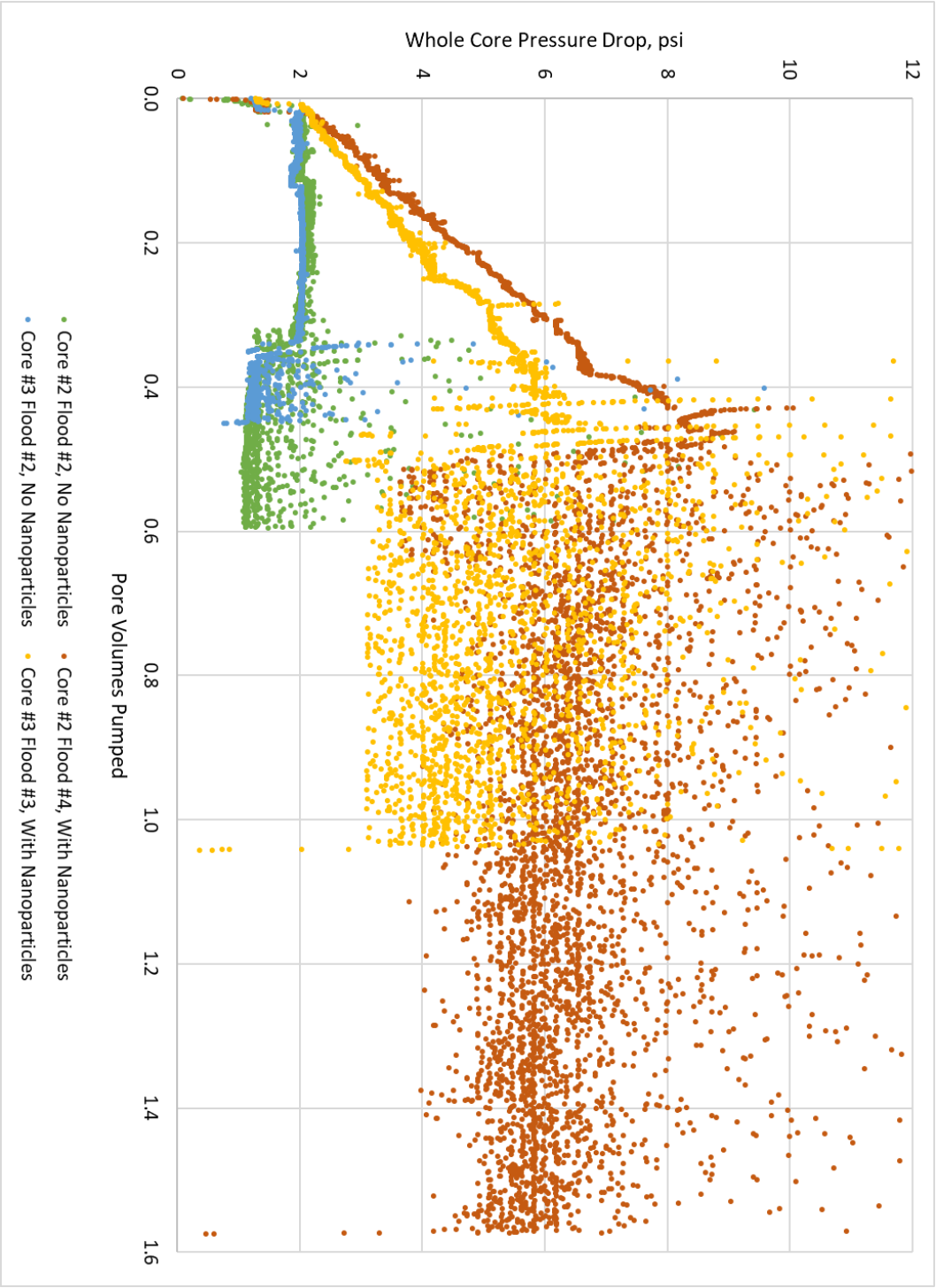

Figure 22: Whole core pressure drop comparison with and without nanoparticles in core #2 and core #3

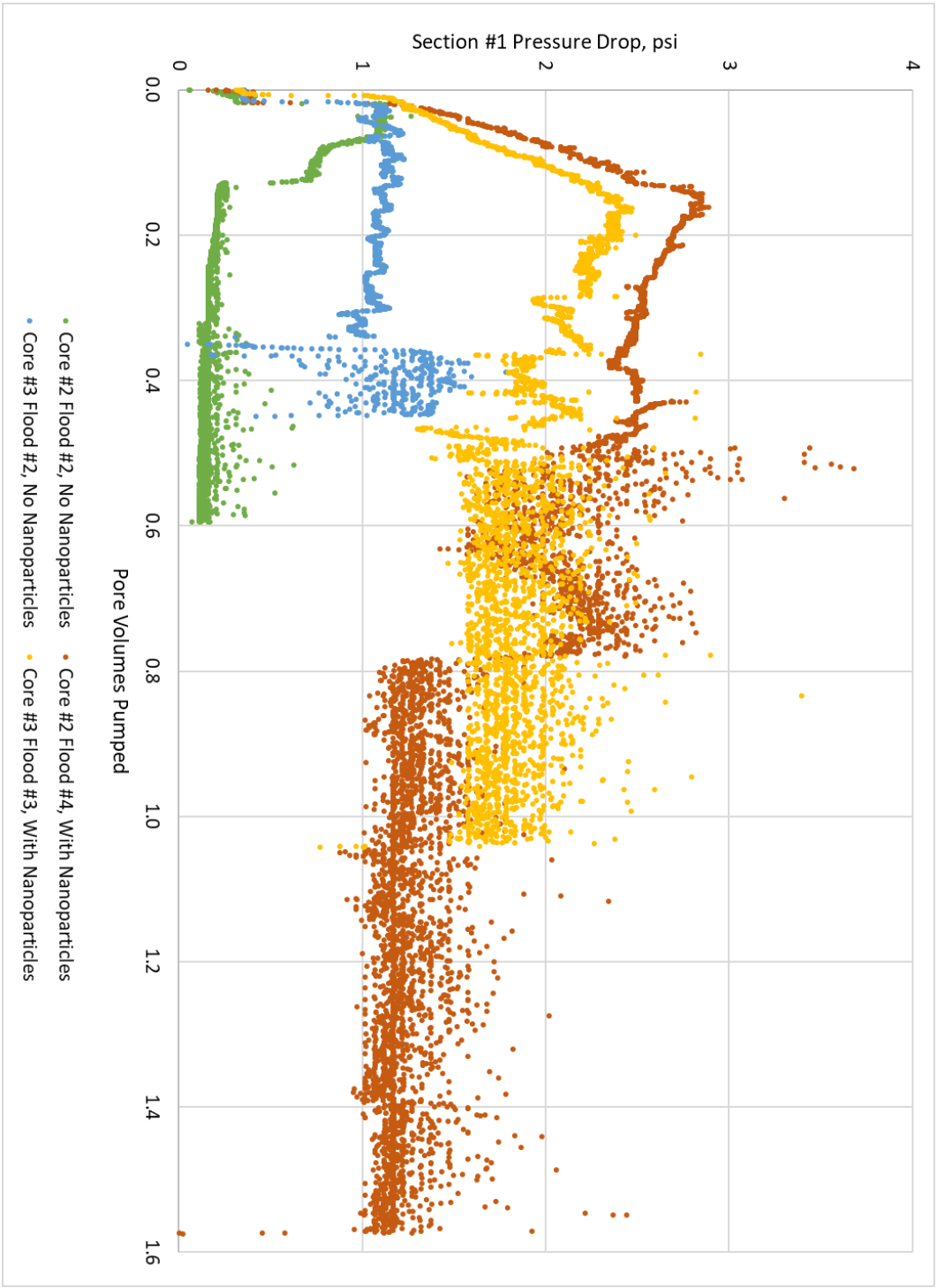

Figure 23: Section #1 pressure drop comparison with and without nanoparticles in core #2 and core #3

Picture 1: Foam-like effluent from CO2 flood with nanoparticles

4.2: Pressure Drop Measurements

Other than the CO_2 floods with nanoparticles, a sudden pressure drop change is observed when a pressure tap is reading through the CO_2 phase while the other is reading through the brine phase. For this reason, any analysis of the pressures needs to take this into account by separating the pressure drop reading into viscous and capillary portions. The method for separating the pressure drops into viscous and capillary portions is discussed in chapter 3.2.2, while the results of this analysis is summarized in Table 8, Table 9, and Table 10. Calculations of mobility, relative permeability and effective permeability shown in this section are performed only on the viscous portion of the pressure drop reading.

4.3: Total Mobility Calculations

Before the CO_2 front has reached a section of the core, only brine flows through that section. The pressure drop in that section would therefore be equivalent to that in a brine flood. After the CO_2 front has passed a section of the core and the capillary pressure effect is no longer present, it is observed that the pressure drop remains constant in that section. That section of the core would be at or very close to irreducible saturation, and therefore only CO_2 would be flowing in that section. The pressure drop reading in that section would differ from that of brine by the change in mobility which includes two opposing factors: the lower viscosity of CO_2 compared to brine, and the effect of relative permeability. Therefore, by assuming the flow of brine in CO_2-swept sections is

negligible and by using the viscosity of CO_2 at experimental conditions, the end-point relative permeability of CO_2 can be calculated in that core. Starting with mobility:

$$\lambda_{CO_2} = \frac{k k_{r\,CO_2}}{\mu_{CO_2}} = \frac{Q_{CO_2}}{A\frac{dP}{dx}}$$

Effective permeability is calculated as follows:

$$k_{eff} = \lambda \cdot \mu_{co_2}$$

For floods without nanoparticles, the CO_2 end-point relative permeability is:

$$k_r = \frac{k_{eff}}{k}$$

The average calculated end-point relative permeabilities were 0.11, 0.11 and 0.07 for cores 1, 2 and 3 respectively. This is summarized in Table 8, Table 9 and Table 10. The flowrates in these tables are in milliliters per minute, and permeability is in millidarcies.

Core #		1		
Flood #		1	2	3
Flowrate	mL/min	0.5		
Brine Permeability	mD	121	120	124
Nanoparticles	Y/N	N	N	Y
Capillary Pressure Reading (psi)	Whole	0.83	0.81	0.85
	#1	0.99	1.27	0.98
	#2	0.69	1.06	
	#3	1.07	1.09	
	#4	1.10	1.08	
	#5	0.90	0.79	
Viscous Pressure Drop (psi)	Whole	1.77	1.68	9.60
	#1	0.56	0.19	3.66
	#2	0.26	0.24	1.98
	#3	0.24	0.24	2.18
	#4	0.22	0.24	1.65
	#5	0.32	0.36	1.62
Total Mobility ($x10^{-12}$ m^2/Pa-s)	Whole	127		19
	#1	160	172	13
	#2	238	258	16
	#3	172	281	14
	#4	221	343	19
	#5			29
Effective Permeability (mD)	Whole	8		1
	#1	10	10	1
	#2	14	16	1
	#3	10	17	1
	#4	13	21	1
	#5			2
CO_2 End-Point Relative Permeability	Whole			
	#1	0.09	0.10	
	#2	0.14	0.13	
	#3	0.07	0.16	
	#4	0.10	0.13	
	#5			

Table 8: Core #1 CO_2 flood analysis

Core #		2			
Flood #		1	2	3	4
Flowrate	mL/min	1.0			
Brine Permeability	mD	305	300	309	310
Nanoparticles	Y/N	N	N	N	Y
Capillary Pressure Reading (psi)	Whole	0.73	0.73	0.72	0.90
	#1	0.71	0.73	0.71	0.91
	#2	0.73	0.81	-0.86	
	#3	0.19	-0.72	-0.74	
	#4	0.79	0.81	0.91	
	#5	0.46	0.81	0.77	
Viscous Pressure Drop (psi)	Whole	1.22	1.31	1.28	7.45
	#1	0.31	0.35	0.33	1.89
	#2	0.21	0.23	0.15	1.51
	#3	0.16	0.17	0.20	1.84
	#4	0.20	0.21	0.21	1.32
	#5	0.30	0.34	0.25	2.62
Total Mobility ($x10^{-12}$ m^2/Pa-s)	Whole	360	334	256	50
	#1	1,159	580		49
	#2	618	687		41
	#3	618	687	309	34
	#4	618		618	47
	#5				35
Effective Permeability (mD)	Whole	22	20	16	3
	#1	70	35		3
	#2	38	42		2
	#3	38	42	19	2
	#4	38		38	3
	#5				2
CO_2 End-Point Relative Permeability	Whole	0.07	0.07	0.05	
	#1	0.21	0.11		
	#2	0.11	0.12		
	#3	0.10	0.13	0.05	
	#4	0.14		0.12	
	#5				

Table 9: Core #2 CO_2 flood analysis

Core #		3			
Flood #		1	2	3	4
Flowrate	mL/min	1.0			
Brine Permeability	mD	303	304	307	307
Nanoparticles	Y/N	N	N	Y	N
Capillary Pressure Reading (psi)	Whole	0.71	0.72	0.76	0.88
	#1	0.77	0.76	0.65	0.71
	#2	0.42	-0.73		-0.75
	#3	0.38	0.56		0.43
	#4	0.53	0.92		
	#5	0.68	0.87		0.90
Viscous Pressure Drop (psi)	Whole	1.12	1.31	5.07	1.13
	#1	0.14	0.35	1.70	0.30
	#2	0.17	0.13		0.13
	#3	0.17	0.17		0.16
	#4	0.17	0.20	2.86	
	#5	0.34	0.35	1.54	0.28
Total Mobility ($x10^{-12}$ m^2/Pa-s)	Whole	331	283	73	328
	#1	662	265	55	309
	#2	364	476		476
	#3	364	364		386
	#4	364	309	22	
	#5	273	265	60	331
Effective Permeability (mD)	Whole	20	17	4	20
	#1	40	16	3	19
	#2	22	29		29
	#3	22	22		23
	#4	22	19	1	
	#5	17	16	4	20
CO_2 End-Point Relative Permeability	Whole	0.07	0.06		0.07
	#1	0.13	0.05		0.06
	#2	0.05	0.08		0.08
	#3	0.06	0.06		0.06
	#4	0.06	0.07		
	#5	0.07	0.06		0.07

Table 10: Core #3 CO_2 flood analysis

4.4: FOAM MOBILITY REDUCTION

The total mobility from the nanoparticle CO_2 flood is divided by the average mobility of the CO_2 floods without nanoparticles to obtain the following mobility ratios. The calculated mobility ratio was an average of 0.08, 0.08 and 0.16 for cores 1, 2 and 3 respectively.

$$M = \frac{\lambda_{CO_2\ with\ nanoparticles}}{\lambda_{CO_2\ without\ nanoparticles}}$$

Core	Transducer	Mobility Ratio
1	Whole	0.15
	#1	0.08
	#2	0.06
	#3	0.06
	#4	0.07
	#5	
2	Whole	0.16
	#1	0.06
	#2	0.06
	#3	0.06
	#4	0.08
	#5	
3	Whole	0.24
	#1	0.12
	#2	
	#3	
	#4	0.06
	#5	0.22

Table 11: Mobility ratio of CO_2 with and without nanoparticles

4.5: CO_2 Saturation at Breakthrough

Figure 24 is the average CO_2 saturation in the core versus pore volumes pumped, with the data point closest to breakthrough made larger for emphasis. Before breakthrough, all lines overlap and are straight with a slope of 1. Shortly after breakthrough, the saturation in the core plateaus, indicating no additional brine is being displaced by the CO_2. The point at which breakthrough occurs, and the value of average CO_2 saturation at that point is equal between the flood before and the flood after nanoparticles. The flood with nanoparticles in comparison has a delayed breakthrough and a greater final saturation.

4.6: CO_2 Saturation Profiles

Figure 68 through Figure 103 in Appendix A2.2 show the CO_2 saturation in the core at different dimensionless times. The saturations are represented by a "jet" color scale that goes from no CO_2 at the blue end of the scale to 100% CO_2 at the red end of the scale. The top slice in these images is at the top of the core, which is at the inlet. The bottom slice is at the bottom of the core, which is at the outlet. The two slices in the middle are picked so that the distance between each slice and the next is almost constant.

Figure 68 through Figure 76 represent different dimensionless times for flood #2, which is without nanoparticles. Figure 77 through Figure 93 are for flood #3, which is with nanoparticles. Figure 94 through Figure 103 are for flood #4, which is after the core was flushed with brine.

The figures show that a preferential flow path exists for the CO_2 in both flood #2 and flood #4. Since the preferential flow path is at the same location for both floods, it is likely to be initiated by heterogeneity in the core and propagated by viscous fingering. In flood #3, the flood is closer to piston-like compared to floods #2 and #4, and the effect of the preferential flow path is greatly dampened. This suggests the nanoparticles suppress the effects of heterogeneity and viscous fingering and help stabilize the flow.

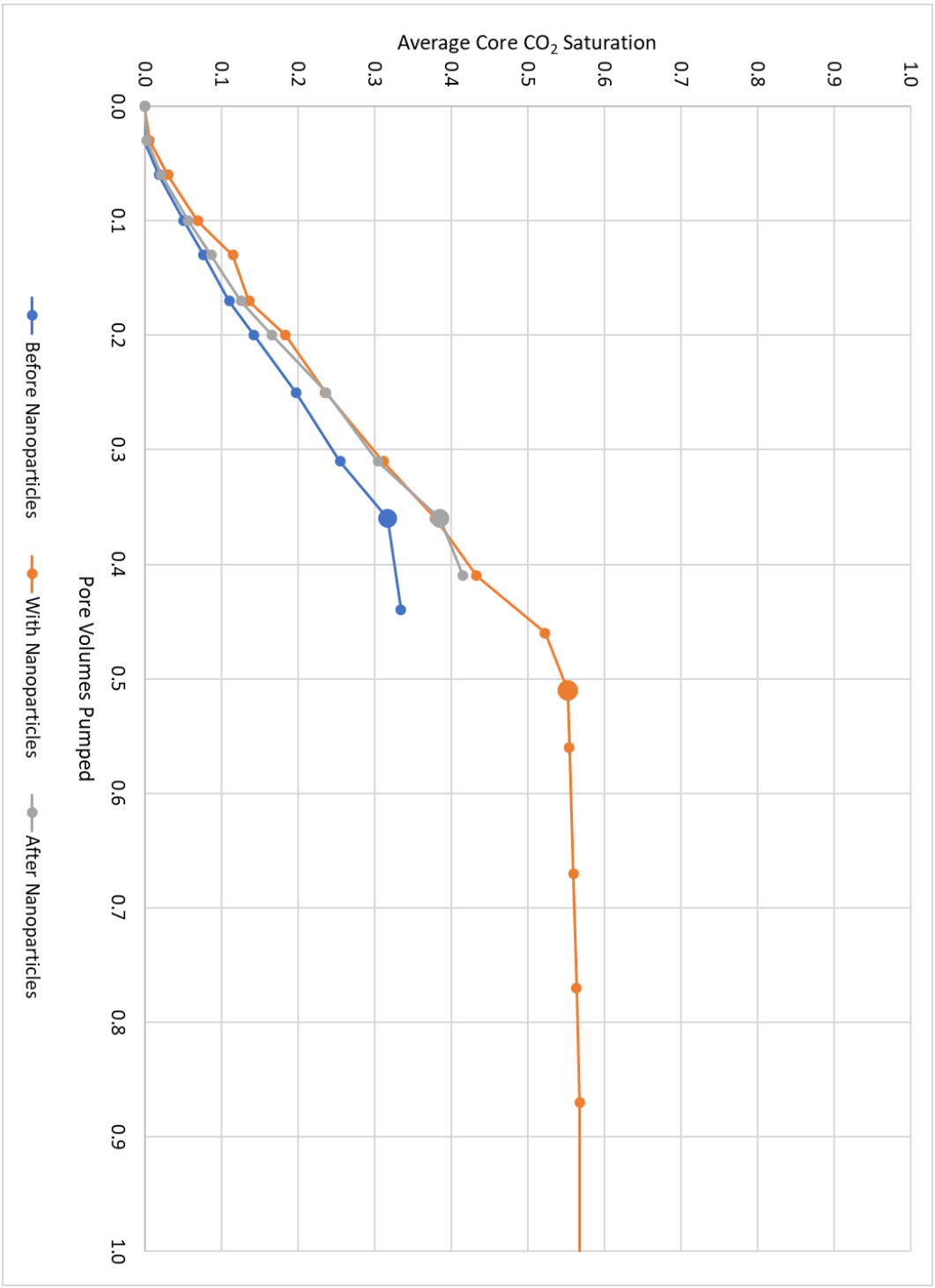

Figure 24: Average CO_2 saturation vs pore volumes pumped

Chapter 5: Conclusions

This study evaluated the use of brine with suspended surface-coated nanoparticles as a means of improving the sweep efficiency of CO_2 floods. Experiments consisted of injecting liquid CO_2 into a brine-saturated core. One of the floods in each core was conducted with the core saturated with surface-coated silica nanoparticle brine. Results from that flood were compared to controls where the core was saturated with brine that does not have nanoparticles prior to CO_2 flooding. The experiments were conducted vertically with the flow direction from top to bottom.

In each flood, pressure drops were measured across the whole core. The core was scanned periodically with a CT scanner, which was used to calculate CO_2 saturations. To extend on previous work, pressure drops were also measured in five sections of the core. Pressure measurements were analyzed to remove the effect of capillary pressure and leave only the viscous portion. The viscous portions of the pressure drops were then used in further analysis to calculate fluid mobilities, effective and relative permeabilities, as well as look at trends in the pressure drop and mobility behavior.

In the CO_2 floods with nanoparticles, the mobility was observed to be ten times lower as compared to floods without nanoparticles. It was also observed that breakthrough was delayed by 45% in the CO_2 floods with nanoparticles. This delay in breakthrough was measured through pressure drop data, CT scanner saturation data, and visual inspection of breakthrough time. The CO_2 saturation front was observed to be sharper in the flood with nanoparticles. The saturation front also went to a greater CO_2

saturation in the nanoparticle case: a jump from zero to 0.46 in the nanoparticle case as opposed to a jump from zero to 0.26 in the control.

The saturation profile along the core consisted of a shock followed by a rarefaction wave, mostly similar to a typical Buckley-Leverett solution of an immiscible displacement. Unlike a typical Buckley-Leverett displacement, the CO_2 saturation at the inlet in this study was measured to not be constant with time but to increase with time.

Consistent with previous work, these effects are interpreted to indicate in-situ formation of CO_2/brine foam. This is supported in this thesis by visually observing a foam-like effluent in the nanoparticle case, as well as an absence of capillary pressure effects in the nanoparticle CO_2 flood, except in the whole core and section #1 transducers. Since those two transducers have reading ports at the core inlet, where CO_2/brine foam would not be expected to have yet formed, they are expected to be exceptions.

The reduction in mobility persisted through the entire flood, lasting more than 1.5 pore volumes. This is well after breakthrough, after CO_2 saturations in the core were almost constant, and when CO_2 saturation at the inlet had reached 0.65.

After the core was flushed with over 4 pore volumes of brine, the subsequent CO_2 flood was similar to that before the introduction of nanoparticles. This indicates these effects are reversible, and that nanoparticles do not permanently adsorb to the rock.

Visual representation CT saturation data show a preferential path for the CO_2. Since these experiments are done vertically, this cannot be explained by buoyancy effects, and is interpreted to be caused by rock heterogeneity. This is supported by the

observation that the preferential flow path was at the same location in both the flood before nanoparticles and the flood after the core was flushed with brine. In the nanoparticle flood, this preferential flow path is suppressed, and the CO_2 front looks much more spread through the entire cross-section. This is a direct observation of nanoparticles improving sweep in CO_2 injection.

Finally, the new measurements and mobility calculations in this study show how nanoparticles stabilize the CO_2 front. Parameters obtained from this analysis can be upscaled from the core-scale to the reservoir scale in reservoir models or simulators.

Appendices

APPENDIX 1: EXPANDED EXPERIMENTAL SETUP

A1.0: Preface

This is an expanded more-detailed section of experimental setup and procedure.

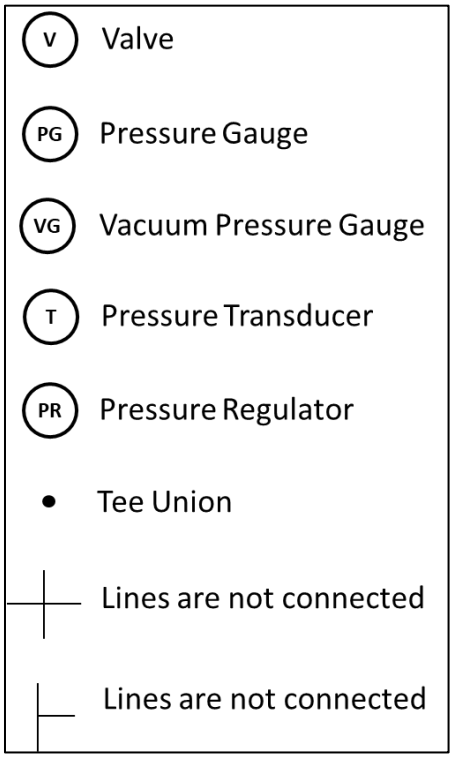

Figure 25: Sketch legend

A1.1: Core Setup

The core is dried in an oven for 12 hours at 348 Kelvin (75 degrees Celsius), then allowed to cool down to room temperature.

The core is then wrapped in a layer of Teflon. This first layer of Teflon acts as a barrier to brine, which would damage the next layer of aluminum foil. The Teflon wrapping extends half a centimeter beyond the edge of the core on either side and seals against the lip of the core holder endcaps. This prevents brine from leaking around either end and reaching the aluminum foil.

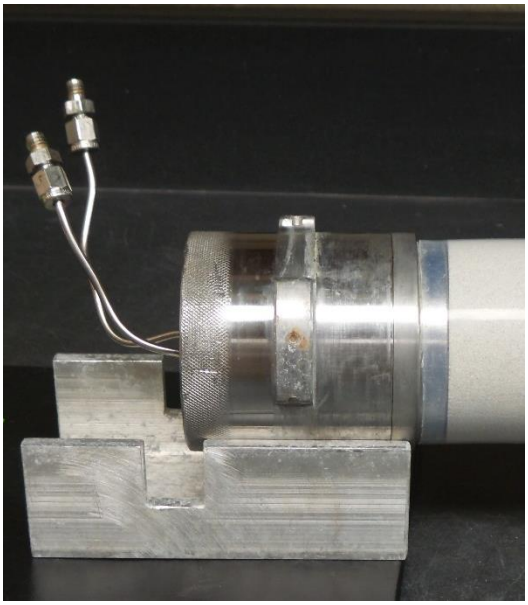

Figure 26: First Teflon layer extended beyond edge of core

The core holder endcaps are placed on either end of the core during the application of the Teflon wrapping to ensure proper shrinking and sizing. A heat gun is used to shrink the Teflon wrapping, with heat applied starting in the middle of the core and going towards the edges to avoid the presence of bubbles and wrinkles in the

wrapping. The core is left to cool with the core holder endcaps in place before proceeding to the next step, to avoid the ends shrinking further with residual heat.

Four layers of aluminum foil are wrapped around the core, which act as a barrier to CO_2 from reaching and damaging the rubber sleeve of the core holder. Then, a second layer of Teflon wrapping is shrunk around the Aluminum foil to keep it in place. Care should be taken not to allow the aluminum foil layers to unwrap before they are secured by the shrunk Teflon layer. The aluminum foil and Teflon layers all extend half a centimeter beyond the edge of the core, as did the first Teflon layer. The core is again allowed to completely cool with the core holder endcaps in place at each end of the core before proceeding to the next step. At this point, a cross section of the core would be as in Figure 27.

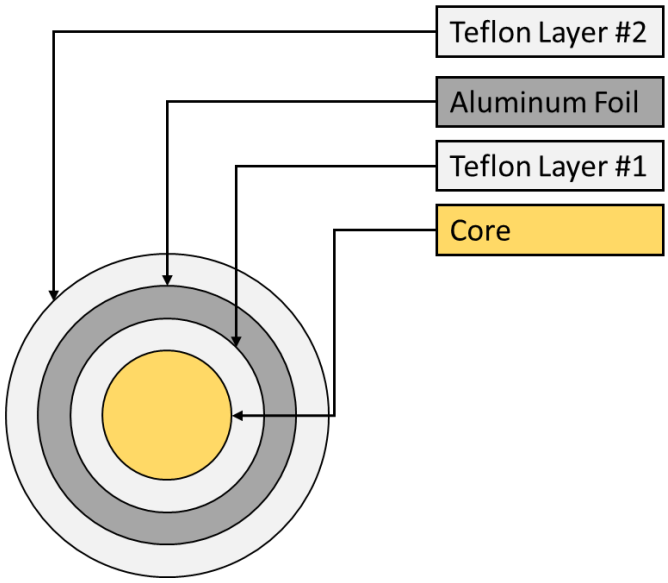

Figure 27: Core cross-section after wrapping

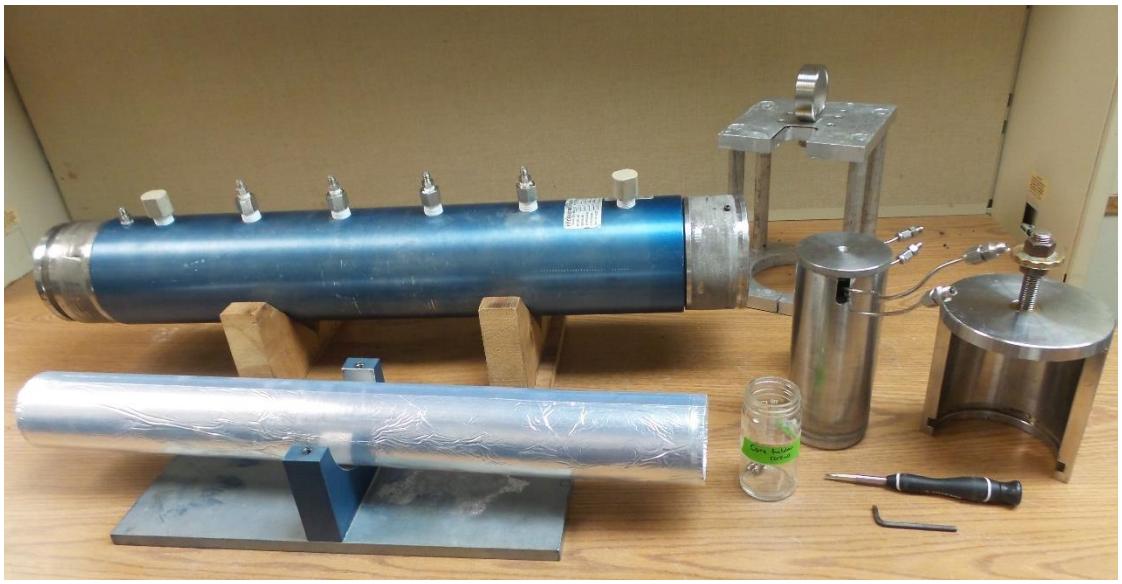
Figure 28: Core wrapped with Teflon and aluminum foil

A1.2: Core Holder Setup

The wrapped core is placed in the core holder and both endcaps are inserted and secured. A cross section of the cored holder would be as in Figure 29. A drill is used to drill holes through the Teflon wrapping and aluminum foil layers through each pressure tap. A cross section of the core holder would be as in Figure 31.

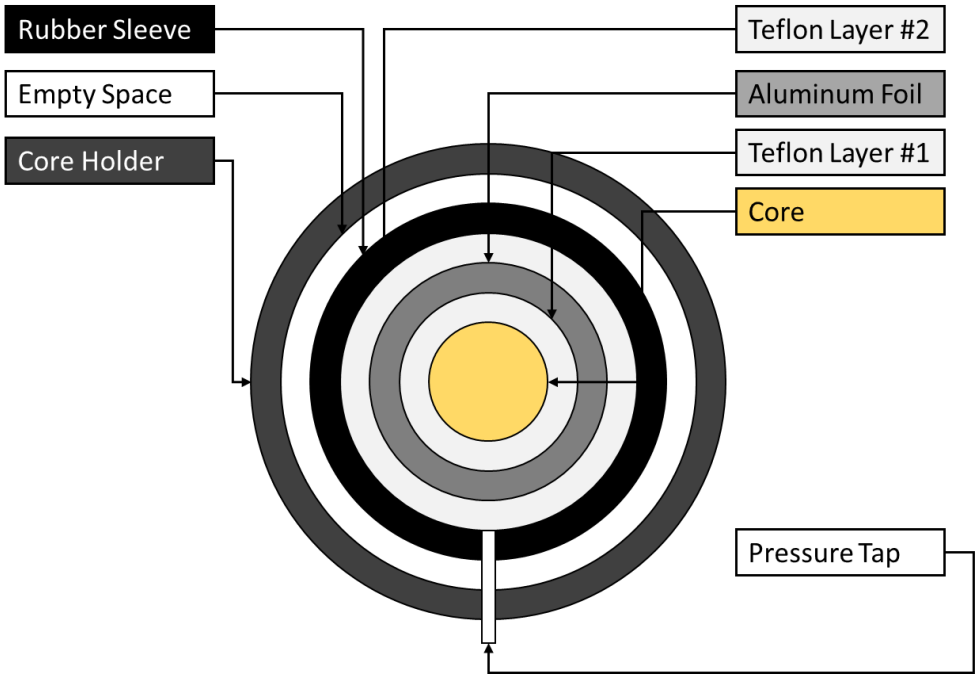

Figure 29: Core cross-section in core holder

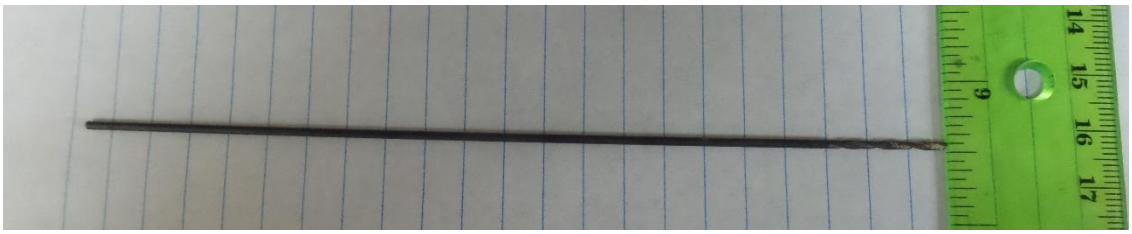

Figure 30: Drill bit size used to drill through pressure taps

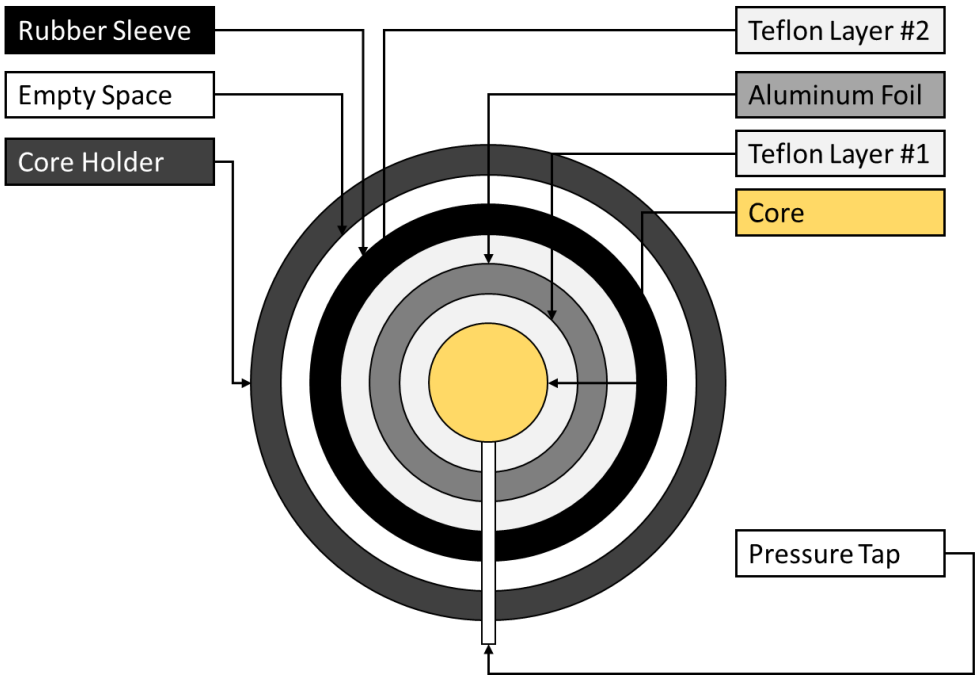

Figure 31: Core cross-section after drilling holes

The core holder is then suspended vertically. A pressure gauge and a two-way valve are connected to the top inlet of the core holder confining pressure inlet. Another two-way valve 2-3 is connected to the bottom inlet. This would look as in Figure 32.

.

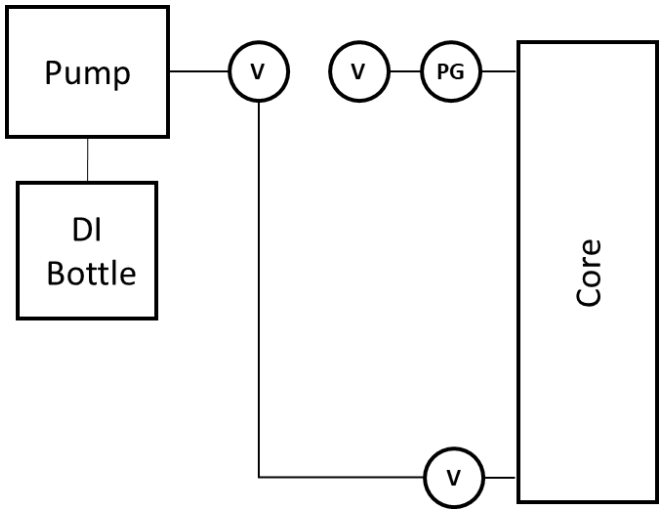

Figure 32: Setting up confining pressure

De-ionized water is then pumped to the bottom inlet of the confining pressure while all valves are open to purge air. When water is observed to come out of the top valve, that valve is closed. Pumping de-ionized water is continued until desired confining pressure is reached. When desired confining pressure is reached, the pump is stopped and both valves connected to the core holder are closed. A cross section of the core holder would be as in Figure 33.

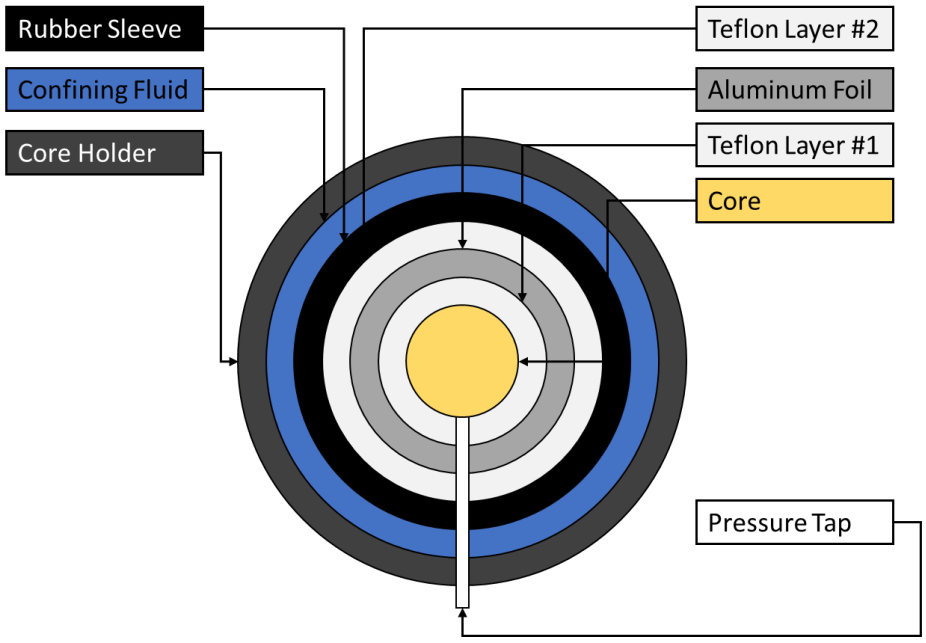

Figure 33: Core cross-section after applying confining pressure

The confining pressure is then monitored for 24 hours to ensure there are no leaks. As the confining fluid presses on the rubber sleeve, it is normal to observe an initial drop in confining pressure.

A1.3: Transducer Line Setup

The internal cavities of the transducers and the tubing lines connecting them must be purged of air to ensure proper pressure difference readings. The lines and bodies must also be pressurized and monitored to ensure there are no leaks. This setup is shown in Figure 34. Each transducer has two vent openings.

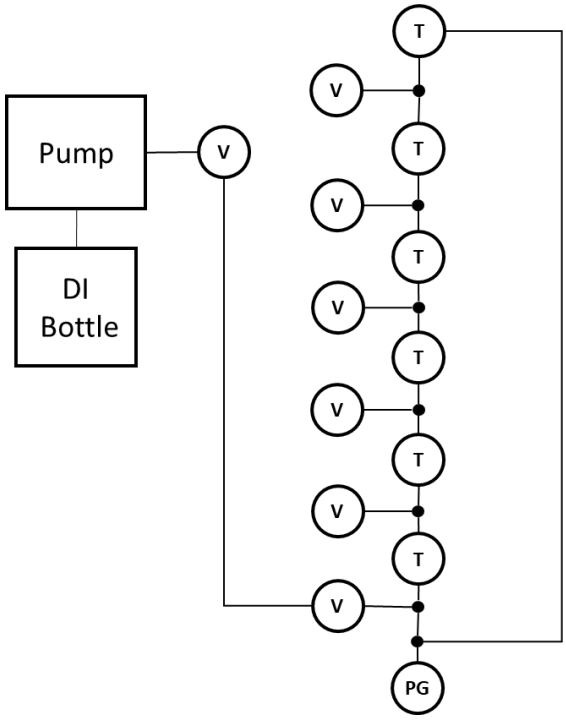

Figure 34: Transducer line setup

Using the vent openings, the valves on the transducer bodies, and the valves connected to the lines, water is forced to purge each part of the system sequentially. When one part is purged, the valves are manipulated to direct the water to a new direction. Water must be observed to come out of the outlet of the section being purged before moving on to the next section. After the entire system is fully purged, all outlets are closed, and the system is pressurized. Pressure is monitored for 24 hours to ensure no leaks are present. Because of the small volume of the transducer lines, even a fluid loss of miniscule volume would result in a large drop in the system pressure. Moreover, the presence of any air in the system would result in a large initial loss of system pressure as that air dissolves into the pressurized water. Vacuuming the transducer lines before attempting to purge them would generally yield better leak tests.

A1.4: Vacuum Saturating the Core

The core is connected to a vacuum pump, and the pressure taps are connected to the valves on the transducer lines, as shown in Figure 35. The valves connecting the core to the transducer system are to remain closed during this procedure. The valves connecting the vacuum pump to the core are opened. The valves isolating the core from the atmosphere are closed. The vacuum pump is turned on for 3 hours, and the pressure is observed through the vacuum pressure gauge in the line connecting the vacuum pump to the core. The vacuum pressure gauge should read close to -1 atm or -30 in. Hg a few seconds after turning on the vacuum pump if proper vacuum is pulled on the core and no leaks are present.

When vacuuming is completed, the valve closest to the vacuum pump is closed, isolating the core from the vacuum pump. The vacuum pump is disconnected from the core holder and allowed to vent before being turned off. The vacuum can then be leak tested by reading pressure from the vacuum pressure gauge. This would be as in Figure 36.

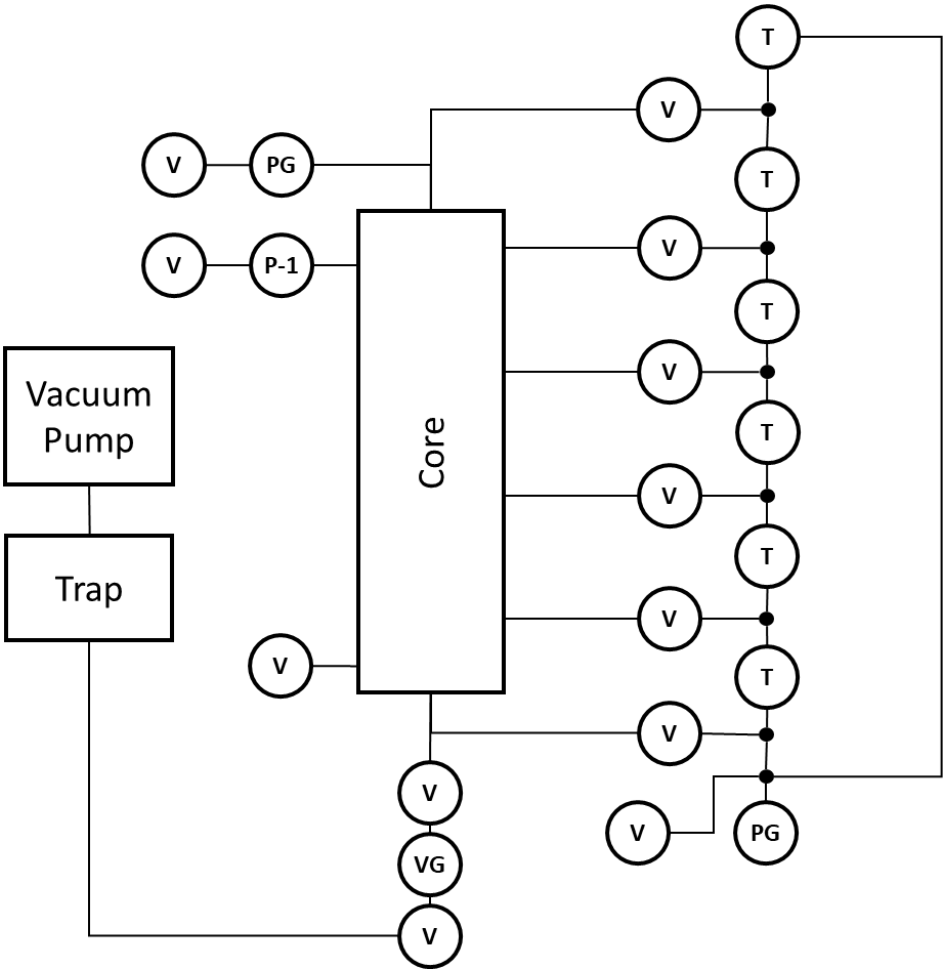

Figure 35: Vacuuming core

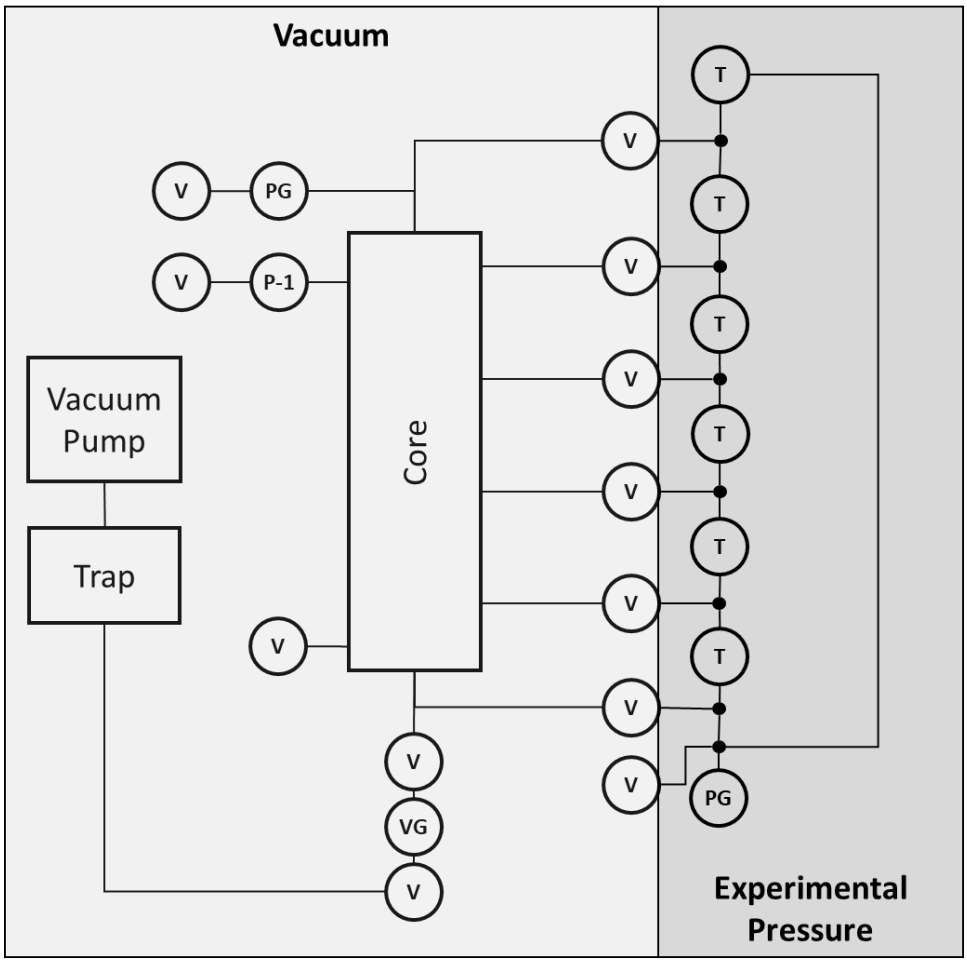

Figure 36: Pressure testing vacuum in core

A1.5: Filling Accumulator with Brine

The accumulator piston is initially positioned at one end of the accumulator. The endcap is screwed onto the same end that has the piston. That end should be at the bottom, as shown in Figure 37. Brine is poured into the accumulator from the top, then the second end-cap is screwed onto the top end of the accumulator, as shown in Figure 38. A three-way valve is installed on both ends of the accumulator. The pump is connected to the bottom end of the accumulator, as shown in Figure 39.

All valves are opened, with the three-way valves opened in the direction of the accumulator. De-ionized water is pumped to the bottom of the accumulator until brine starts to flow out of the top, indicating all air is purged. The top accumulator valve is closed, and additional de-ionized water is pumped until the brine is at desired experimental pressure. The final setup will be as in Figure 40.

Figure 37: Empty accumulator

Figure 38: Accumulator with brine

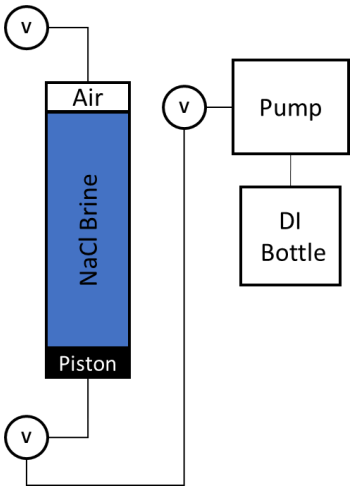

Figure 39: Accumulator connected to pump

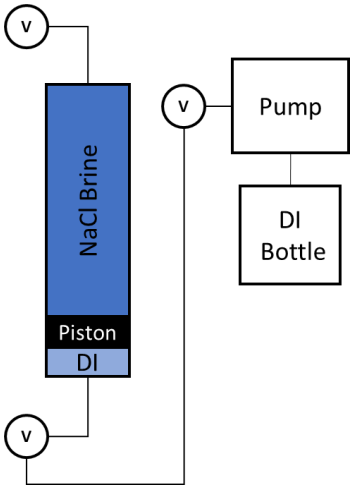

Figure 40: Brine accumulator ready for experiment

A1.6: Saturating the Core

Brine is pumped to the core from the brine accumulator, as shown in Figure 41. Valves from the pump to the accumulator, and from the accumulator to the core are opened, while others are closed so that the core is isolated from the atmosphere.

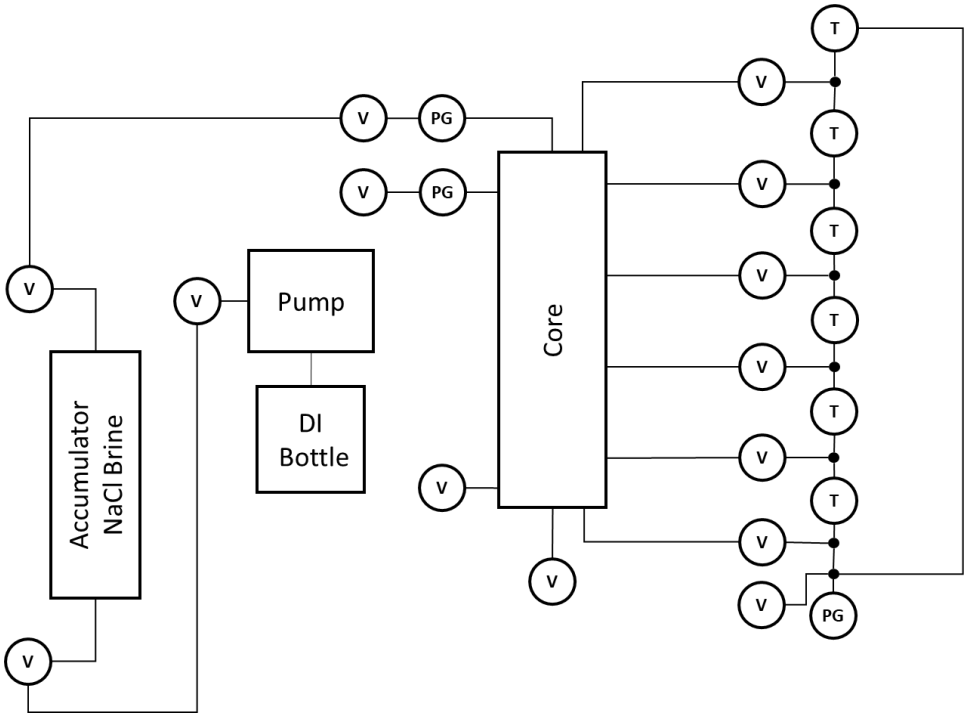

Figure 41: Setup for saturating core with brine

As the core is initially vacuumed, pump pressure will be zero until one pore volume is pumped. Afterwards, pressure will start to increase. The point at which pressure starts increasing is recorded as a measurement of pore volume and is used to calculate porosity. When the core is at experimental pressure, the pump is stopped and the valve between the core and the accumulator are closed. The core is then leak tested for 24 hours by observing the pressure gauge at the top of the core holder.

A1.7: Setting Up the Back-Pressure Regulator (BPR)

The dome side of the BPR is connected to a pressure gauge and a two-way valve, then to the Nitrogen tank, as shown in Figure 42. First, the valve closest to the Nitrogen tank is opened and the regulator is used to adjust for desired pressure. The valve next to the pressure regulator is opened next. If no signs of a leak are observed, the valve closest to the back-pressure regulator is also opened. The pressure regulator is then adjusted so that the pressure gauge on the back-pressure regulator reads the desired pressure. All valves are closed, the line connecting the BPR to the tank is disconnected from the BPR. The BPR is leak tested by reading the pressure gauge connected to it. If a leak exists, soap water can be used to determine its location. The BPR diaphragm needs to be a material compatible with CO_2 such as graphite-impregnated Teflon. Viton rubber is not compatible with CO_2. Picture 2 shows a Viton rubber BPR diaphragm damaged by CO_2, causing complete blockage of the fluid path within the BPR.

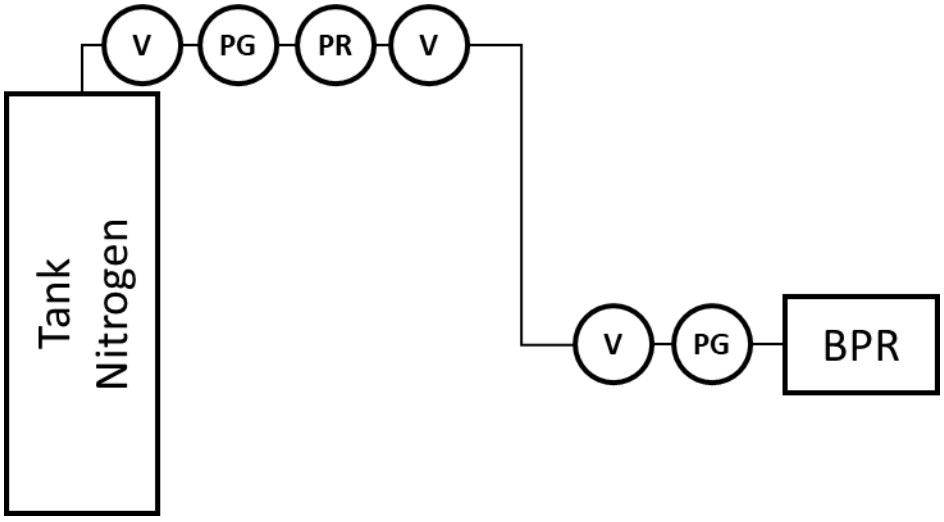

Figure 42: Setting up a back-pressure regulator (BPR)

Picture 2: Viton rubber BPR diaphragm damaged by CO_2

A1.8: Filling Accumulator with CO_2

The accumulator is first filled with de-ionized water. This would be as shown in Figure 43. The valves used are two-way valves.

A BPR is connected to the accumulator on the side opposite the piston and is set to a pressure that slightly lower than that of the vapor pressure of CO_2, which was measured to be 840 psi in these experiments. This is so that the CO_2 can push the piston and displace the water in the accumulator. The reason for the water, and the BPR only being slightly lower than CO_2 vapor pressure is to make sure the accumulator is filled up slowly. This minimizes the loss of pressure in the CO_2 below its vapor pressure as it

transfers, which reduces the amount of gas that will end up in the accumulator and increases the final usable volume of liquid CO_2 in the accumulator. The liquid CO_2 tank is connected to the accumulator from the side of the piston. This is as shown in Figure 44.

The valves between the liquid CO_2 tank and the accumulator are opened, while the valve between the accumulator and the BPR remains closed. The pressure gauge between the liquid CO_2 tank and the accumulator should read the vapor pressure of CO_2. The lines between the liquid CO_2 tank and the accumulator should be checked for leaks with soap water.

The valve between the accumulator and the BPR is opened to allow CO_2 to fill the accumulator while water is collected in the waste bucket. When no more water flows out of the accumulator and the volume of water in the bucket is equal to the accumulator capacity, the accumulator is full of CO_2. At the end of this process, the setup would be as shown in Figure 45.

Figure 43: Accumulator with de-ionized water

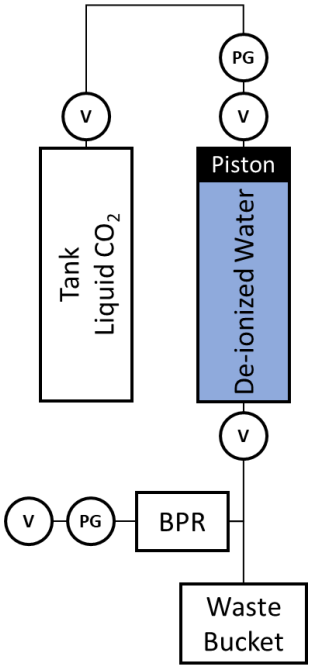

Figure 44: Accumulator connected to CO_2 tank

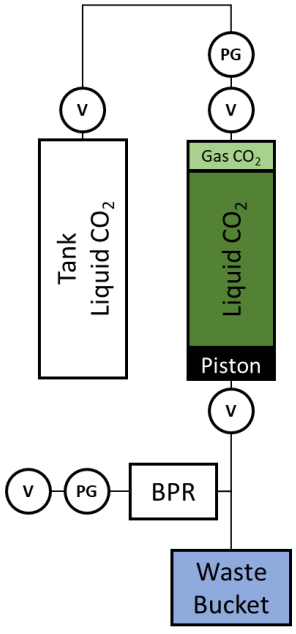

Figure 45: Accumulator with gas & liquid CO_2

All valves are closed. The accumulator is disconnected from the liquid CO_2 tank and connected to a pump, as shown in Figure 46.

Valves between the pump and the accumulator are opened, but the valve at the outlet of the accumulator is to remain closed. Water is pumped to the accumulator, which is a closed system in this setup. This will compress the CO_2 and force free CO_2 gas to condense to liquid. During this process, pressure in the accumulator will remain constant at the vapor pressure of CO_2. When pressure starts increasing, it is a sign that all CO_2 gas has been liquified. Pumping is continued until the accumulator is at desired experimental pressure. In these experiments, liquifying all CO_2 gas and further increasing the CO_2 pressure from 840 psi to 1,000 psi required pumping 300 milliliters of water into the 1,500-milliliter accumulator. This means there was a usable liquid CO_2 volume of 1,200 milliliters from the accumulator each time it was filled. This is as shown in Figure 47.

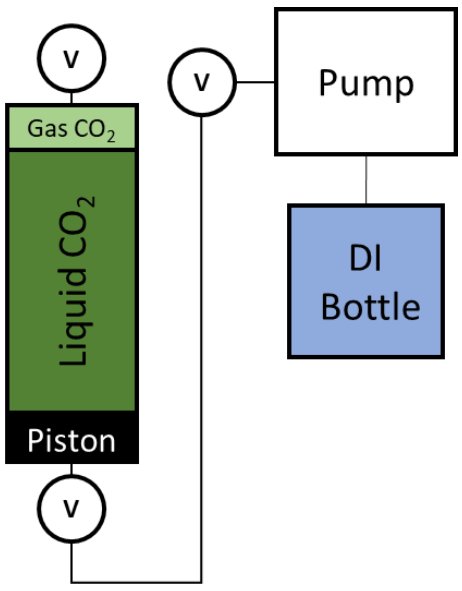

Figure 46: CO_2 accumulator connected to pump

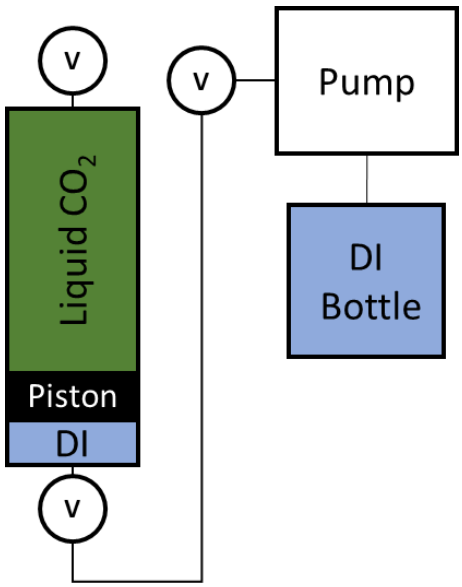

Figure 47: Accumulator with liquid CO_2

A1.9: Opening Transducers to Core

All equipment is set up as in Figure 48. Valves from the pump to the accumulators and from the accumulators to the core are to be open. Three-way valve in the accumulator setup is to be open to the brine side. Two-way valves connected to the CO_2 accumulator are to remain closed, as well as valves from the core to the BPR. Valves from core holder to transducer are opened, then the middle valves on the transducer bodies are closed. When these valves are closed, the compression of water inside the transducer bodies could cause a small pressure drop reading that should dissipate in a few seconds. All transducers should read zero psi a few seconds after their middle valves are closed.

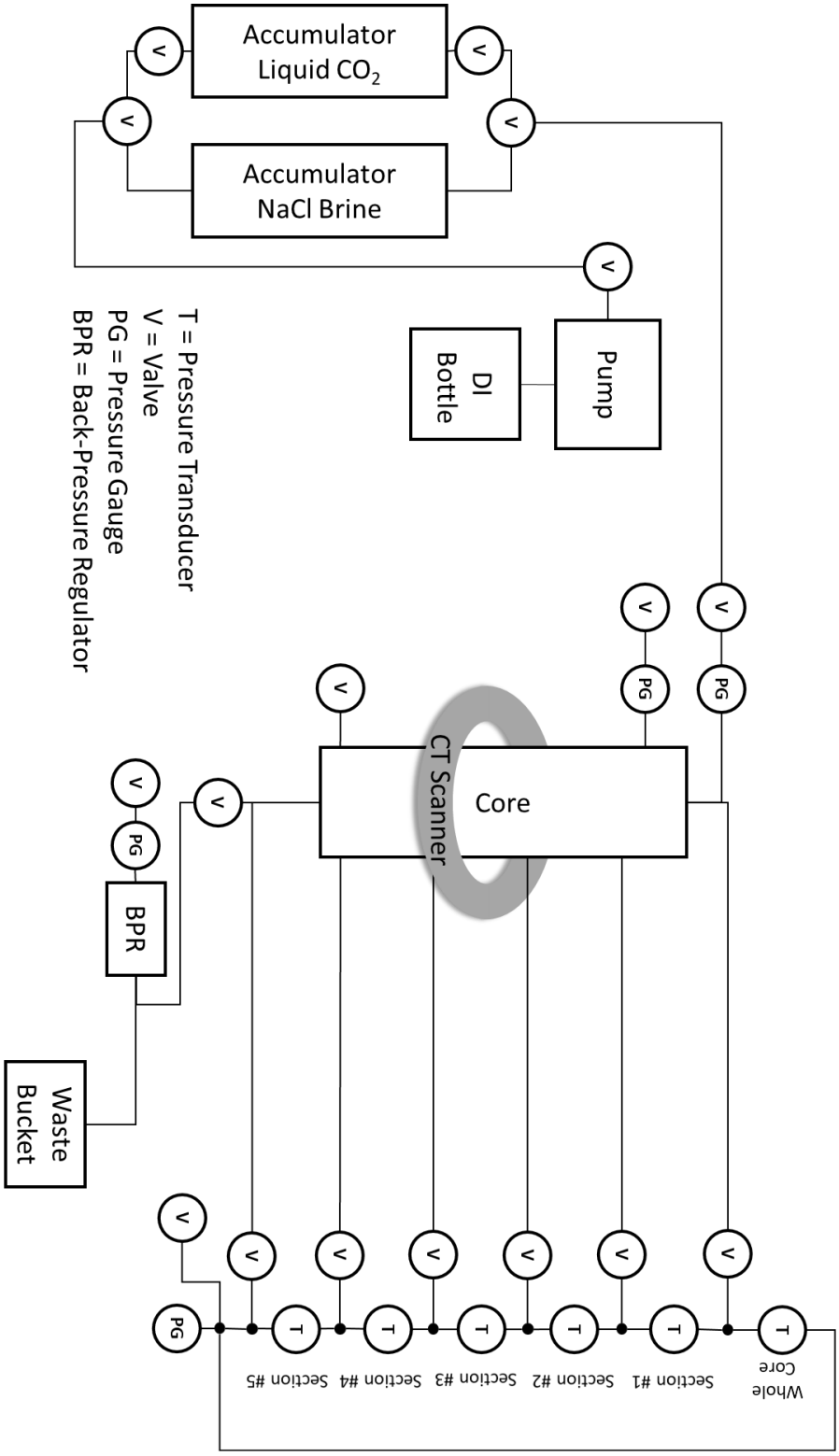

Figure 48: Complete experimental setup

A transducer reading anything other than zero is an indication of a plug or leak in one of the lines or in the fittings and connections of the transducer itself. A pressure drop equal in magnitude but opposite in sign observed in two adjacent transducers is an indication there is either a plug or leak in the line or connections between them. If this is observed after a CO_2 flood, it is likely caused by damage to the core holder rubber sleeve at the location of the pressure tap of the line in question. As the Teflon and aluminum foil at the pressure tap location are drilled, it does cause some contact between CO_2 and the rubber sleeve at that location. Damage to the rubber sleeves at the locations of the pressure taps was a common problem encountered in these experiments. Some small parts of the rubber sleeve have been observed to get into the lines and plug them, which was remedied by flushing the lines. The rubber at the pressure tap location could also swell and plug the opening, which was remedied by re-drilling at those locations.

A1.10: Other Considerations

The BPR is set to desired experimental pressure, which should be greater than the vapor pressure of CO_2 to ensure no CO_2 gas evolves inside the core. When CO_2 breaks through in a CO_2 flood, its rapid expansion from experimental pressure on one side of the BPR to atmospheric pressure on the other side causes large pressure pulses, which show up as noise in the pressure drop measurements.

A1.11: Brine Floods

A brine flood of at least 1 pore volume is done before every CO_2 flood, including the first. When recording pressure using LabView, recording should be started a few minutes before the flood starts so several readings are taken at zero flow. These readings can be used to gauge the noise and uncertainty of the pressure transducers.

Before the brine flood is concluded, flow should be done at three different flow rates, giving each flowrate enough time to stabilize and get several pressure drop readings. Pressure drop readings are checked for expected linear dependency on flowrate. This is shown in Figure 49, which is a brine flood at 1, 2 and 4 mL/min. Deviation would indicate a problem in the setup.

Permeability is calculated for each of the flow rates, keeping in mind the difference in length of sections. The calculated permeability should be independent of flowrate as shown in Figure 50, which is the same flood as in Figure 49.

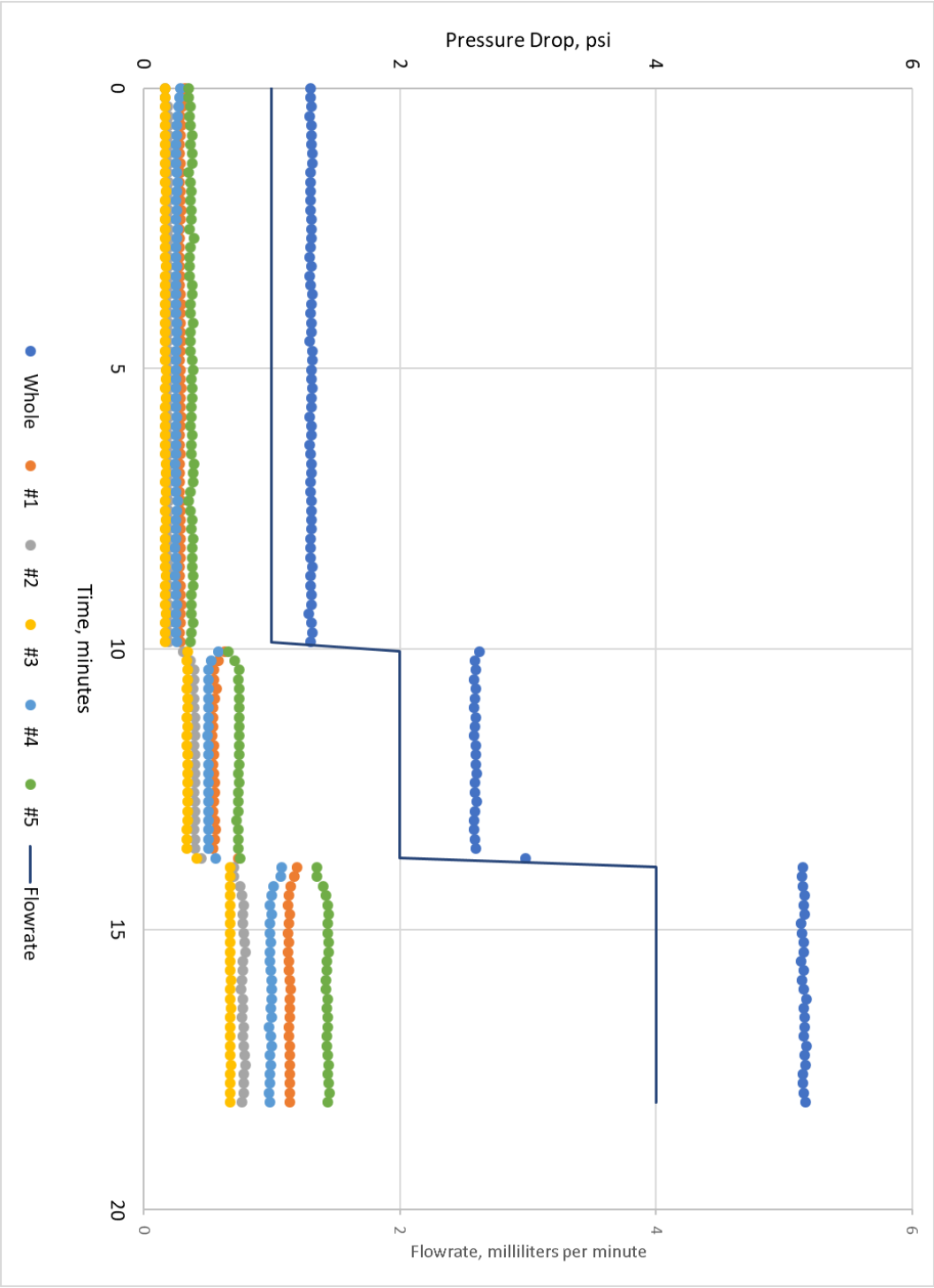

Figure 49: Pressure drops of brine flood with changing flowrate (1, 2 and 4 mL/min)

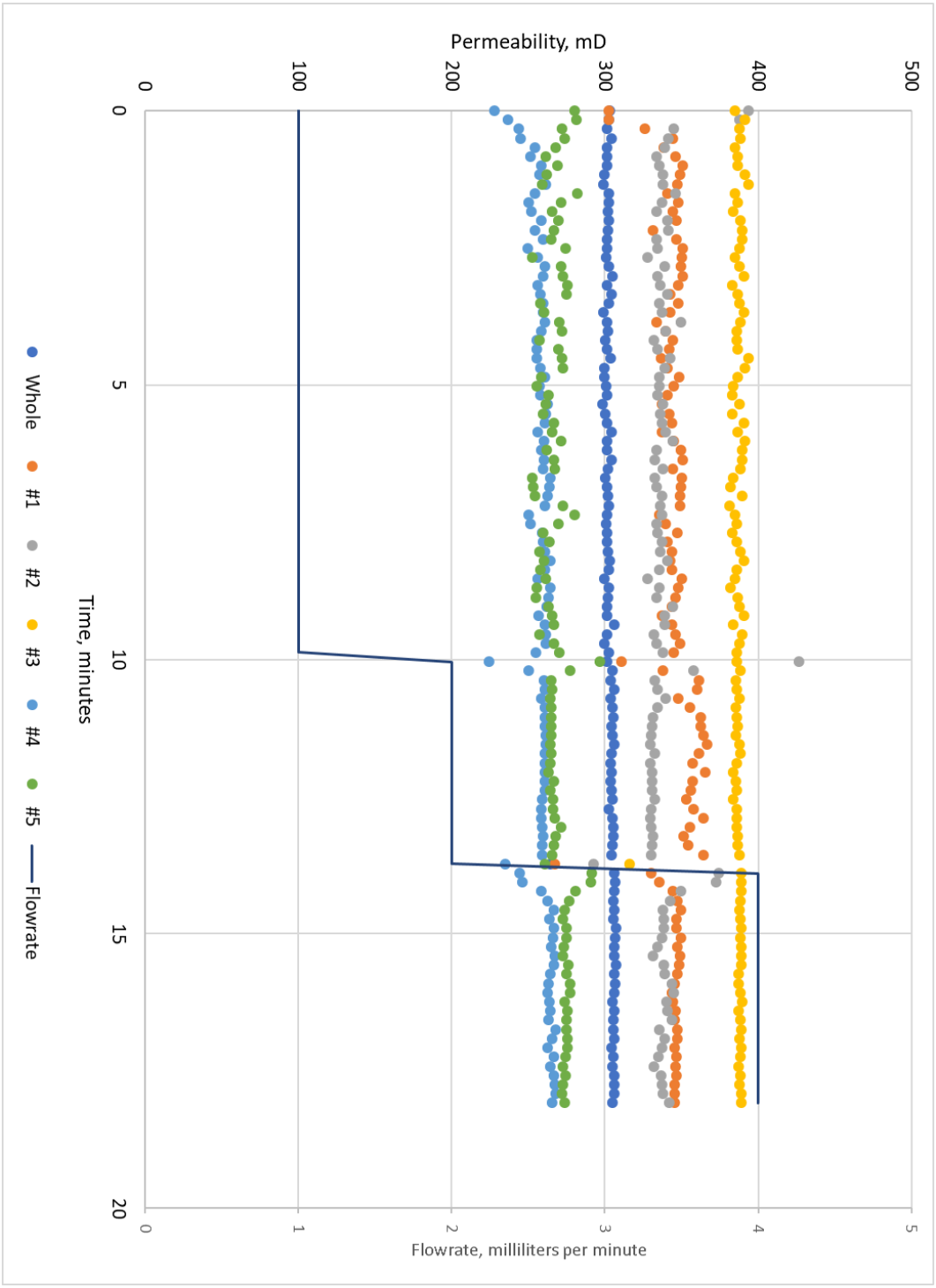

Figure 50: Permeability of brine flood with changing flowrate (1, 2 and 4 mL/min)

A1.12: CO_2 Flood

After the brine flood is complete and the pump is stopped, valves from the pump to the accumulators, from the accumulators to the core and from the core to the BPR are all closed. The valves from the core to the transducers are kept open. The transducers should all read zero shortly after. The valve from the pump to the accumulators are opened, and the three-way valve is turned to the CO_2 accumulator side. The pressure in the CO_2 accumulator is checked by pumping a small amount of water and made to be at experimental pressure. The valves from the accumulator to the core are opened, then the valve from the core to the BPR. In these experiments, flow rates were low enough that flowing to a fume hood was not necessary given the small amount of CO_2 flowing out of the core.

A1.13: Resaturating Core with Brine

When the CO_2 flood is complete, the pump is shut down, then the valve from the pump to the accumulators, the valve from the accumulators to the core, and the valve from the core to the BPR. Transducers not reading zero in this instance is not indicative of any issue, because of capillary pressure effects on the pressure drop readings. The line at the outlet of the core is disconnected from the BPR and anchored in the fume hood inside a waste bottle. It is important that the line is anchored at multiple locations with zip ties, as venting CO_2 will cause it to flail. Before the CO_2 is vented, the valves in the middle of the transducer bodies are opened, then the valves between the transducers and the core are closed. The valve at the outlet of the core is opened slowly until CO_2 starts to flow. When the core is at zero pressure, start pumping brine to the core. When brine is observed to come out of the outlet line, close the valve at the core outlet and keep

pumping brine into the core. When the core is again at experimental pressure, stop the pump. Reconnect the outlet line to the BPR. Do a brine flood that is 1 or more pore volumes before proceeding to the next CO_2 flood.

A1.14: CT Scanning

The CT scanner protocol used in these experiments was modified from the "Orbits" protocol, which is a term for the eye-sockets in the skull. One scan of the core required 59 separate slices of 10mm thickness each, and scanning the entire core took 6 minutes and 5 seconds on average. The slices within one scan were treated in the analysis as if they were all taken instantly at the time the first slice was taken. Each set of slices is saved as a separate file. For the calculation method used in these experiments, two base scans are required: one with the core full of air and another with the core saturated with water. The time at which pressure data recording was started, pumping CO_2 was started and each CT scan was started or completed was recorded separately in a notebook. This is used to synchronize pressure and CT data, and to calibrate CT data. A new base scan with the core saturated with brine is taken before each CO_2 flood. Settings used for the scanner are:

- Voltage: 130 kv
- Current: 100 mA
- Scan Time: 1 s
- Index: -10 mm
- Thickness: 10 mm

The index is how much the couch will move after each slice is taken. The "home" of the VPS at the top is couch position 30mm, and the positive direction is downwards. A

positive index means the core will be lowered after each slice, while a negative index means the core will be raised after each slice. In these experiments, the core started at the bottom and was raised after each scan. This meant scanning started at the top of the core and ended at the bottom and is why the index is negative.

A1.15: CT Data

The output of the CT scanner is a 2D array for each slice, with each number representing the average CT number in that voxel. Figure 51 is an unprocessed CT image, and Figure 52 shows stainless steel pressure tap interference. The images shown are a gray-scale plot of the 2D array using the MATLAB function imshow, with the display range set to a low of 700 and a high of 2100. This means a CT number of 700 or below is black, a CT number of 2100 or above is white and anything between 700 and 2100 is a shade of gray. The white in the figures below is the core holder. The gray circle in the middle is the core. The black between the core and the core holder is the confining water and the rubber sleeve, which are indistinguishable in the display since they are both below a CT number of 700. Figure 51 and Figure 53 are the same slice, but with different display ranges. The display range of 0 to 2200 in Figure 53 shows a color distinction between confining water and the core holder rubber sleeve.

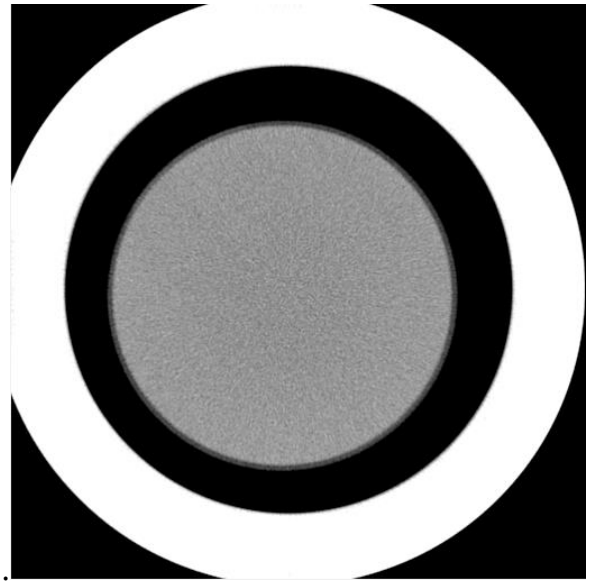

Figure 51: Unprocessed CT image with display range of 700 to 2100

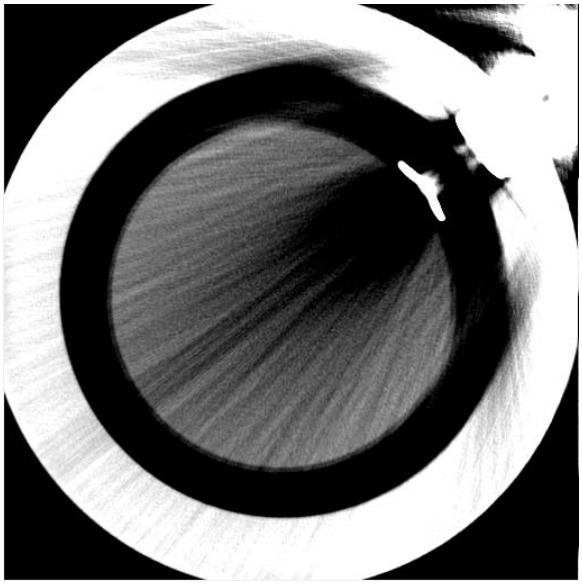

Figure 52: Unprocessed CT image with pressure tap interference

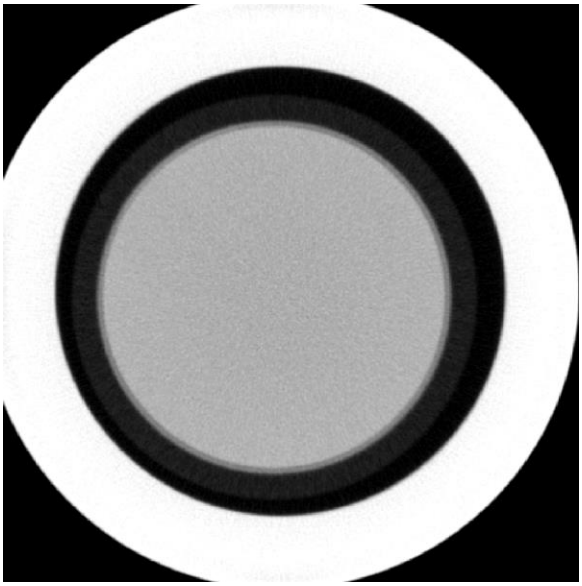

Figure 53: Unprocessed CT image with display range of 0 to 2200

MATLAB is used to cut a circle that transcribes the core at each slice, keeping the data inside the circle and making everything outside the circle zero. This is repeated for all slices in the scan, then values in each slice are averaged together. This results in a 2D array for each slice, and another 1D vector that contains the averages of each slice in that scan. The following calibration and calculations are adapted from an internal communication document by Dr. DiCarlo (DiCarlo, 2019). As core porosity was previously calculated when saturating, the following equation is used to get the attenuation constant difference between experimental brine and air:

$$a_{brine} - a_{air} = \frac{1}{N\bar{\phi}} \sum_{z=1}^{N} \left[CT_{brine\ saturated}(z) - CT_{air\ filled}(z) \right]$$

The attenuation constant difference between 2% NaCl brine and air was calculated to be between 800 and 900 in these experiments. It is then used to calculate average slice porosity:

$$\phi(z) = \frac{CT_{brine}(z) - CT_{air}(z)}{a_{brine} - a_{air}}$$

The average porosity of each voxel within the slice is similarly calculated:

$$\phi(x,y) = \frac{CT_{brine}(x,y) - CT_{air}(x,y)}{a_{brine} - a_{air}}$$

As the volume of CO_2 pumped into the core is being recorded, the average saturation of CO_2 and brine inside the core is known at any given point before breakthrough, t1. The attenuation constant difference between brine and CO_2 is thus calculated using a scan before breakthrough:

$$a_{brine} - a_{\mathrm{CO_2}} = \frac{1}{N\bar{\phi}} \cdot \frac{1}{(1 - \overline{S_w})}\Big|_{t=t1} \sum_{z=1}^{N} [CT_{brine\ saturated}(z) - CT_{t=t1}(z)]$$

The attenuation constant difference between 2% NaCl brine and liquid CO_2 was calculated to be between 200 and 250 in these experiments. It is then used to calculate average slice saturation for all scans:

$$S_{CO_2}(z)\big|_t = \frac{CT_{brine\ saturated}(z) - CT_t(z)}{\left(a_{brine} - a_{\mathrm{CO_2}}\right) \cdot \phi(z)}$$

The saturation for each voxel within the slice is similarly calculated:

$$S_{CO_2}(x,y)\big|_t = \frac{CT_{brine\ saturated}(x,y) - CT_t(x,y)}{\left(a_{brine} - a_{\mathrm{CO_2}}\right) \cdot \phi(x,y)}$$

The arrays obtained will have a “salt and pepper” noise effect. A 2D median filter is applied to smoothen the values before graphing.

APPENDIX 2: ADDITIONAL EXPERIMENTAL RESULTS

A2.1: Saturations

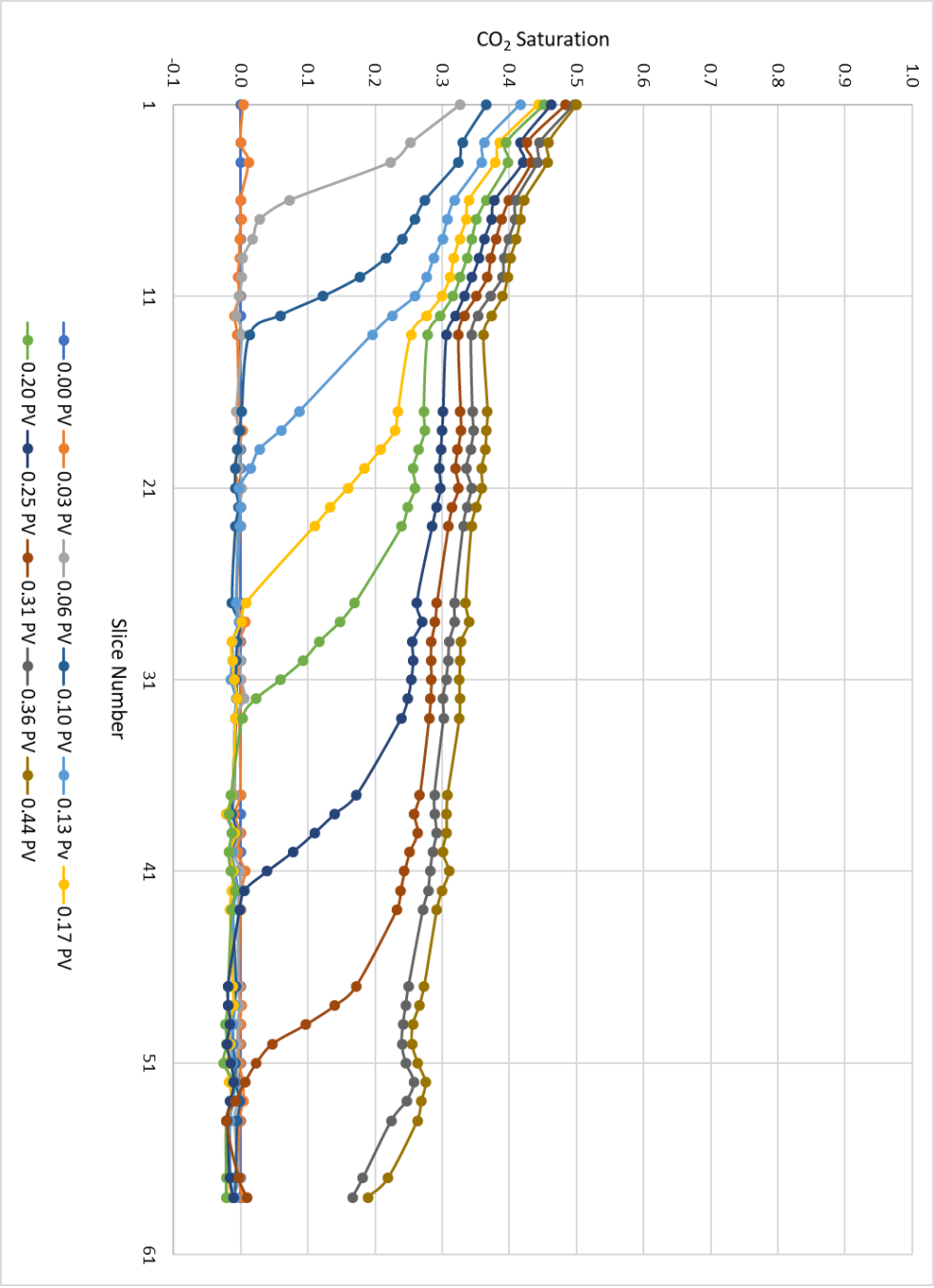

Figure 54: Experiment #3 flood #2 saturation profiles without nanoparticles

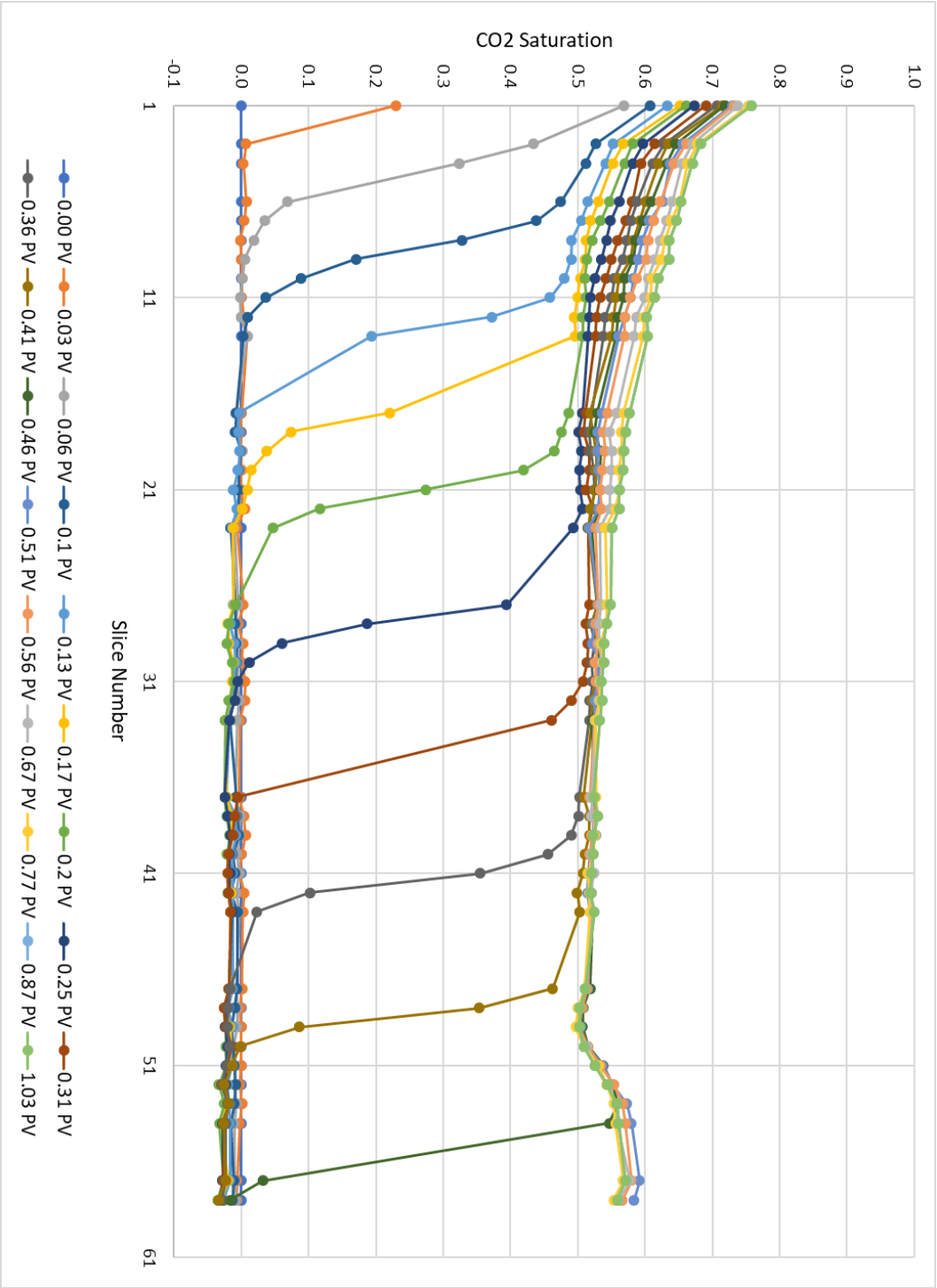

Figure 55: Experiment #3 flood #3 saturation profiles with nanoparticles

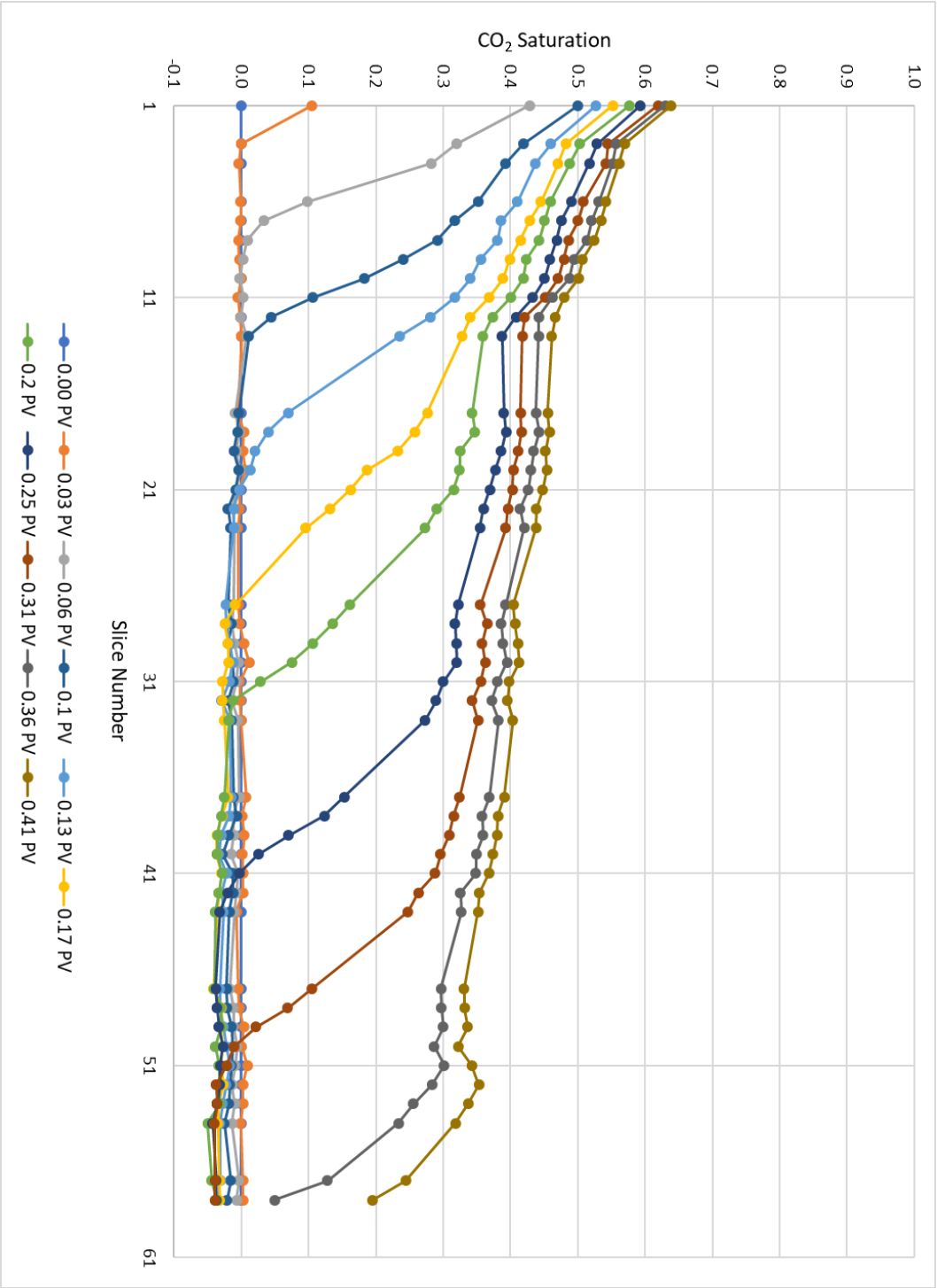

Figure 56: Experiment #3 flood #4 saturation profiles flushed with brine

A2.2: Pressures

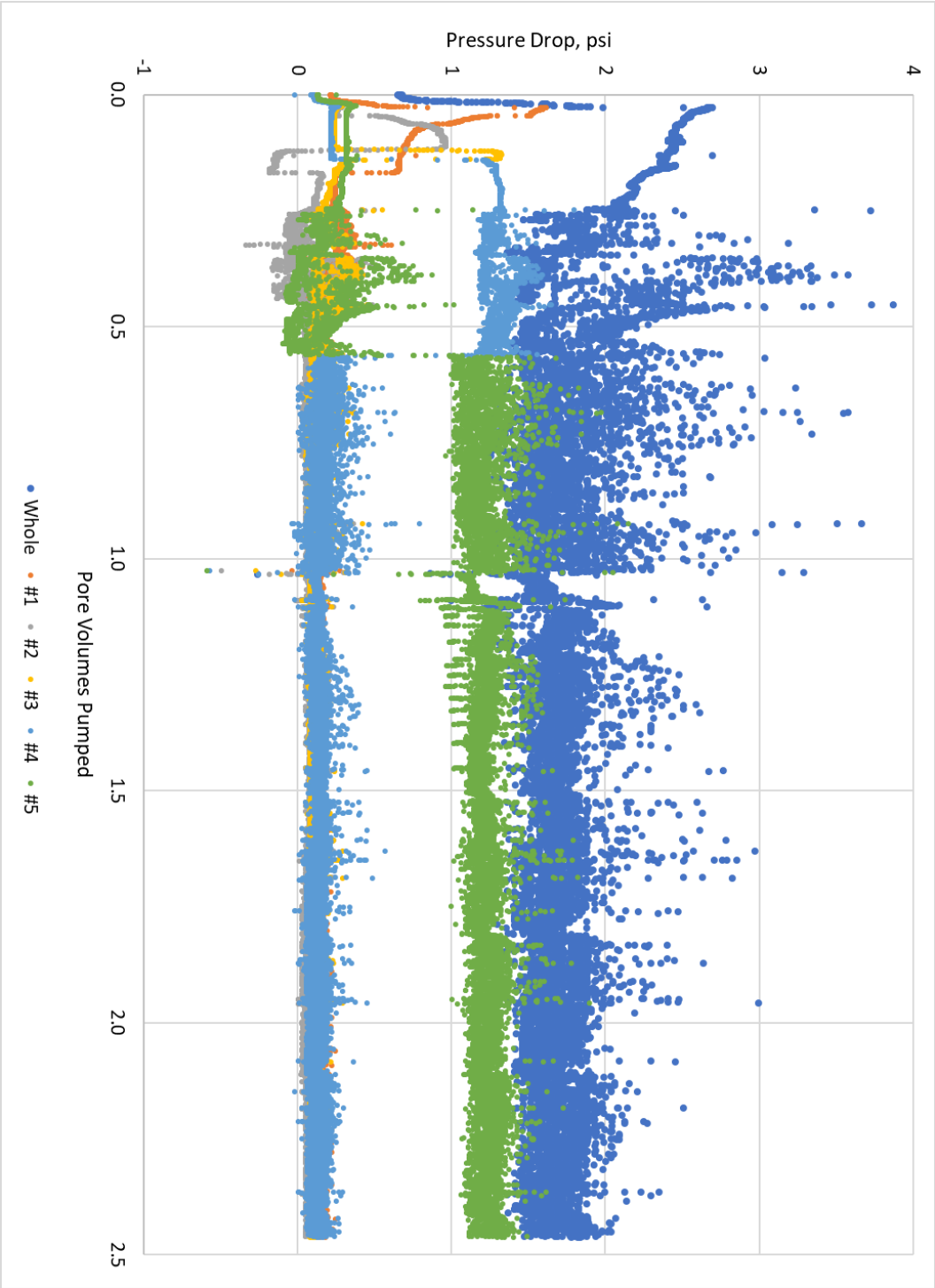

Figure 57: Core #1 flood #1 pressure drops without nanoparticles

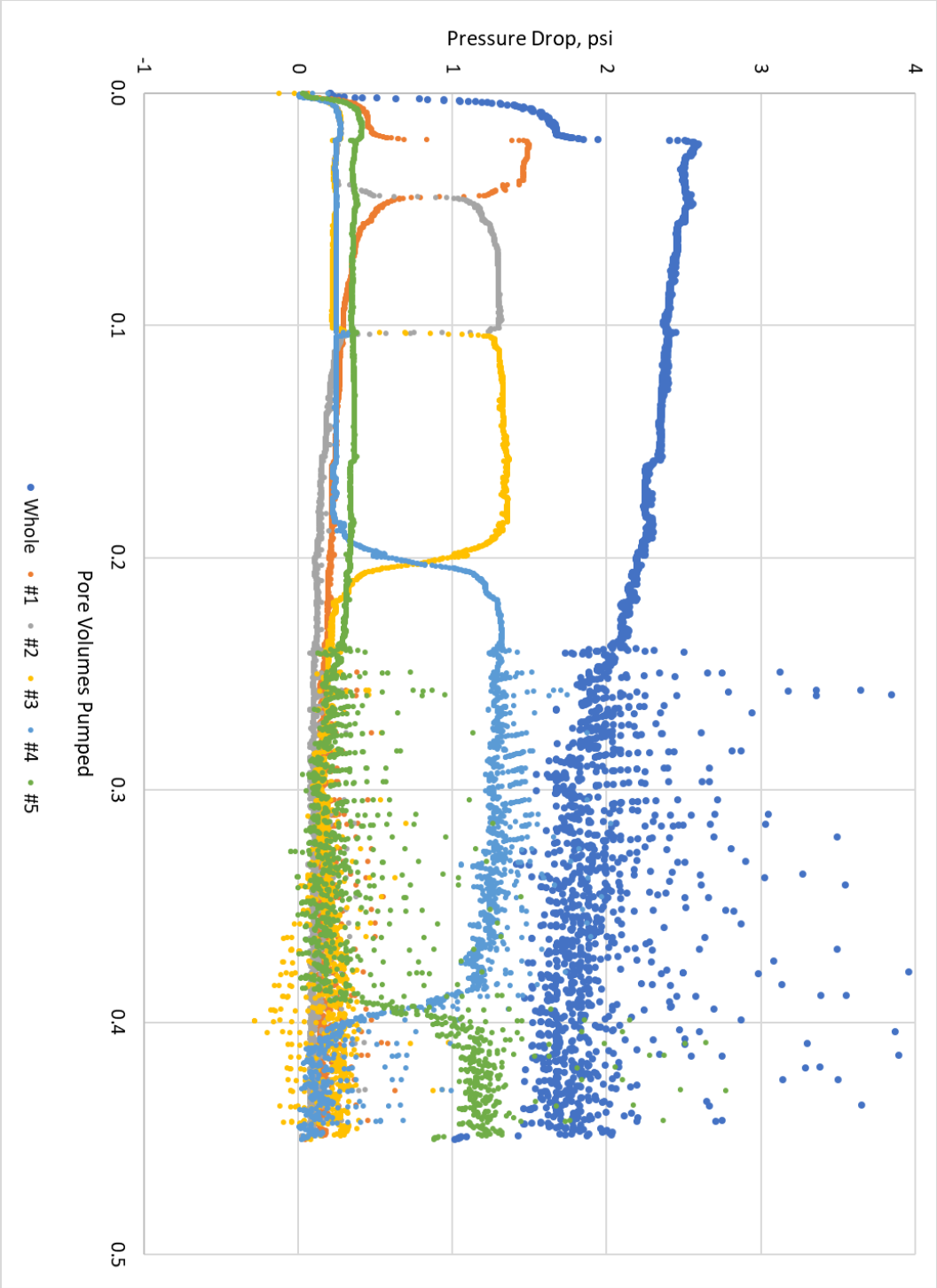

Figure 58: Core #1 flood #2 pressure drops without nanoparticles

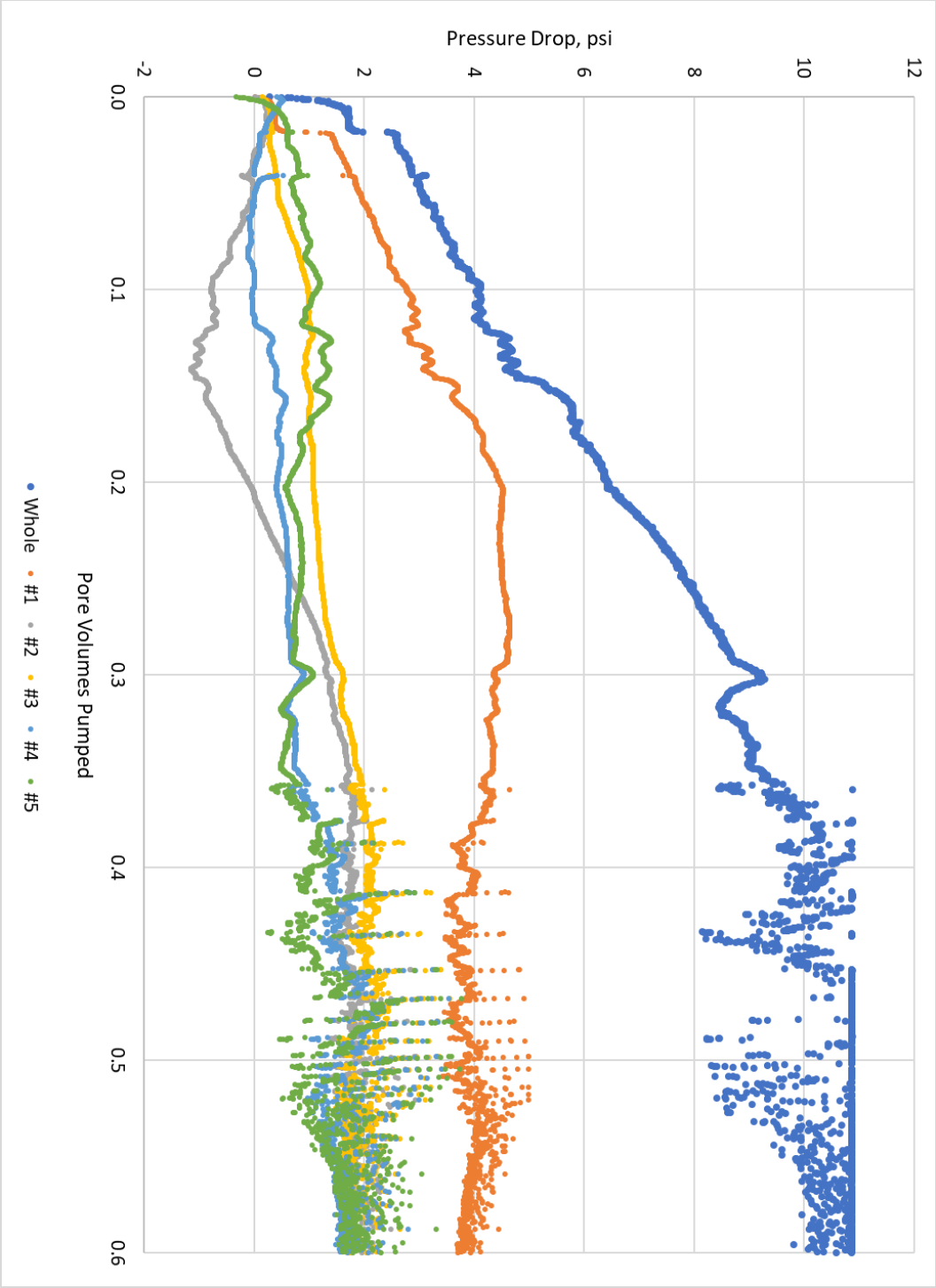

Figure 59: Core #1 flood #3 pressure drops with nanoparticles

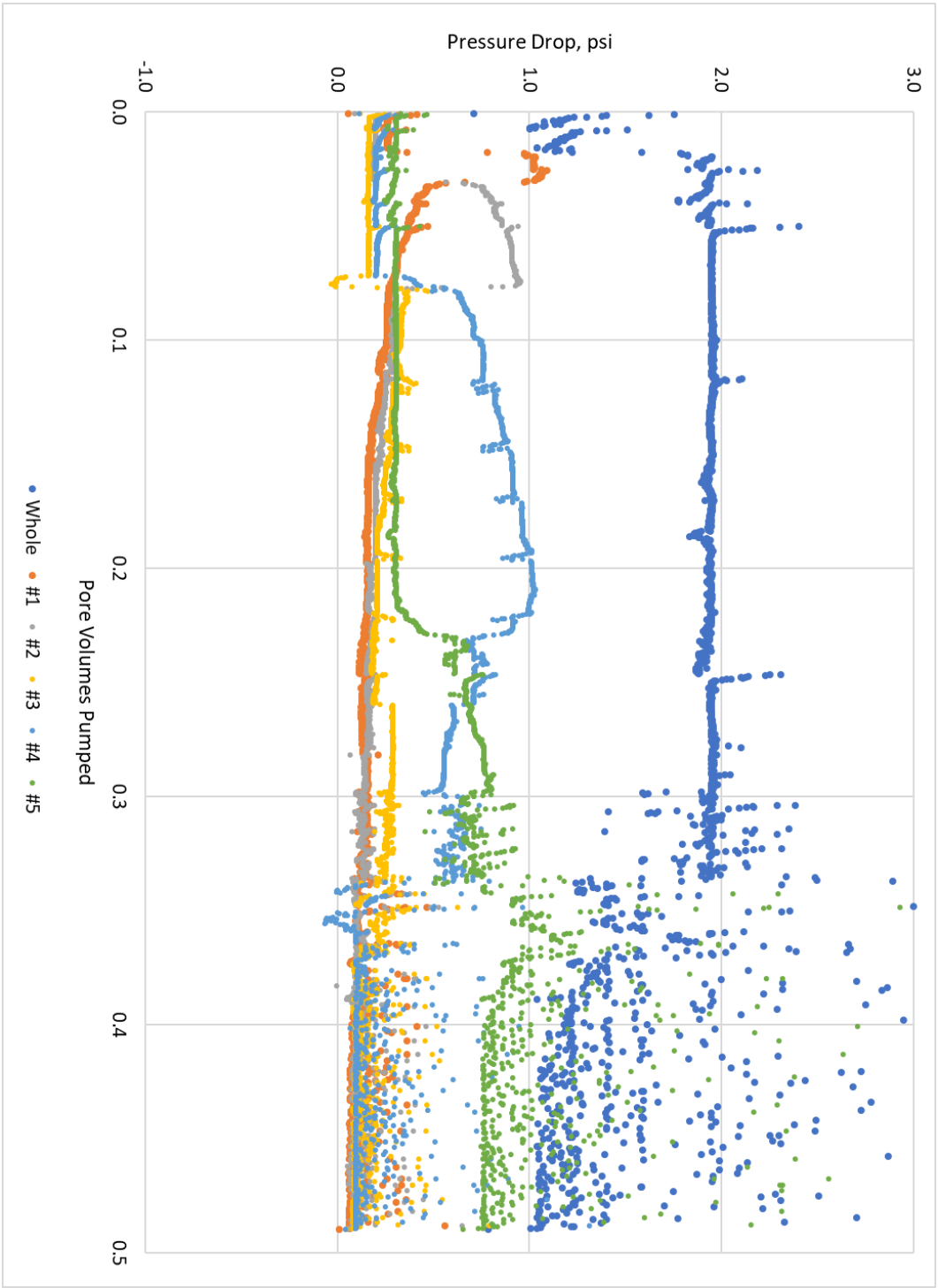

Figure 60: Core #2 flood #1 pressure drops without nanoparticles

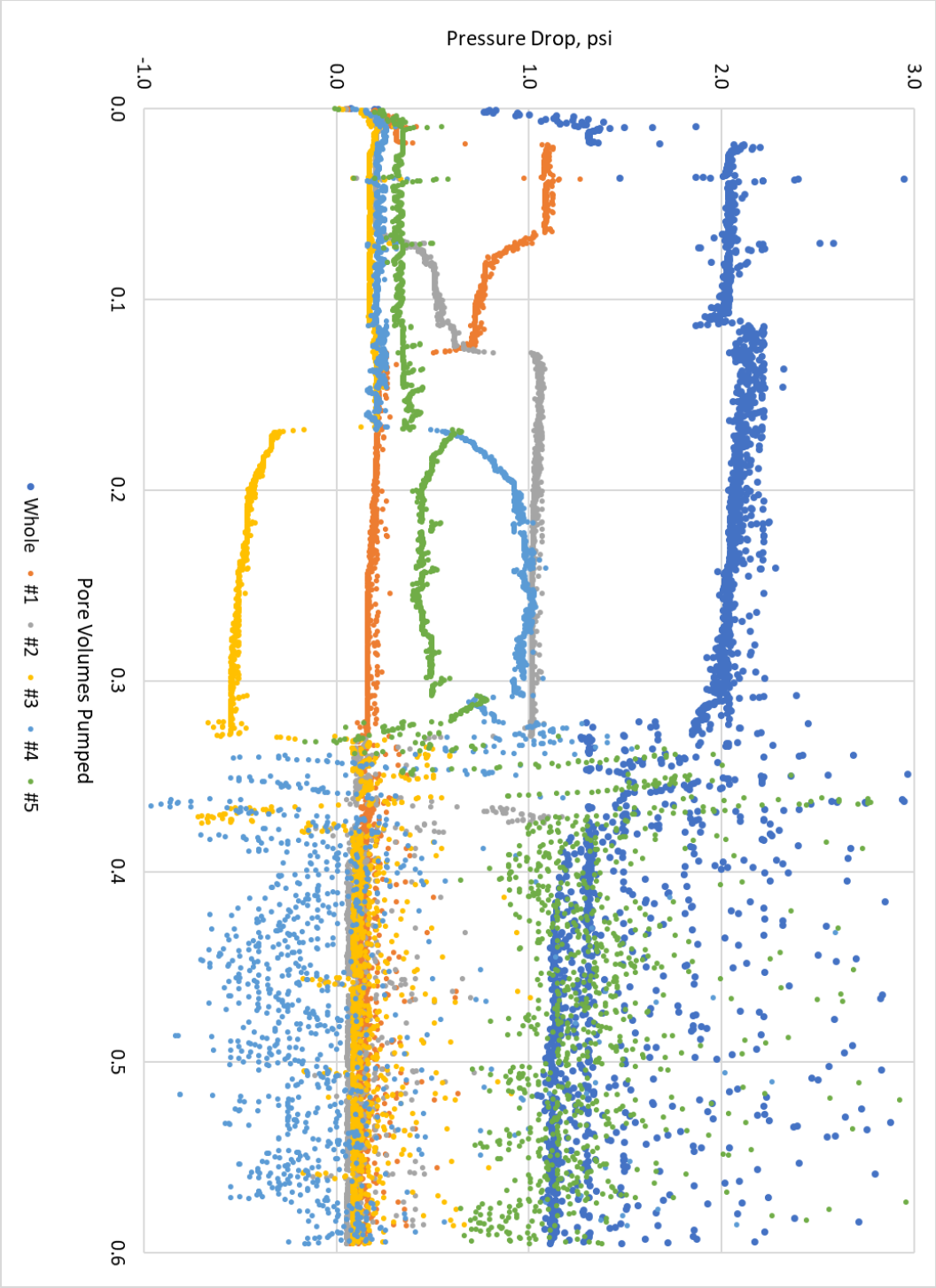

Figure 61: Core #2 flood #2 pressure drops without nanoparticles

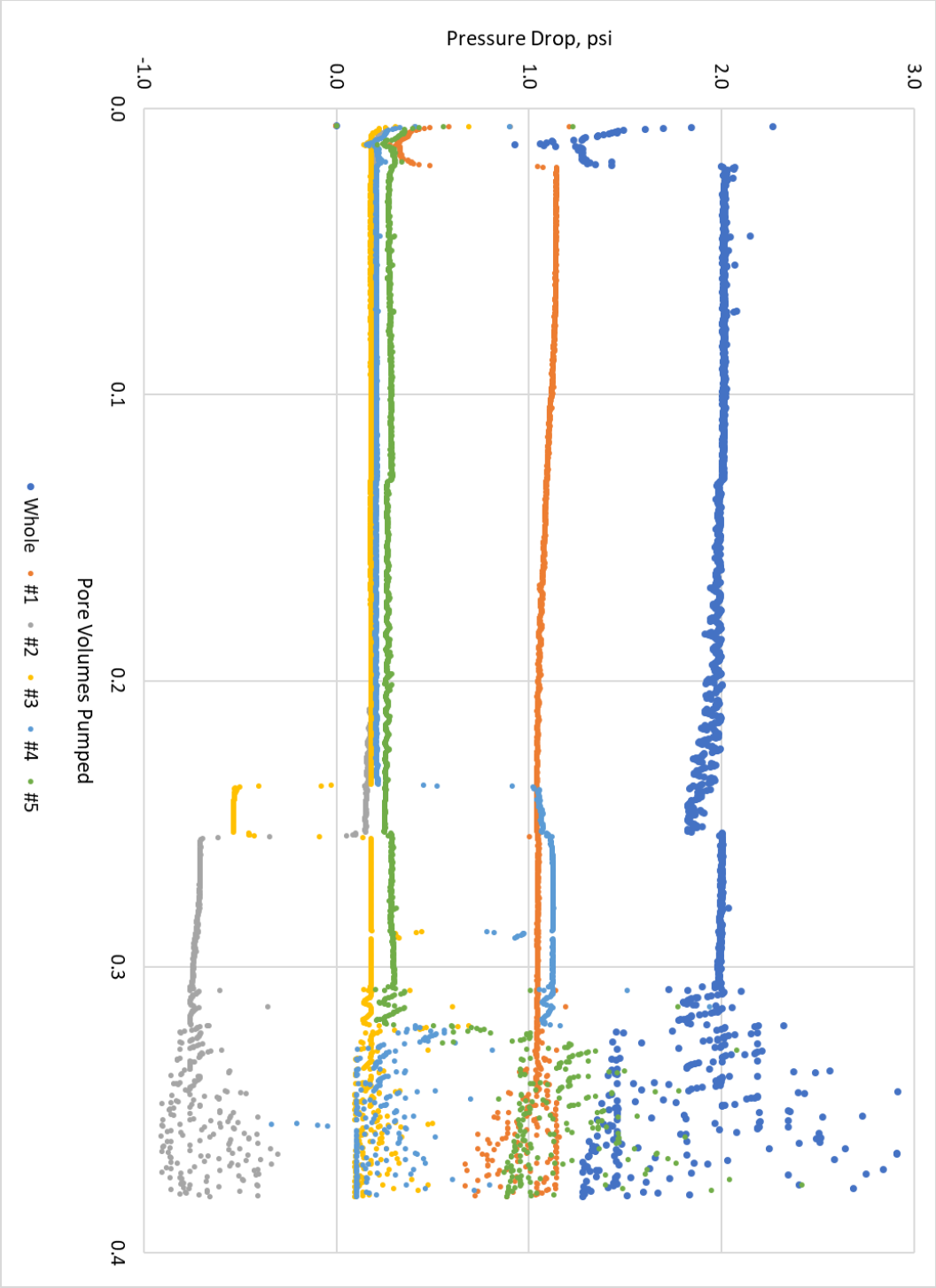

Figure 62: Core #2 flood #3 pressure drops without nanoparticles

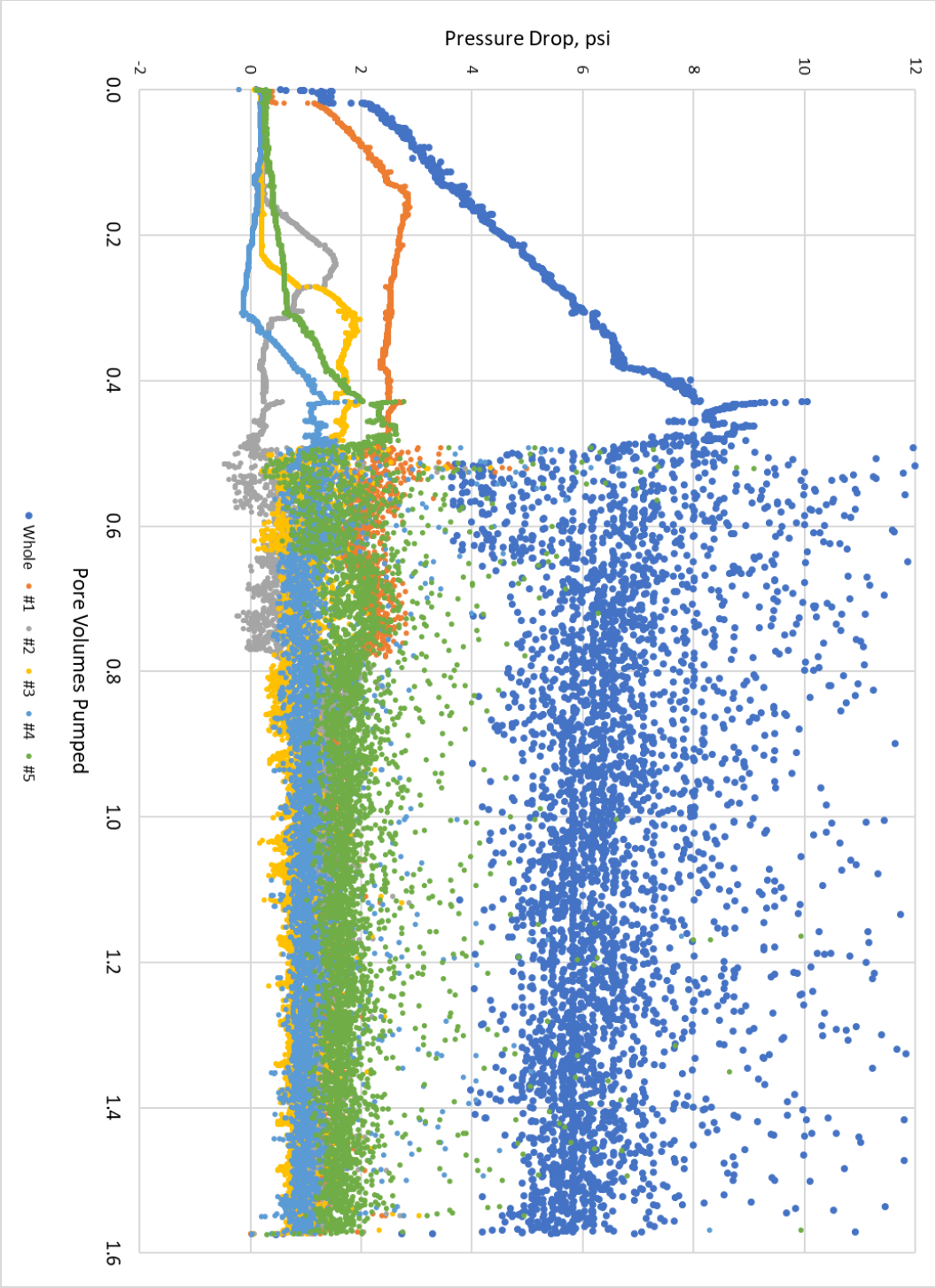

Figure 63: Core #2 flood #4 pressure drops with nanoparticles

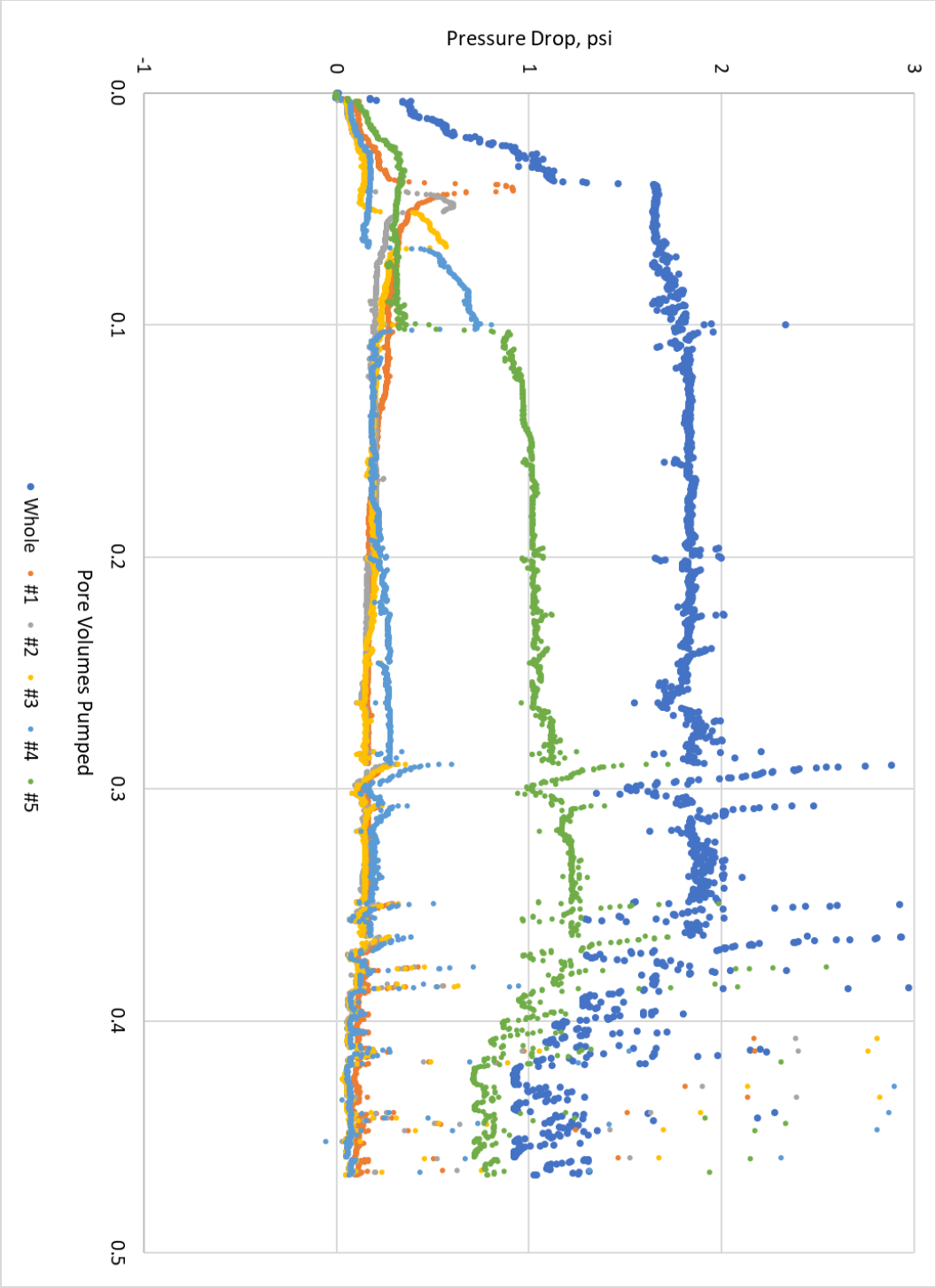

Figure 64: Core #3 flood #1 pressure drops without nanoparticles

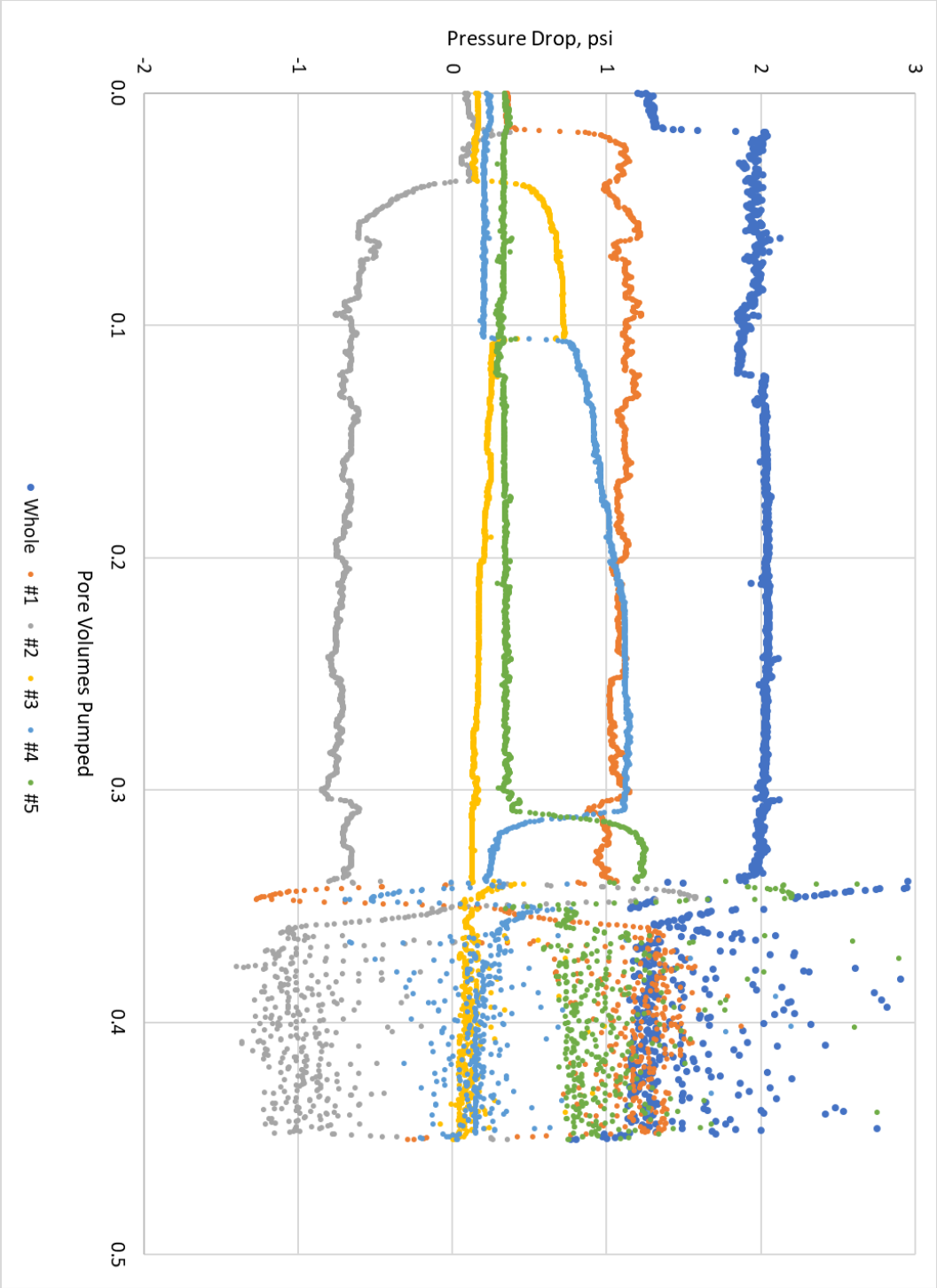

Figure 65: Core #3 flood #2 pressure drops without nanoparticles

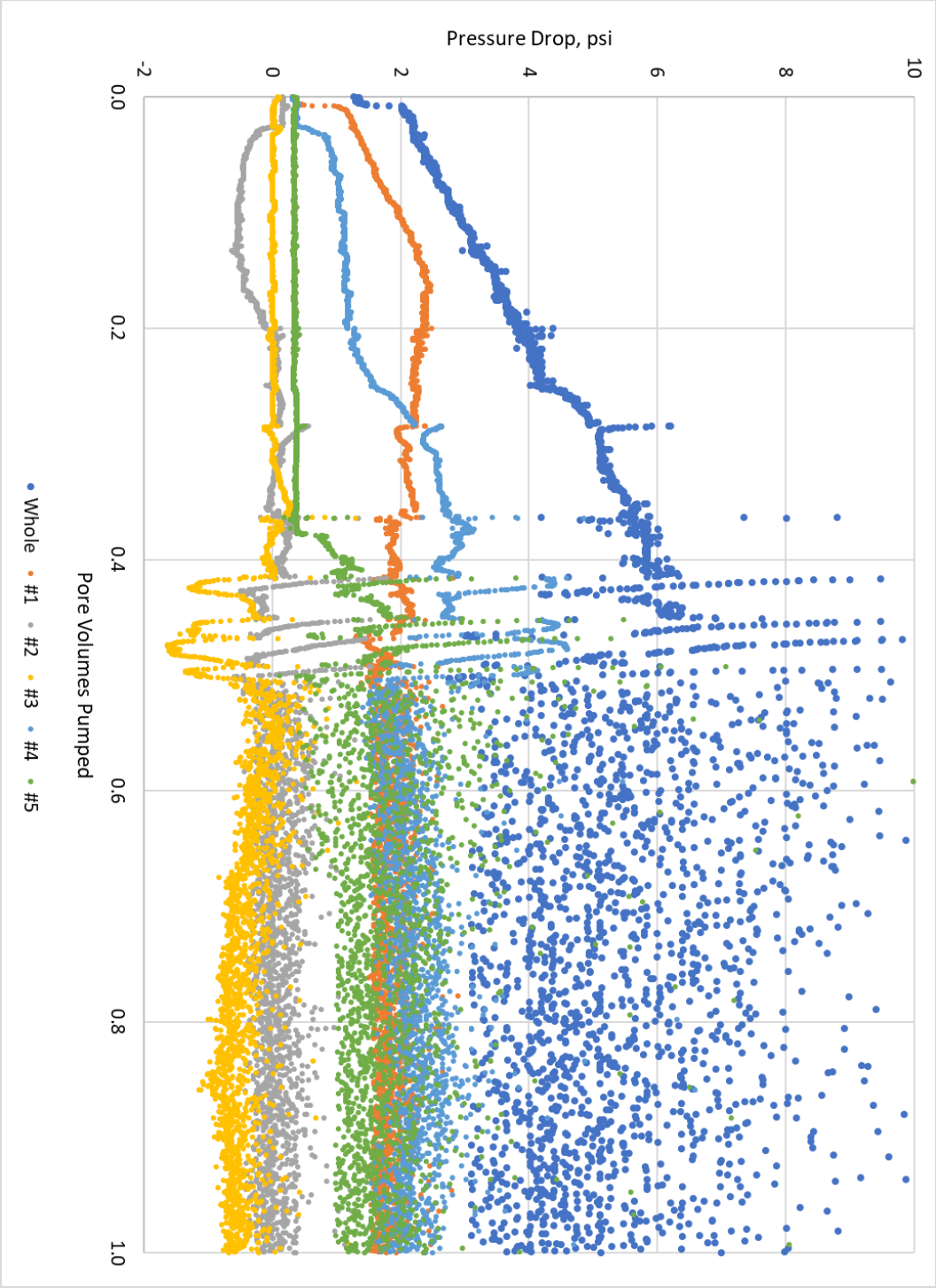

Figure 66: Core #3 flood #3 pressure drops with nanoparticles

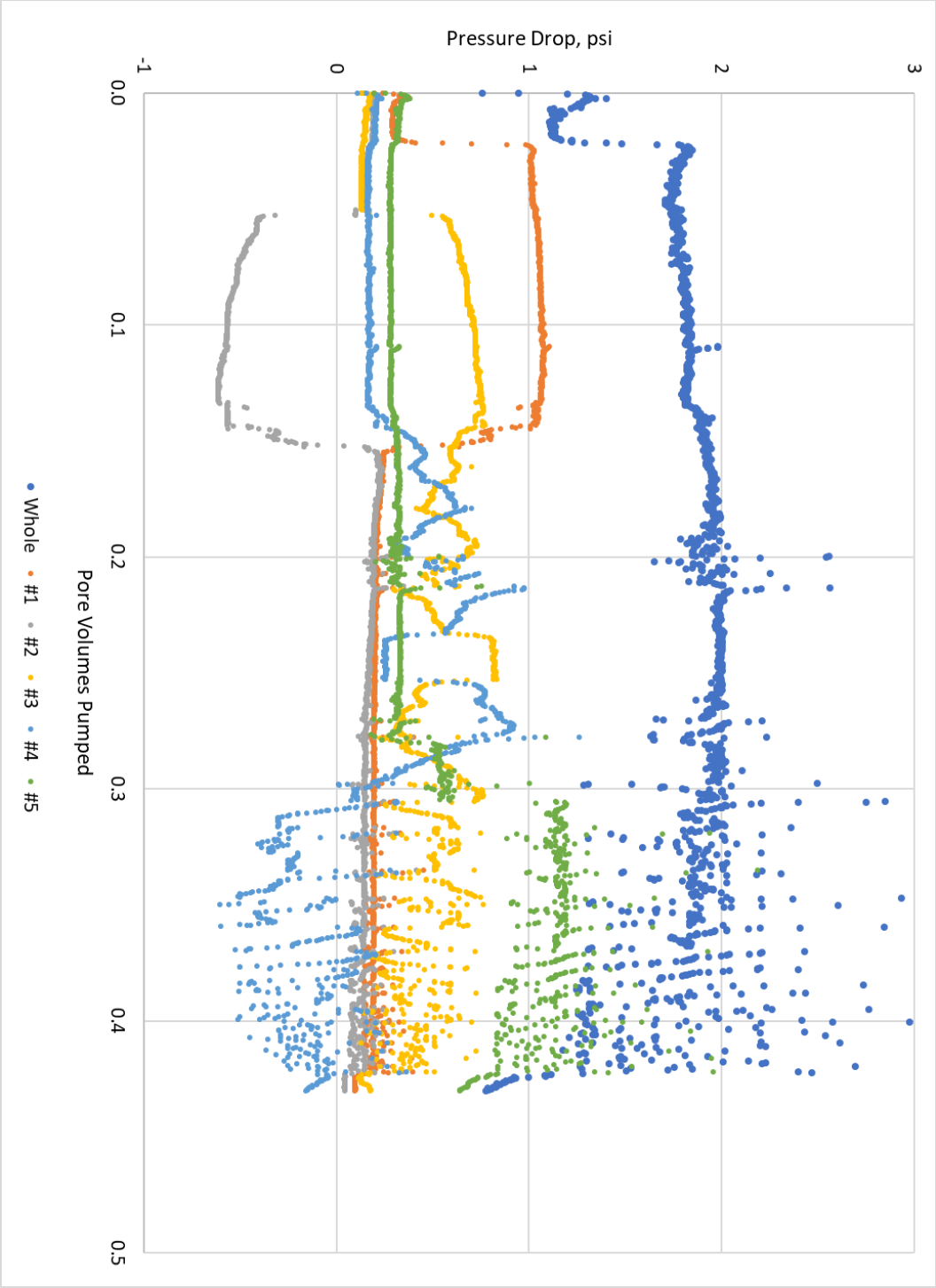

Figure 67: Core #3 flood #4 pressure drops post brine flush

A2.2: CO_2 Saturation Profiles

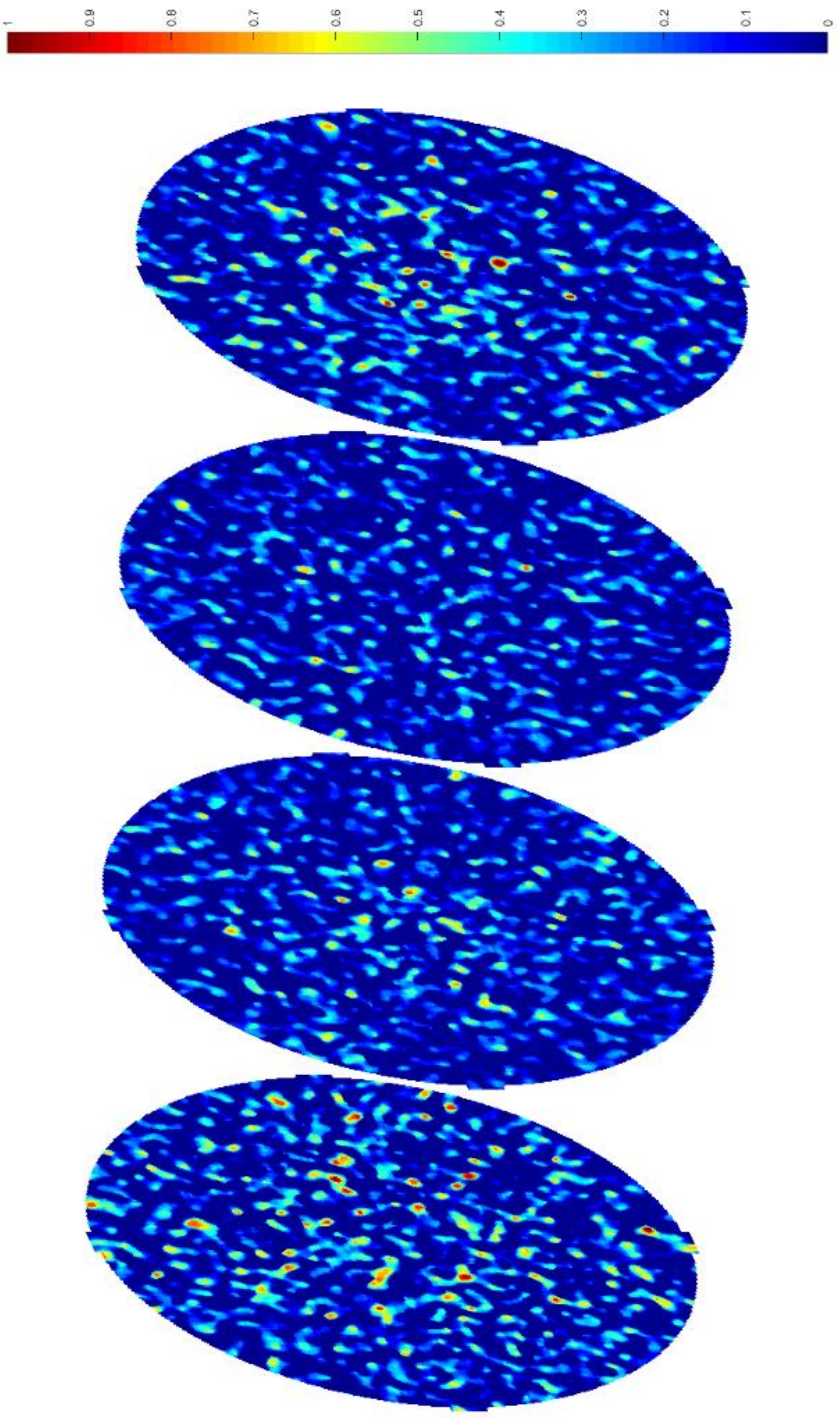

Figure 68: Core #3 flood #2 saturation at 0.03 pore volumes pumped

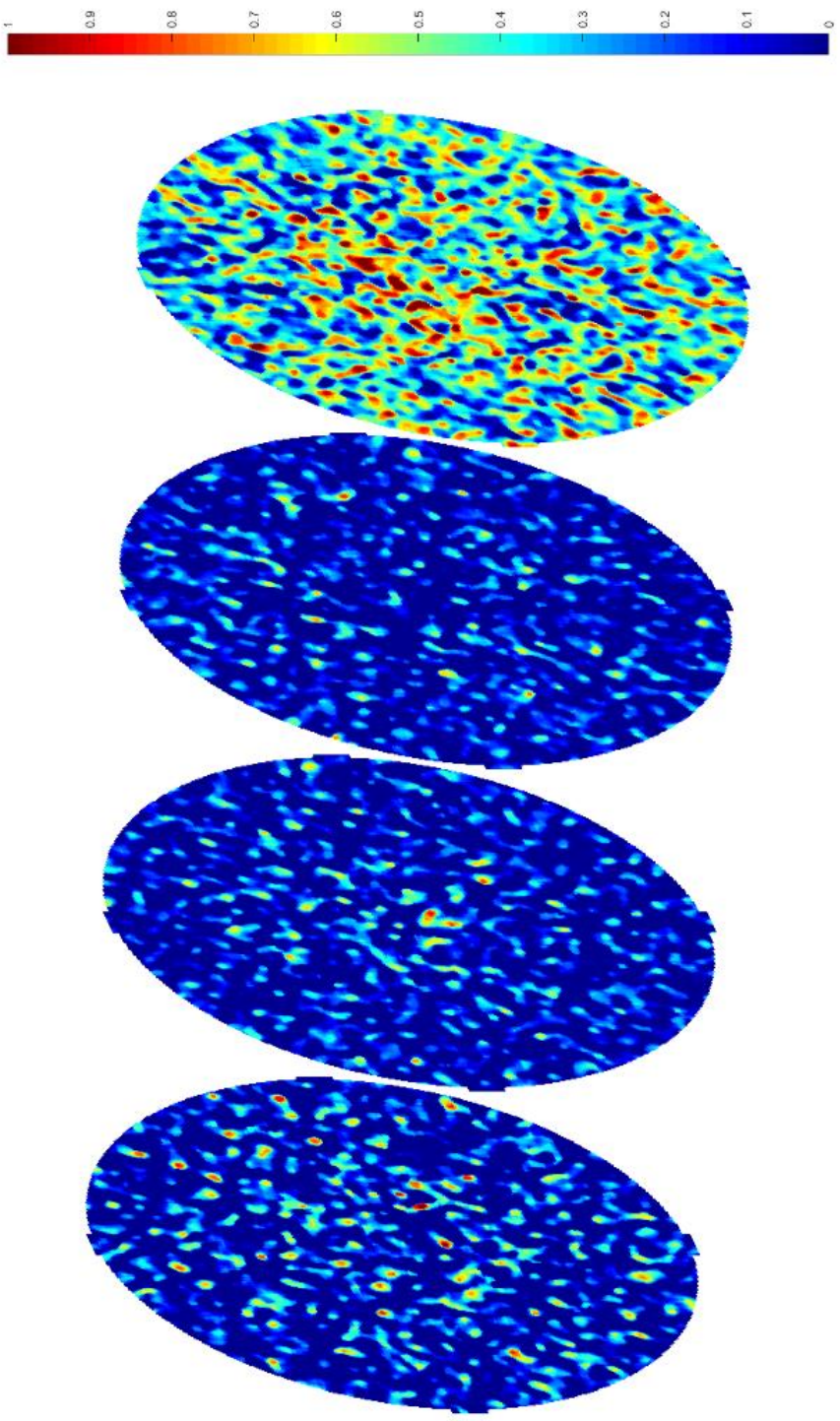

Figure 69: Core #3 flood #2 saturation at 0.06 pore volumes pumped

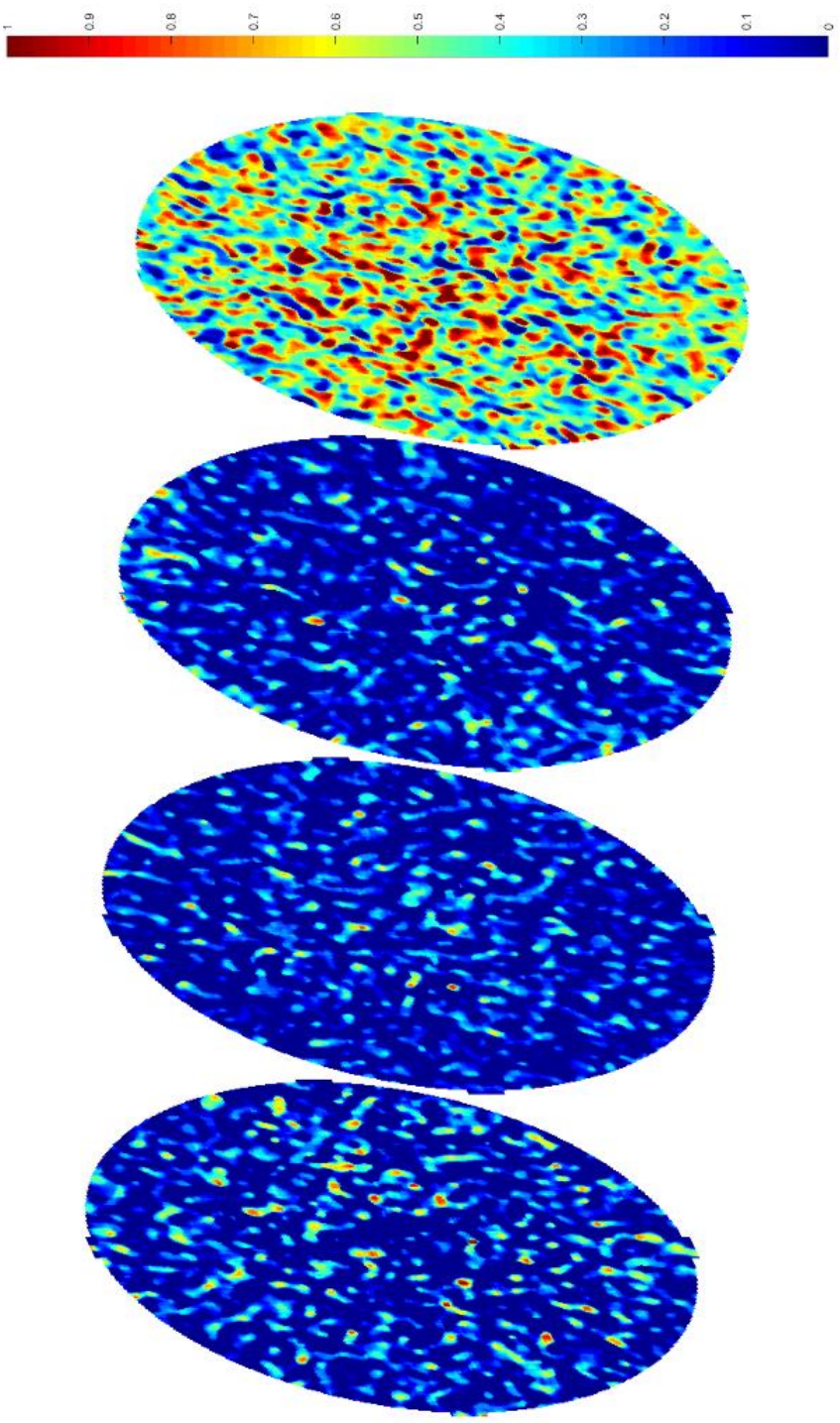

Figure 70: Core #3 flood #2 saturation at 0.13 pore volumes pumped

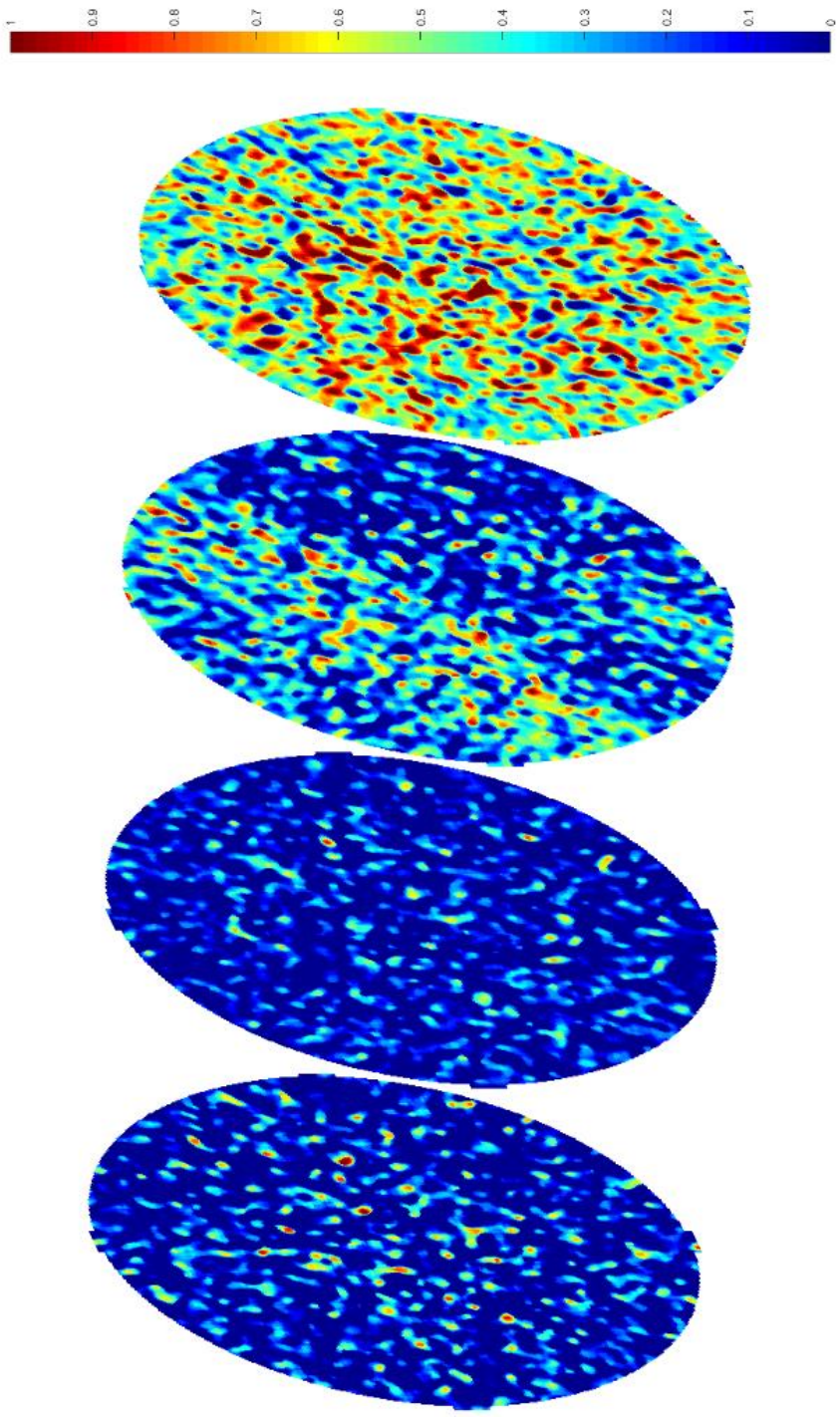

Figure 71: Core #3 flood #2 saturation at 0.17 pore volumes pumped

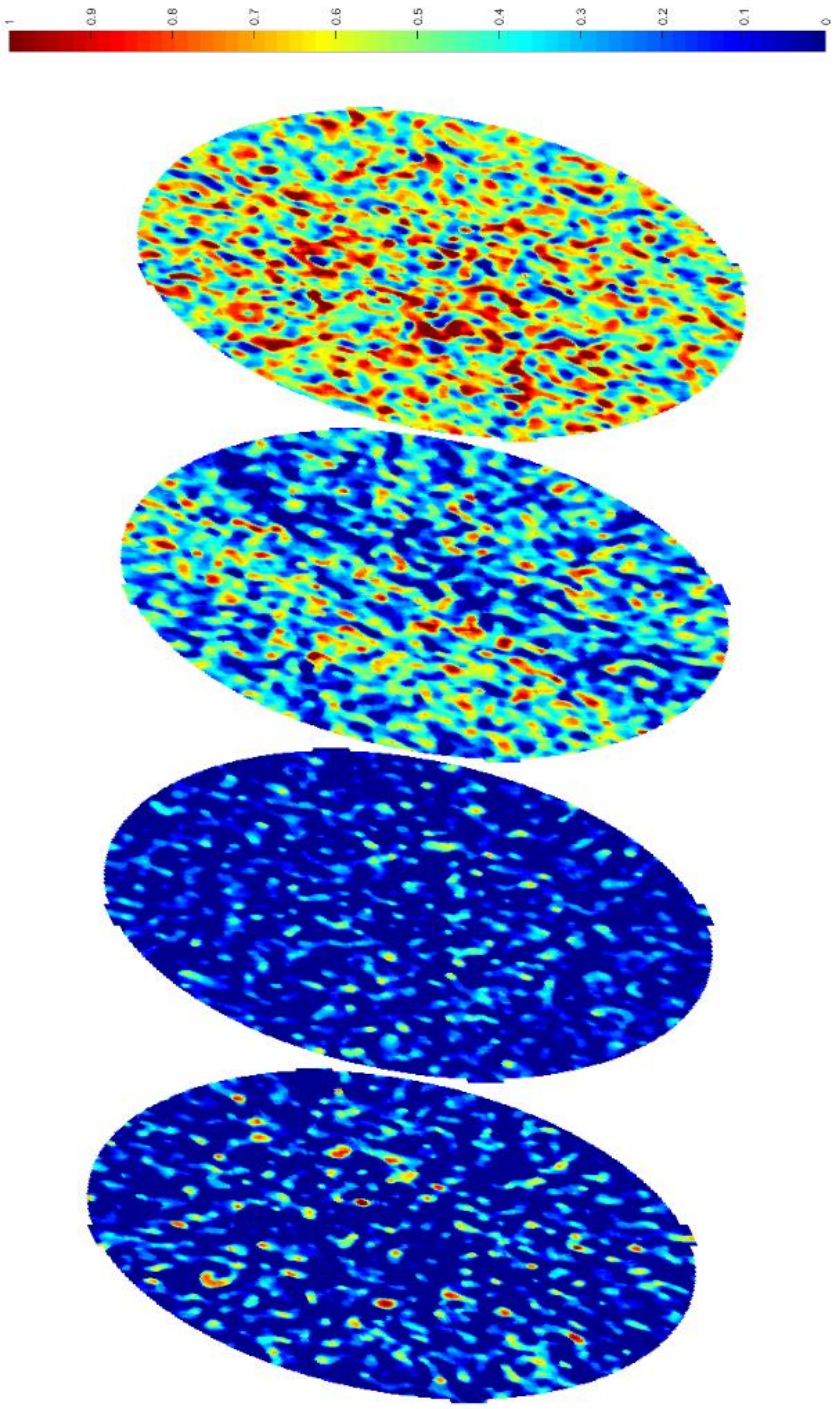

Figure 72: Core #3 flood #2 saturation at 0.20 pore volumes pumped

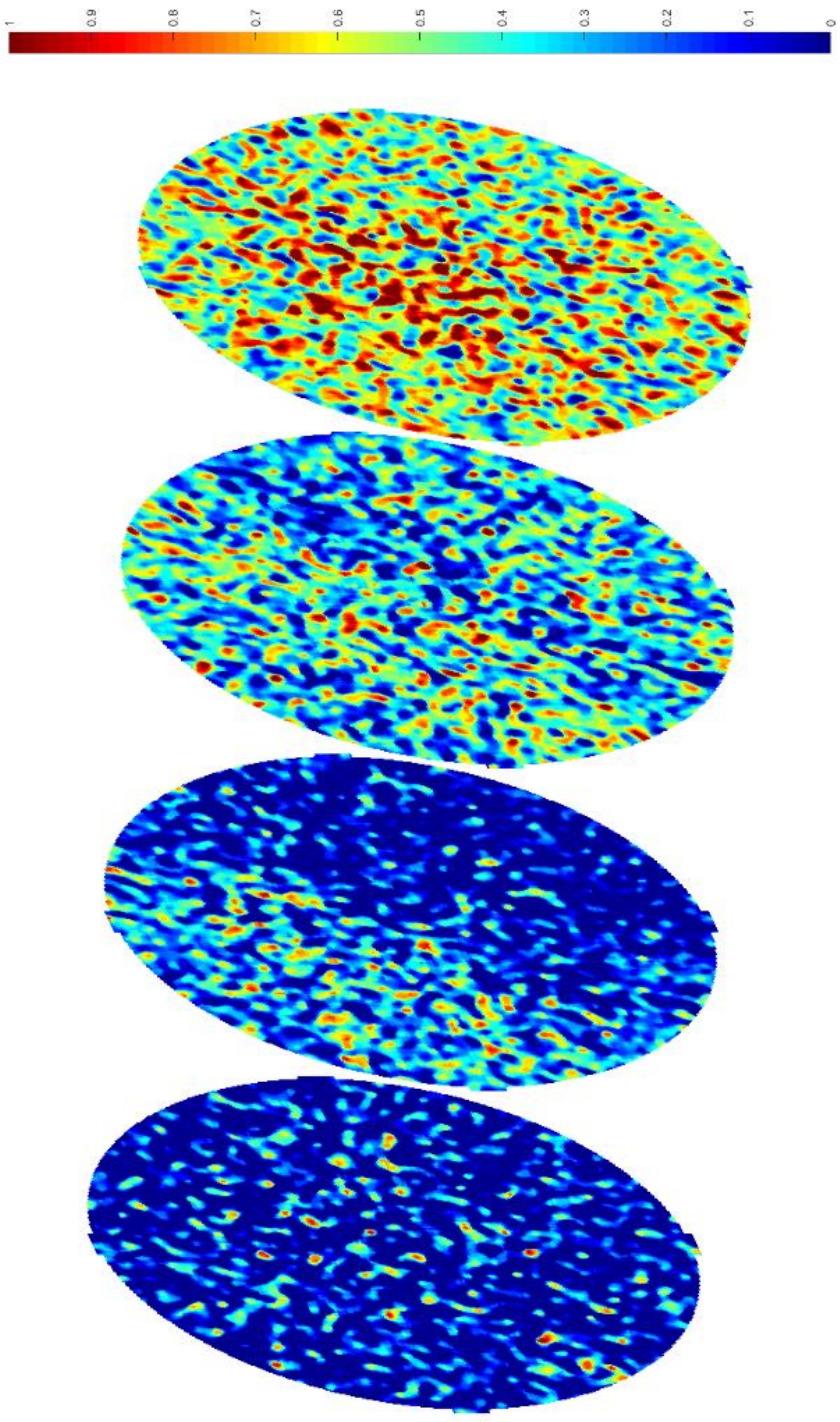

Figure 73: Core #3 flood #2 saturation at 0.25 pore volumes pumped

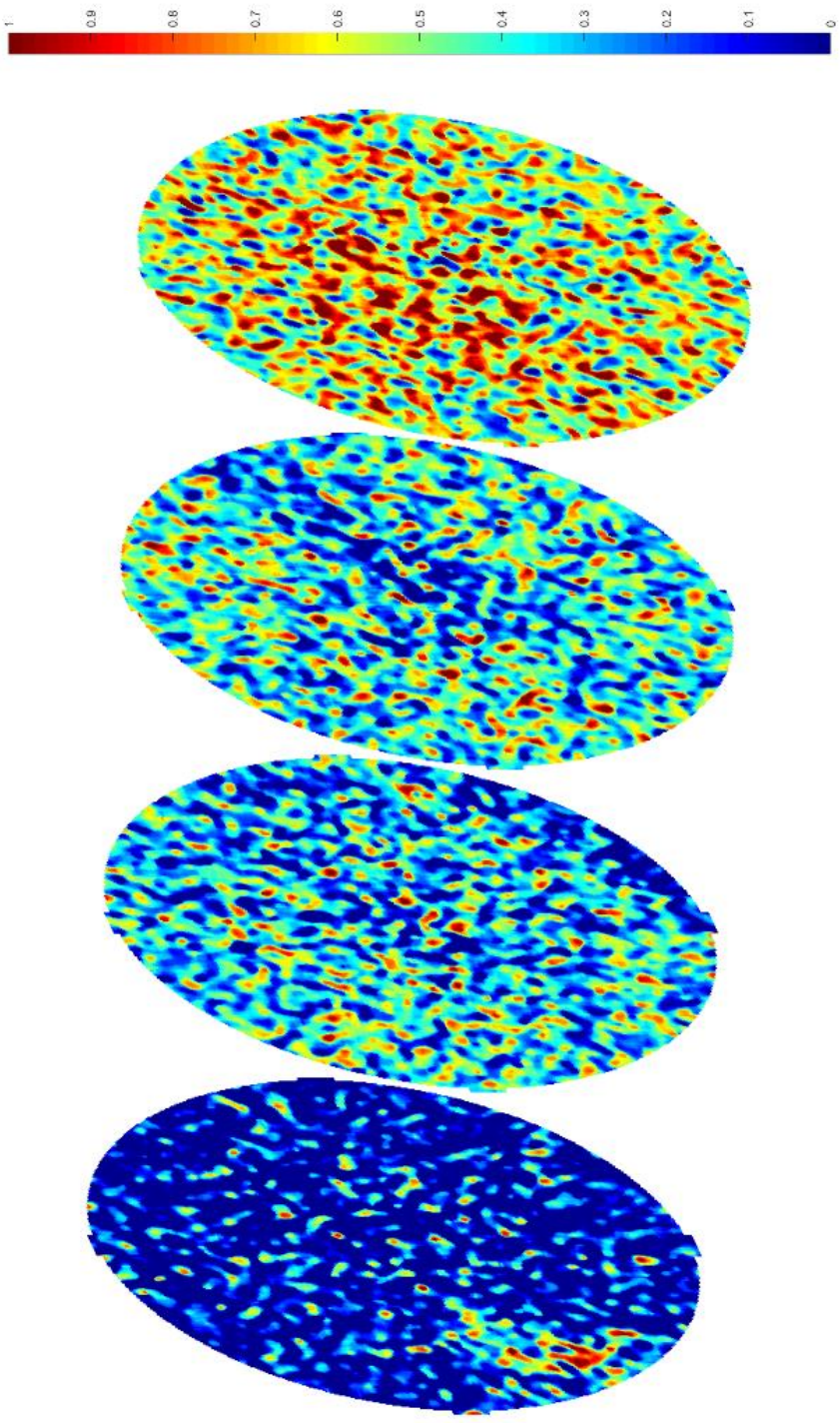

Figure 74: Core #3 flood #2 saturation at 0.31 pore volumes pumped

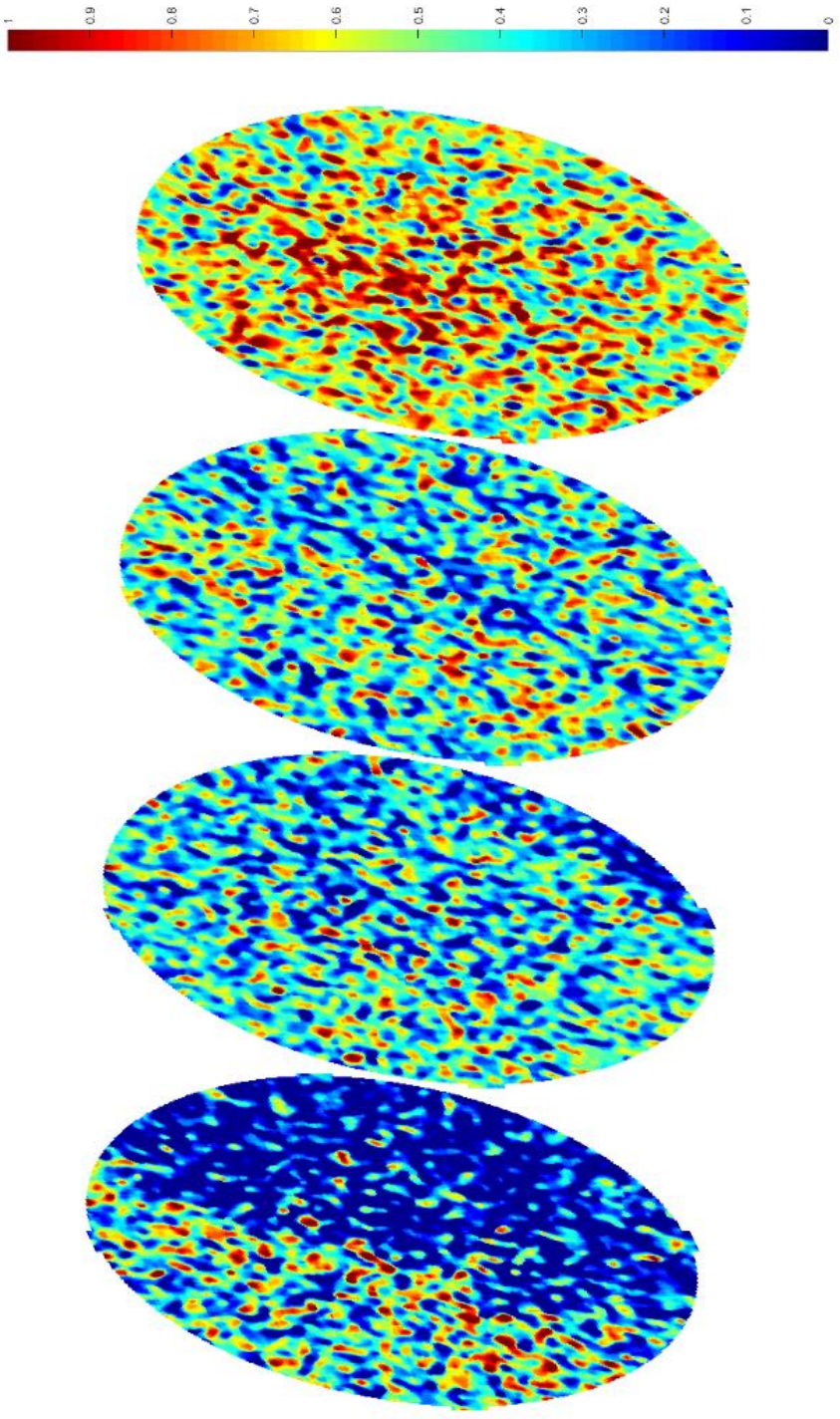

Figure 75: Core #3 flood #2 saturation at 0.36 pore volumes pumped

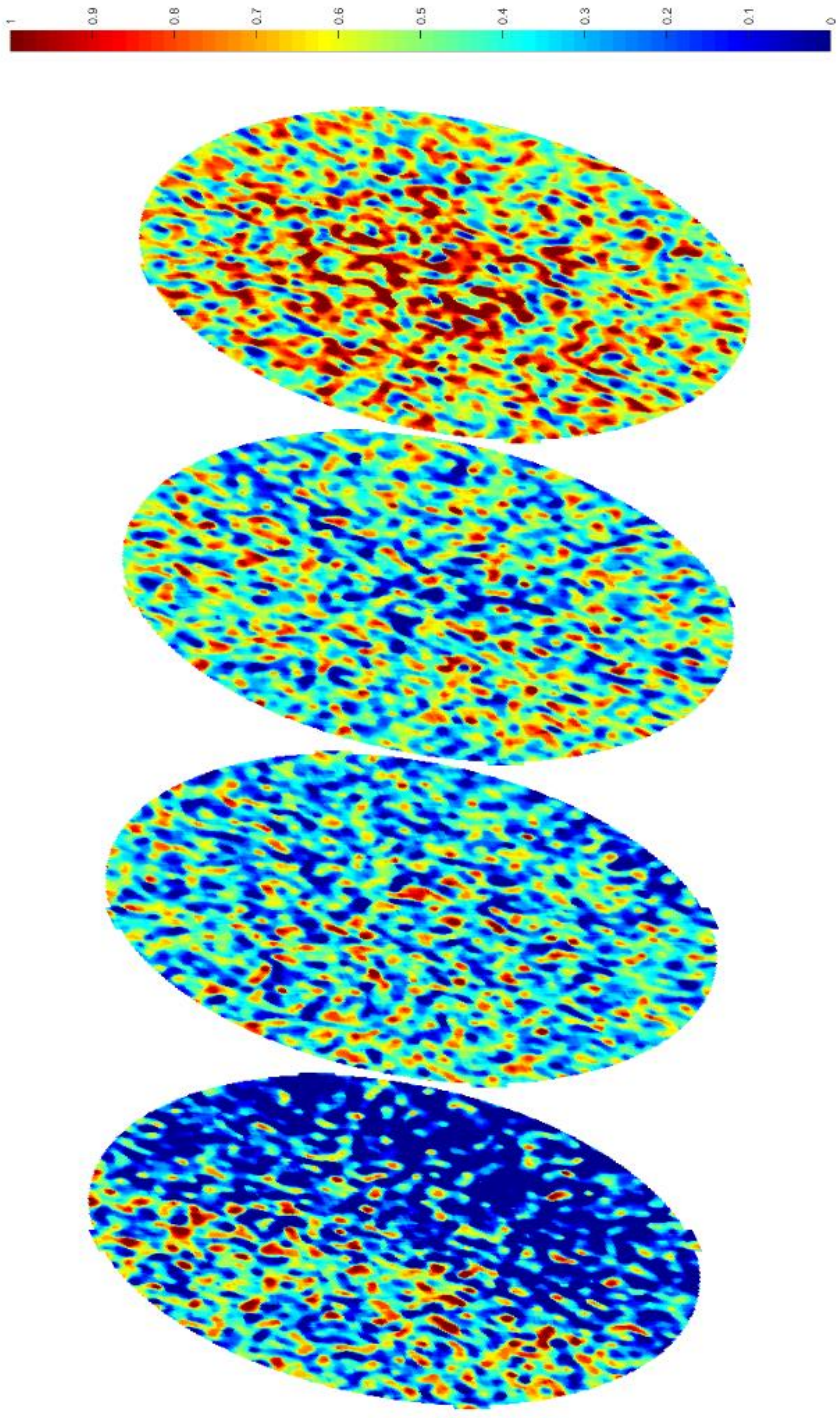

Figure 76: Core #3 flood #2 saturation at 0.44 pore volumes pumped

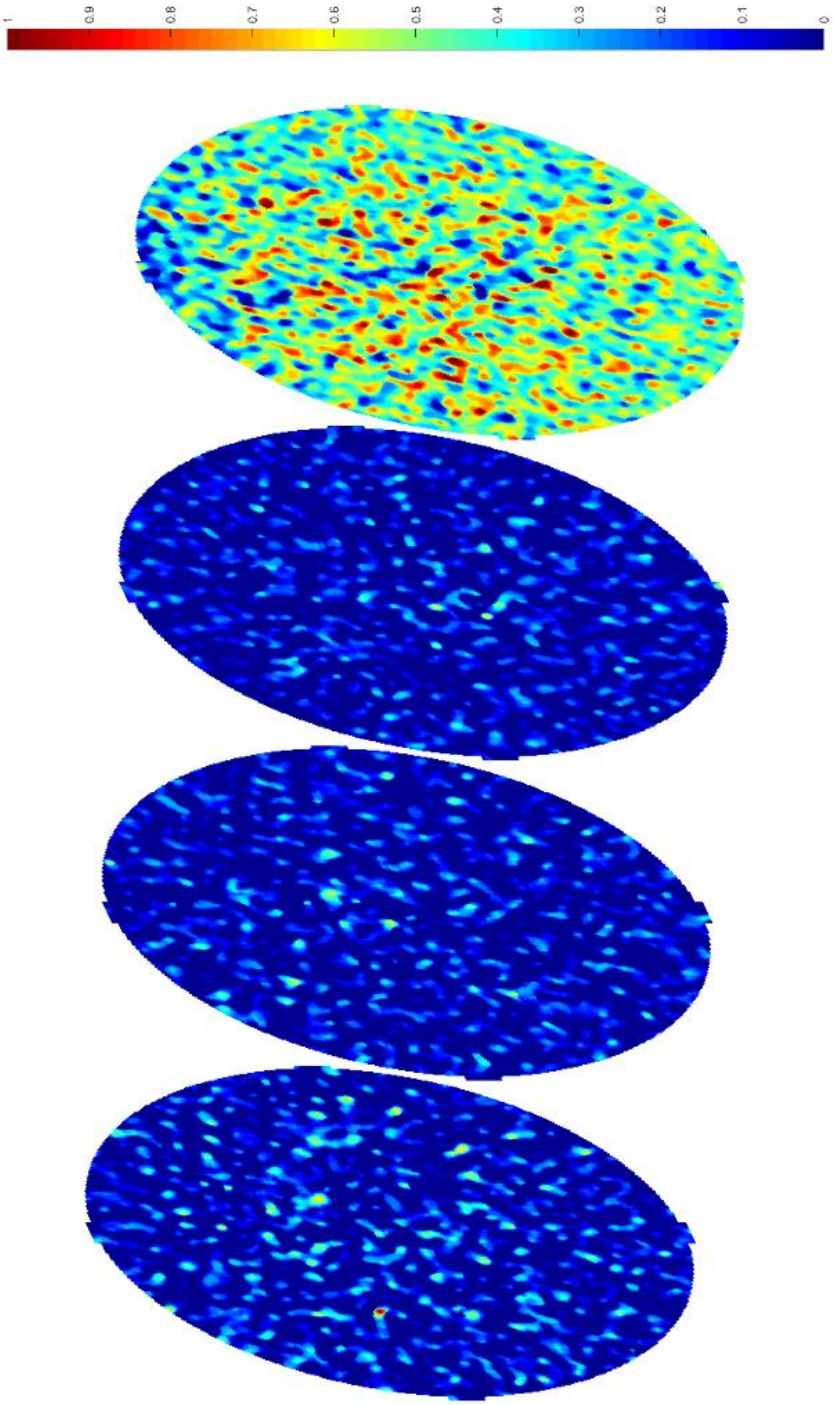

Figure 77: Core #3 flood #3 saturation at 0.03 pore volumes pumped

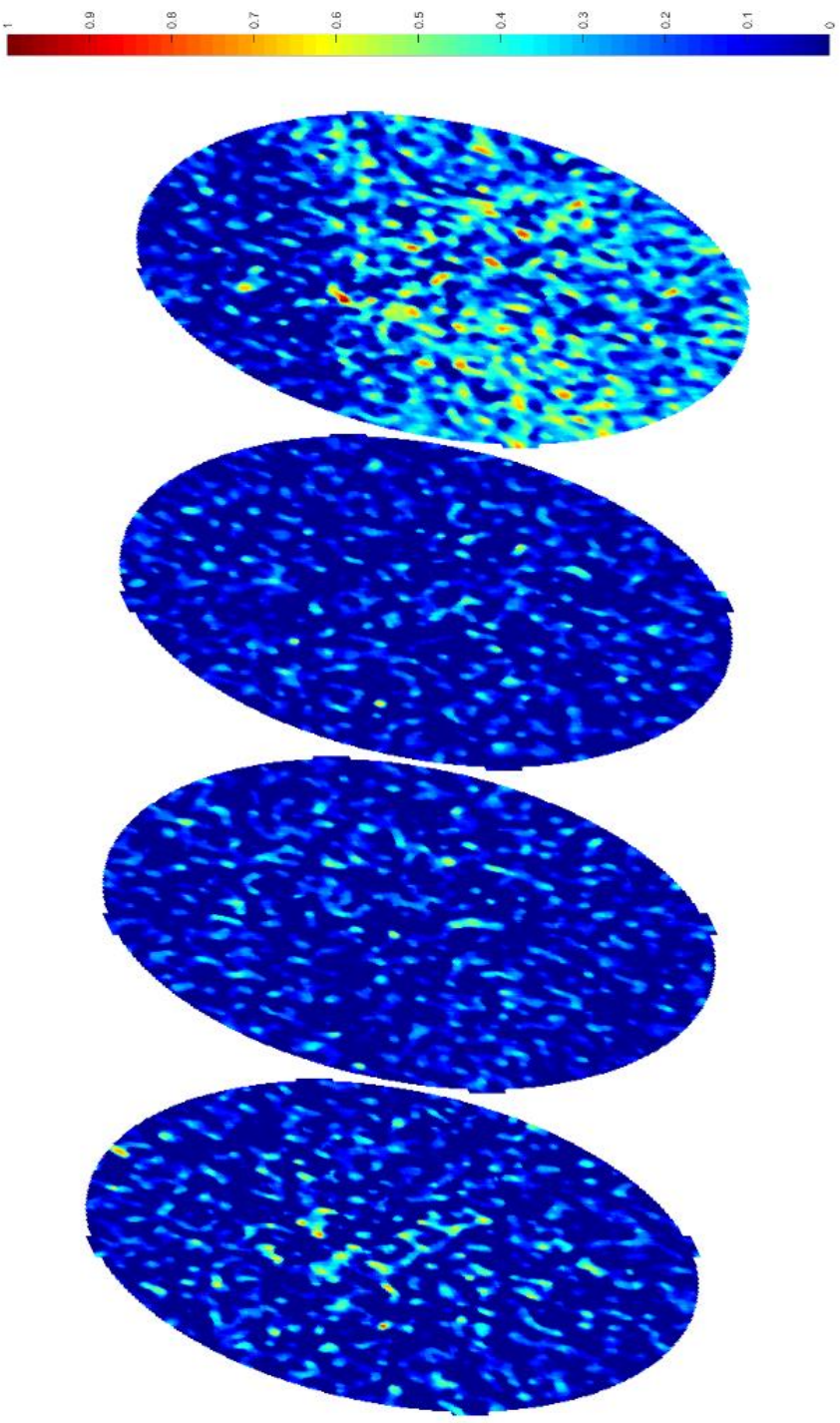

Figure 78: Core #3 flood #2 saturation at 0.06 pore volumes pumped

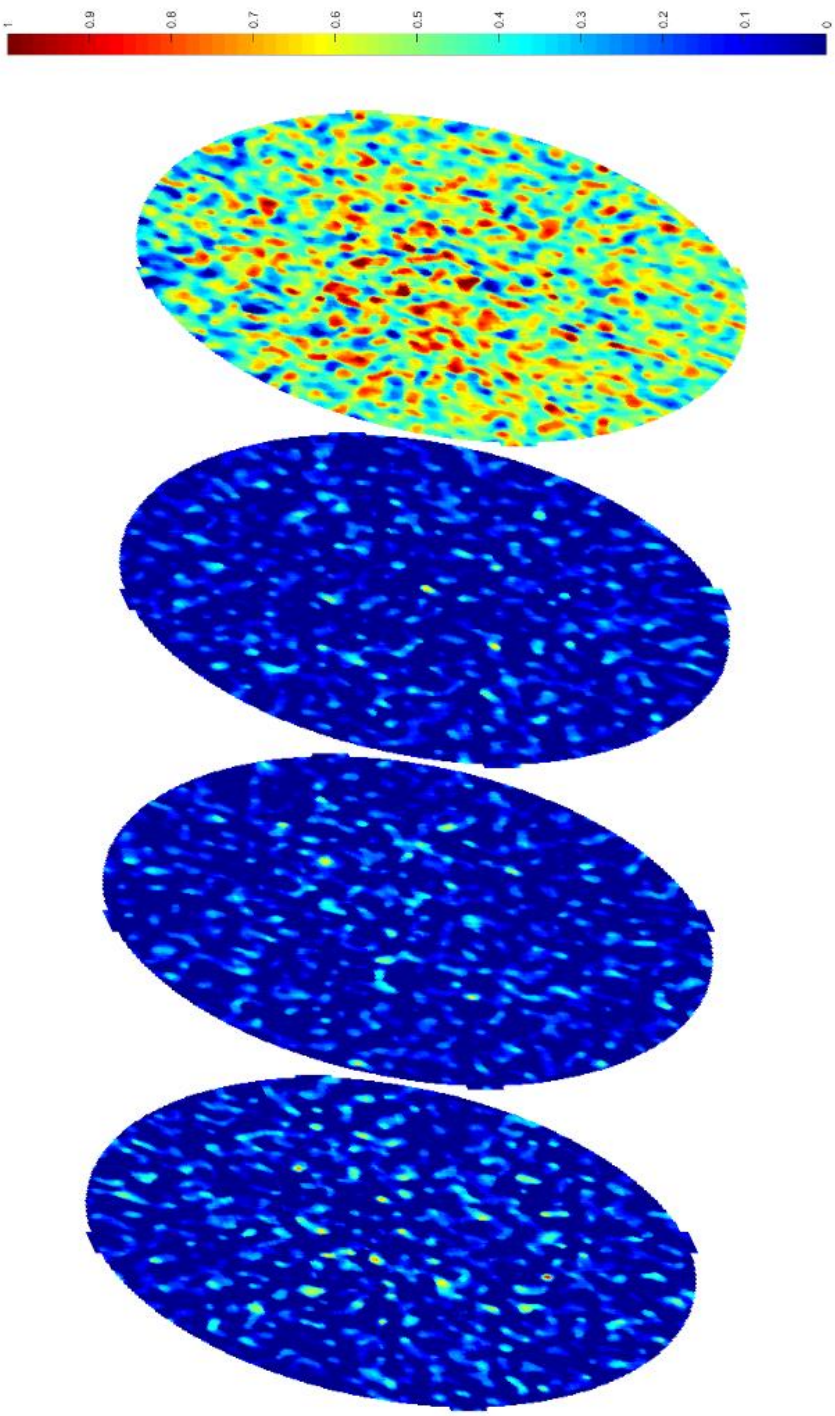

Figure 79: Core #3 flood #2 saturation at 0.10 pore volumes pumped

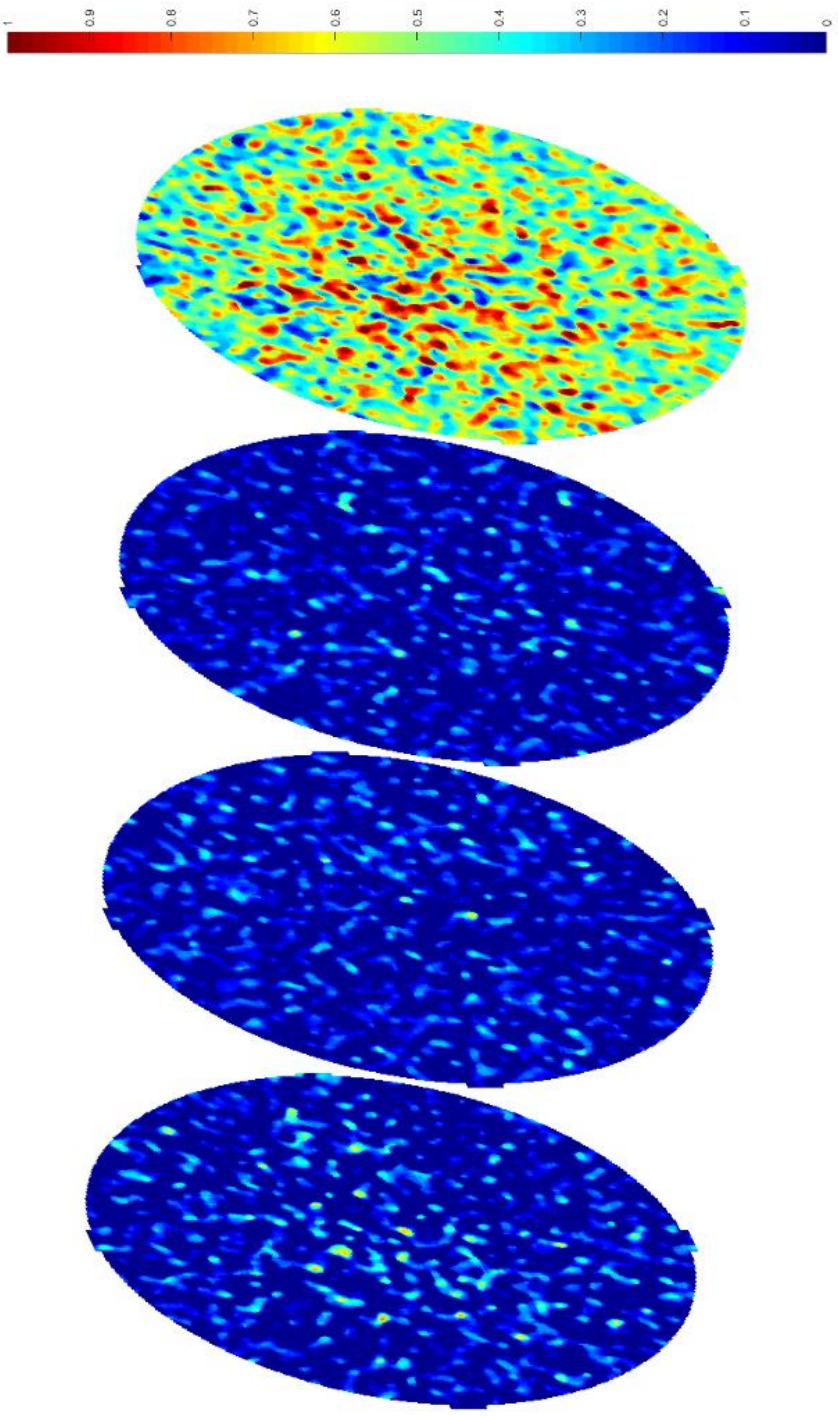

Figure 80: Core #3 flood #2 saturation at 0.13 pore volumes pumped

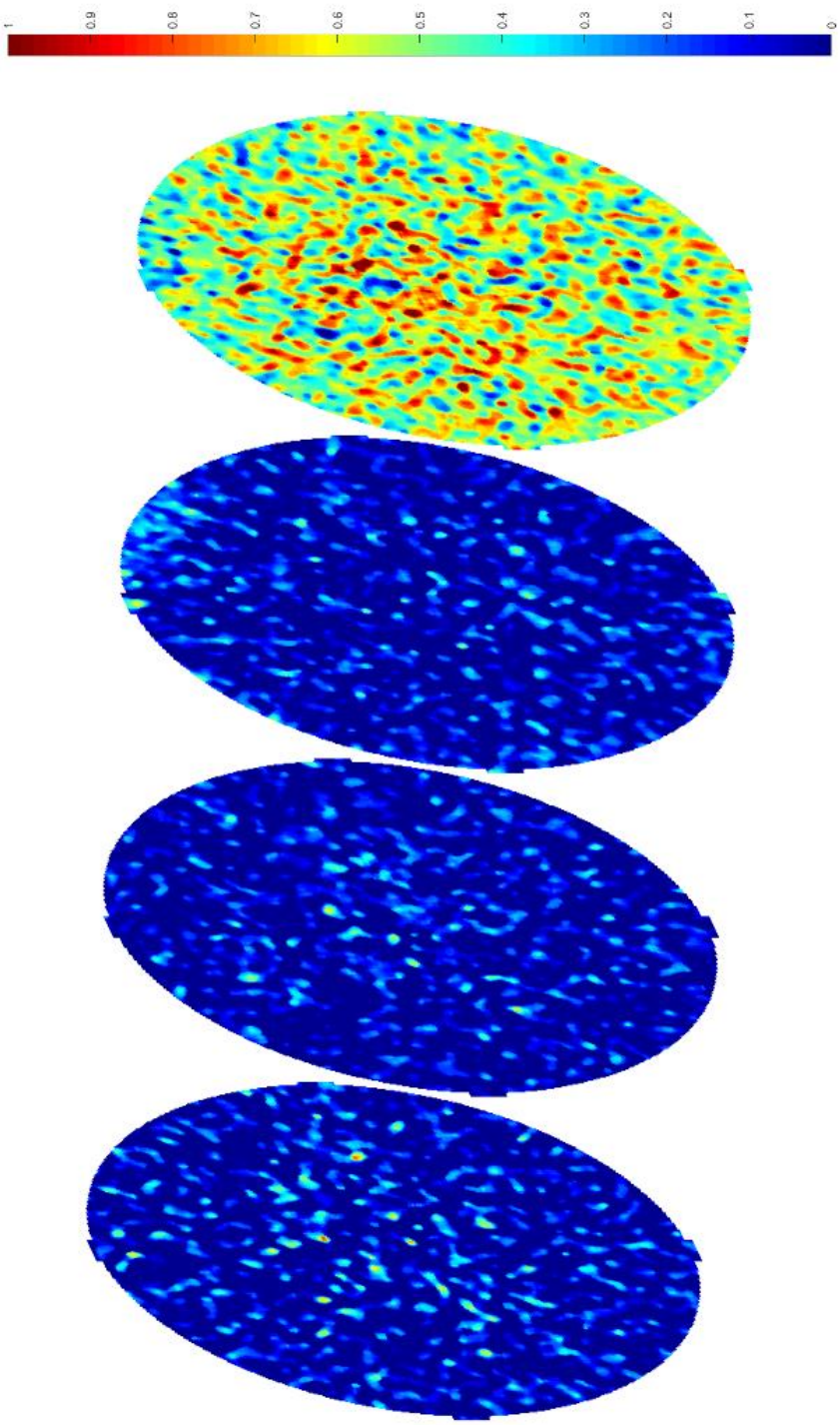

Figure 81: Core #3 flood #2 saturation at 0.17 pore volumes pumped

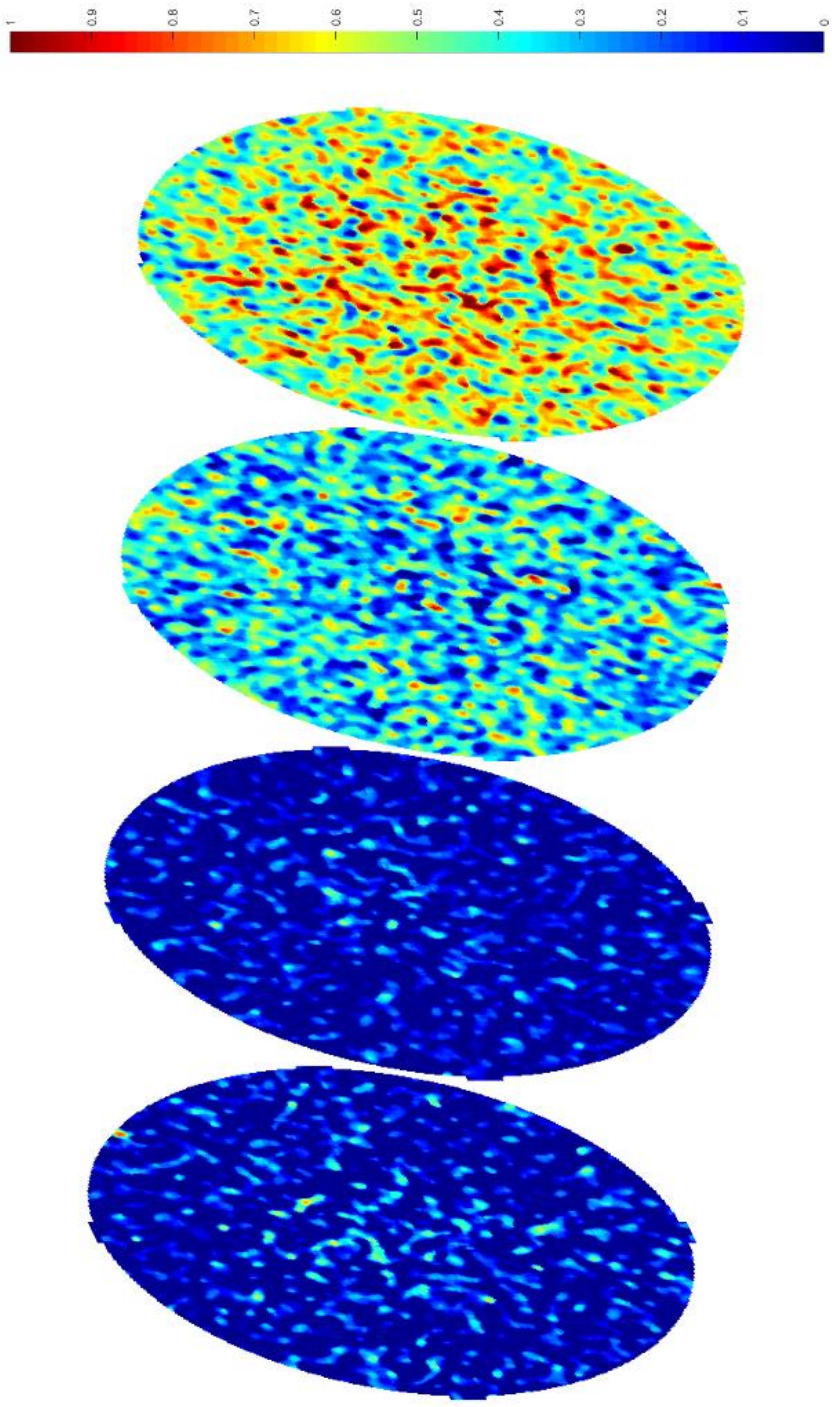

Figure 82: Core #3 flood #2 saturation at 0.20 pore volumes pumped

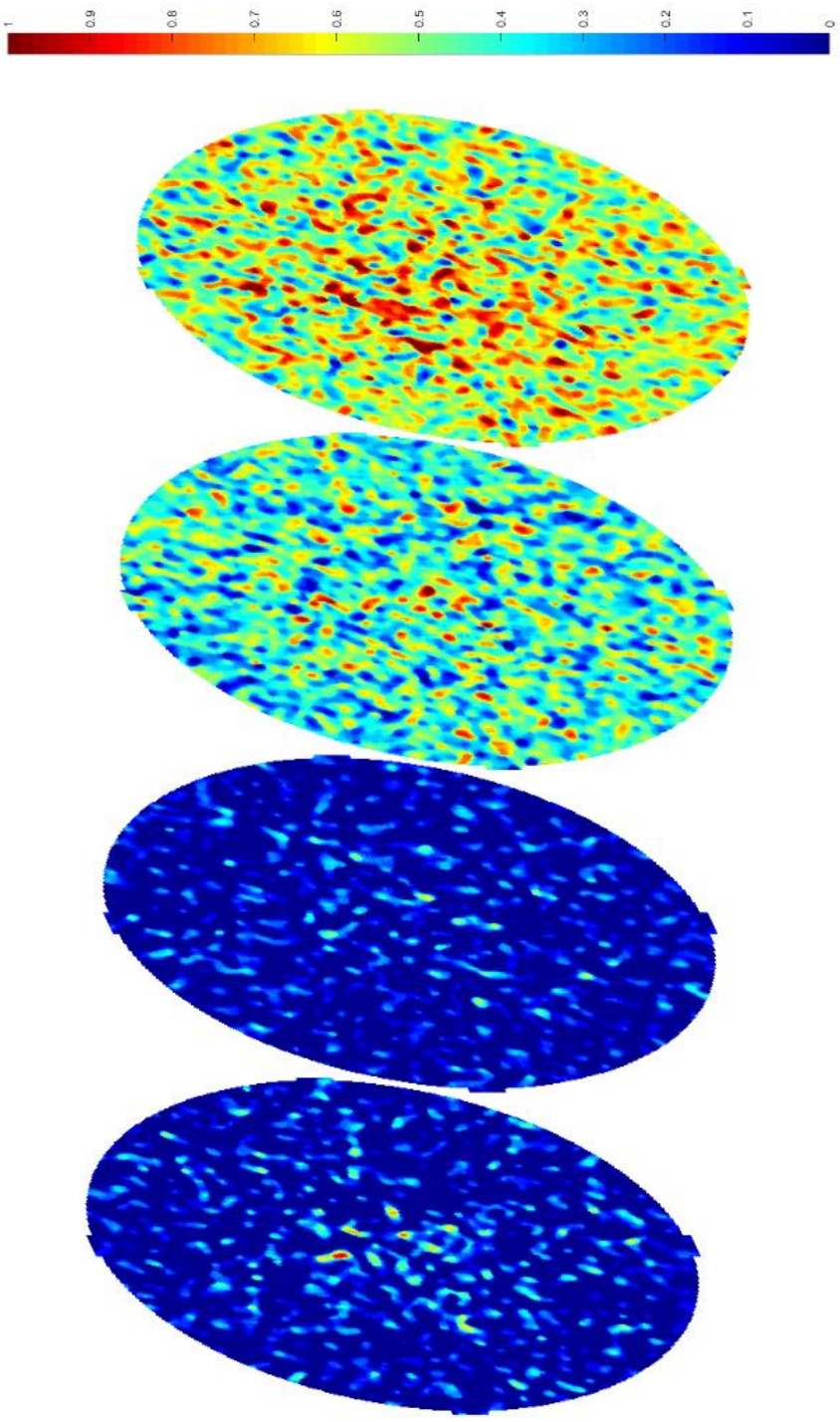

Figure 83: Core #3 flood #2 saturation at 0.25 pore volumes pumped

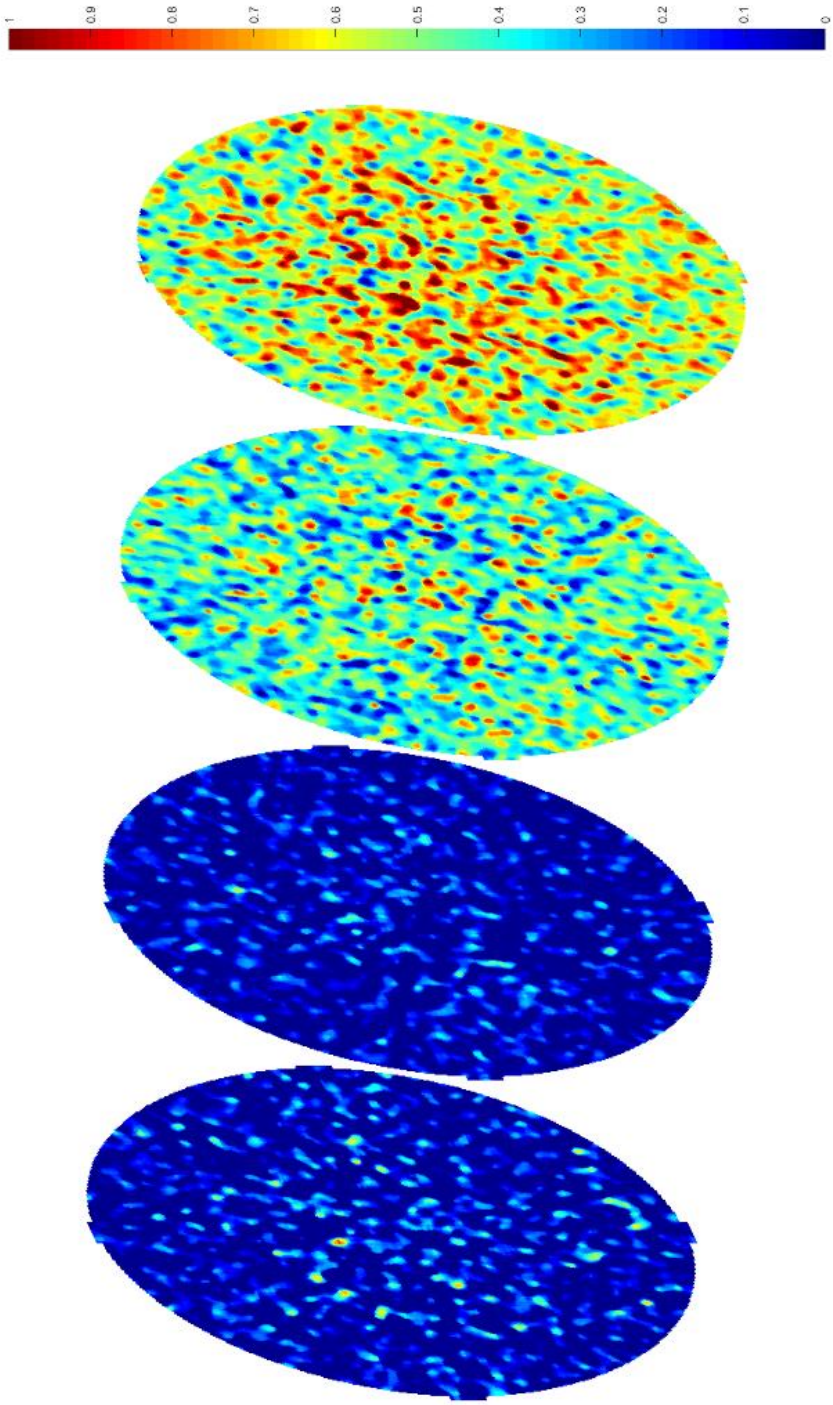

Figure 84: Core #3 flood #2 saturation at 0.31 pore volumes pumped

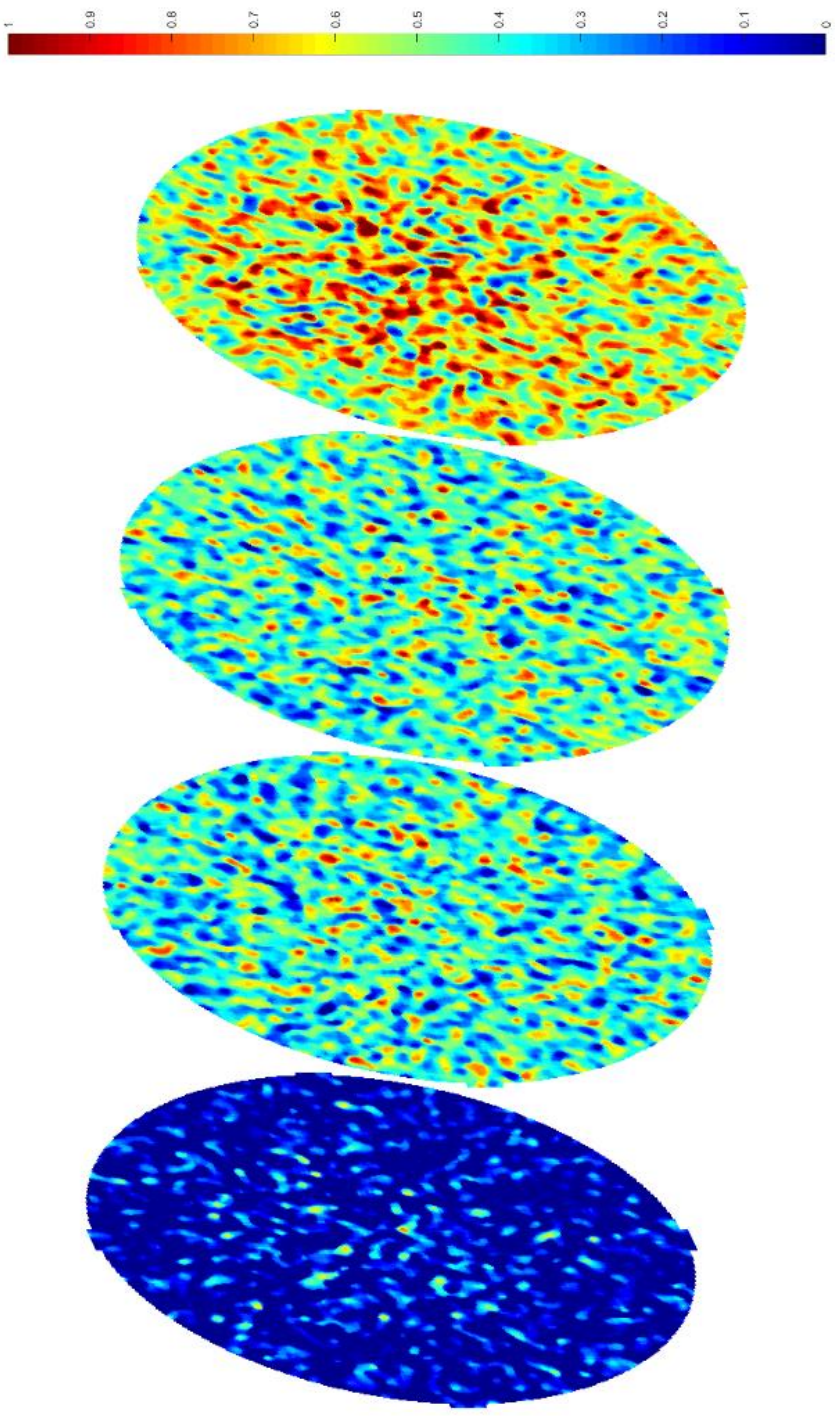

Figure 85: Core #3 flood #2 saturation at 0.36 pore volumes pumped

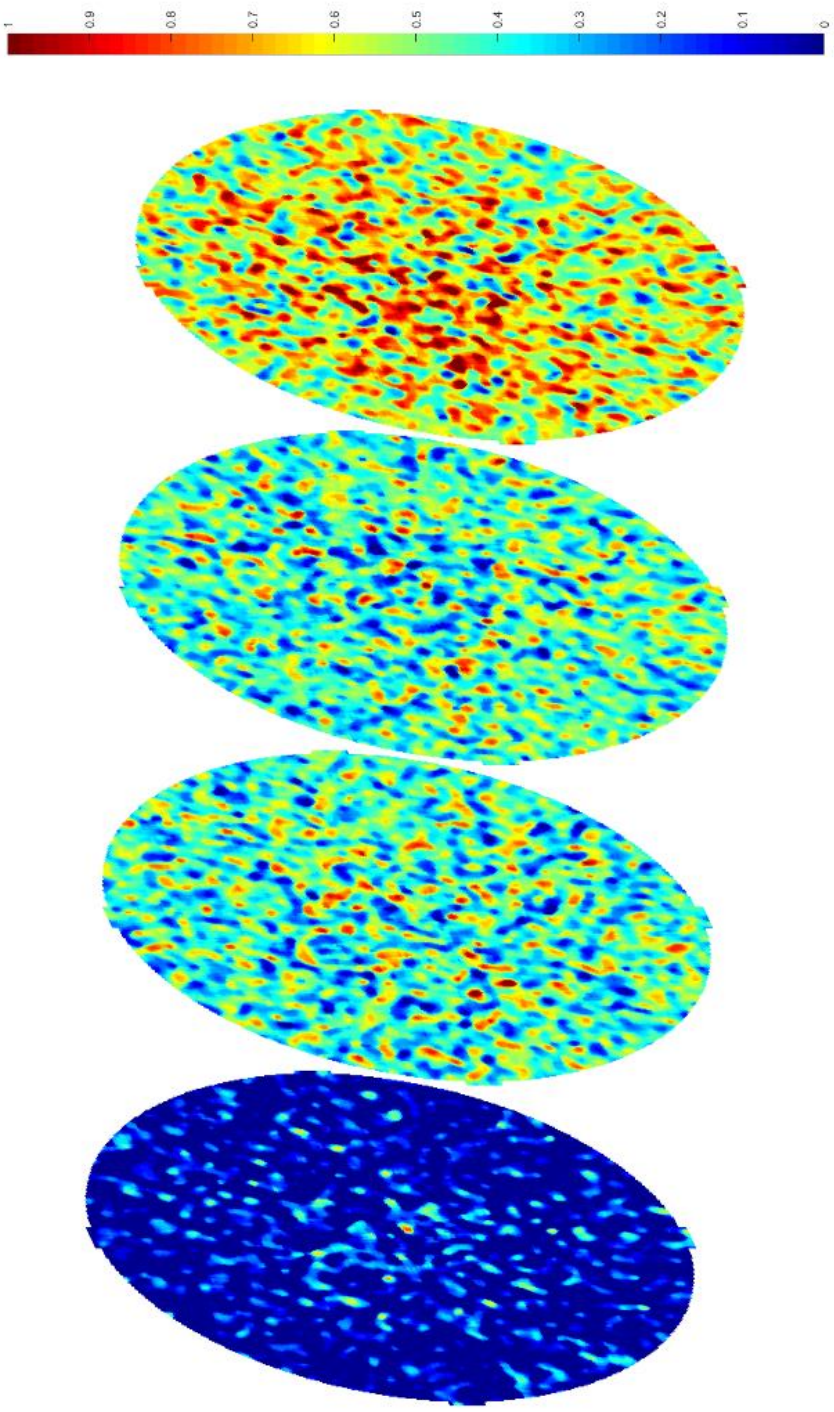

Figure 86: Core #3 flood #2 saturation at 0.41 pore volumes pumped

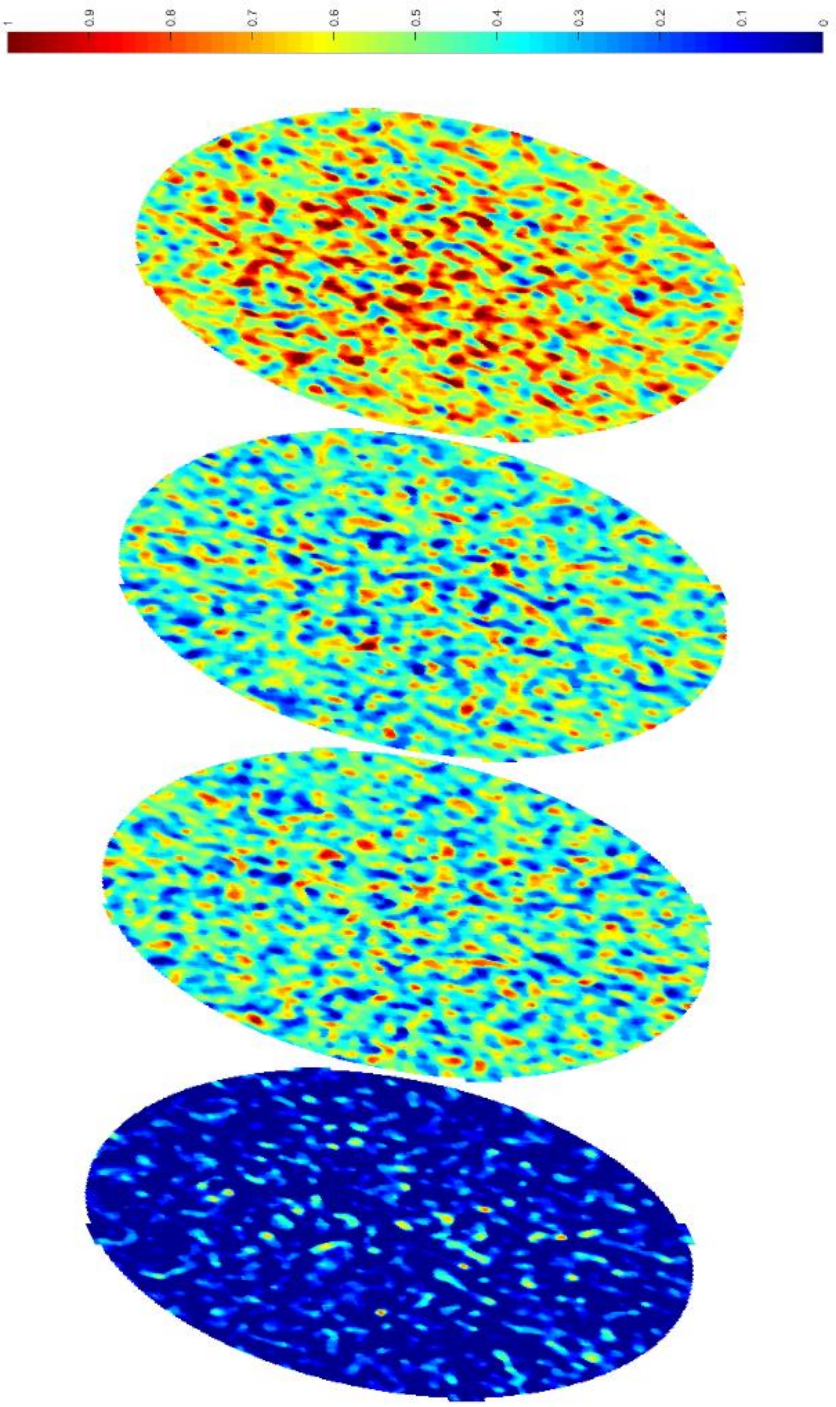

Figure 87: Core #3 flood #2 saturation at 0.46 pore volumes pumped

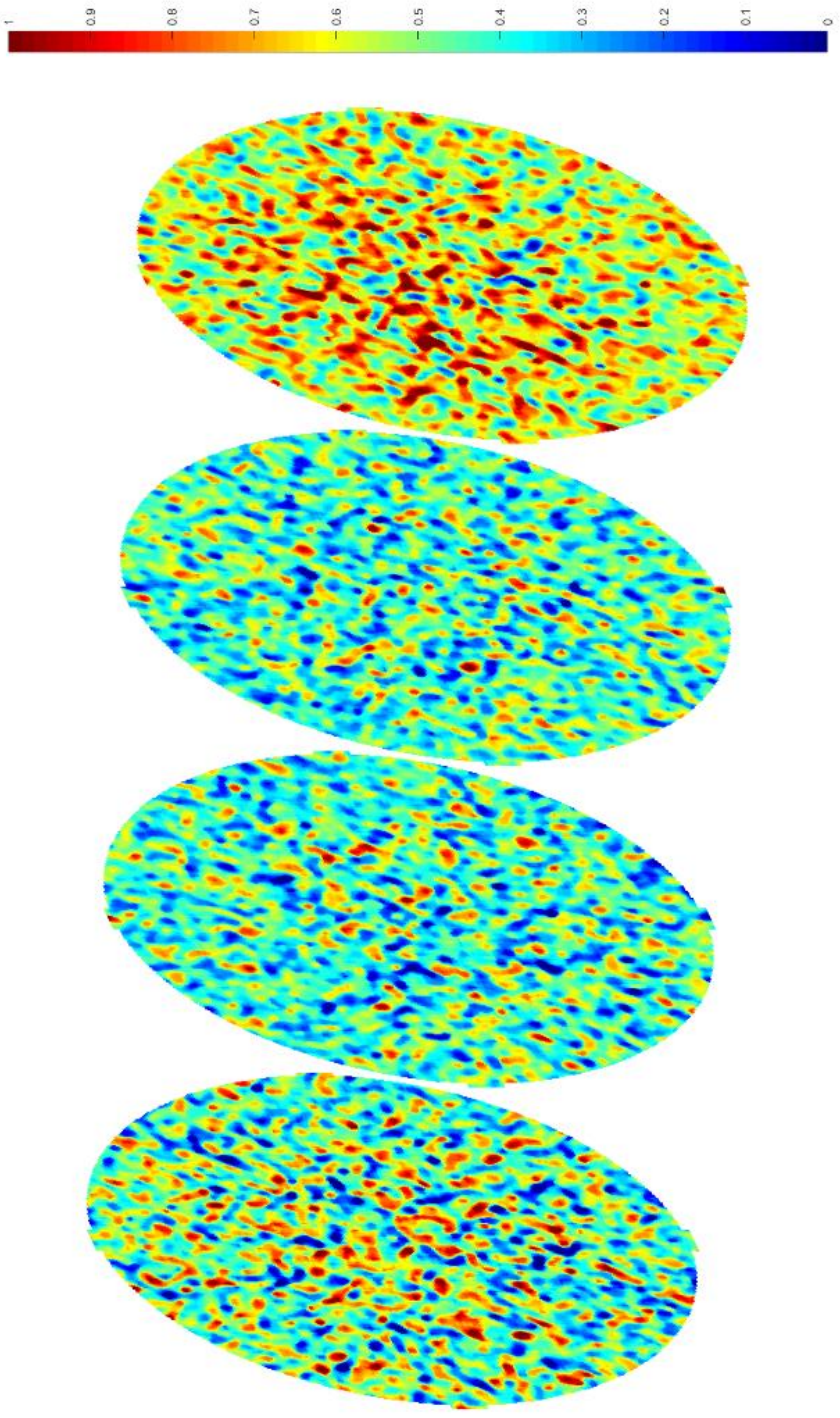

Figure 88: Core #3 flood #2 saturation at 0.51 pore volumes pumped

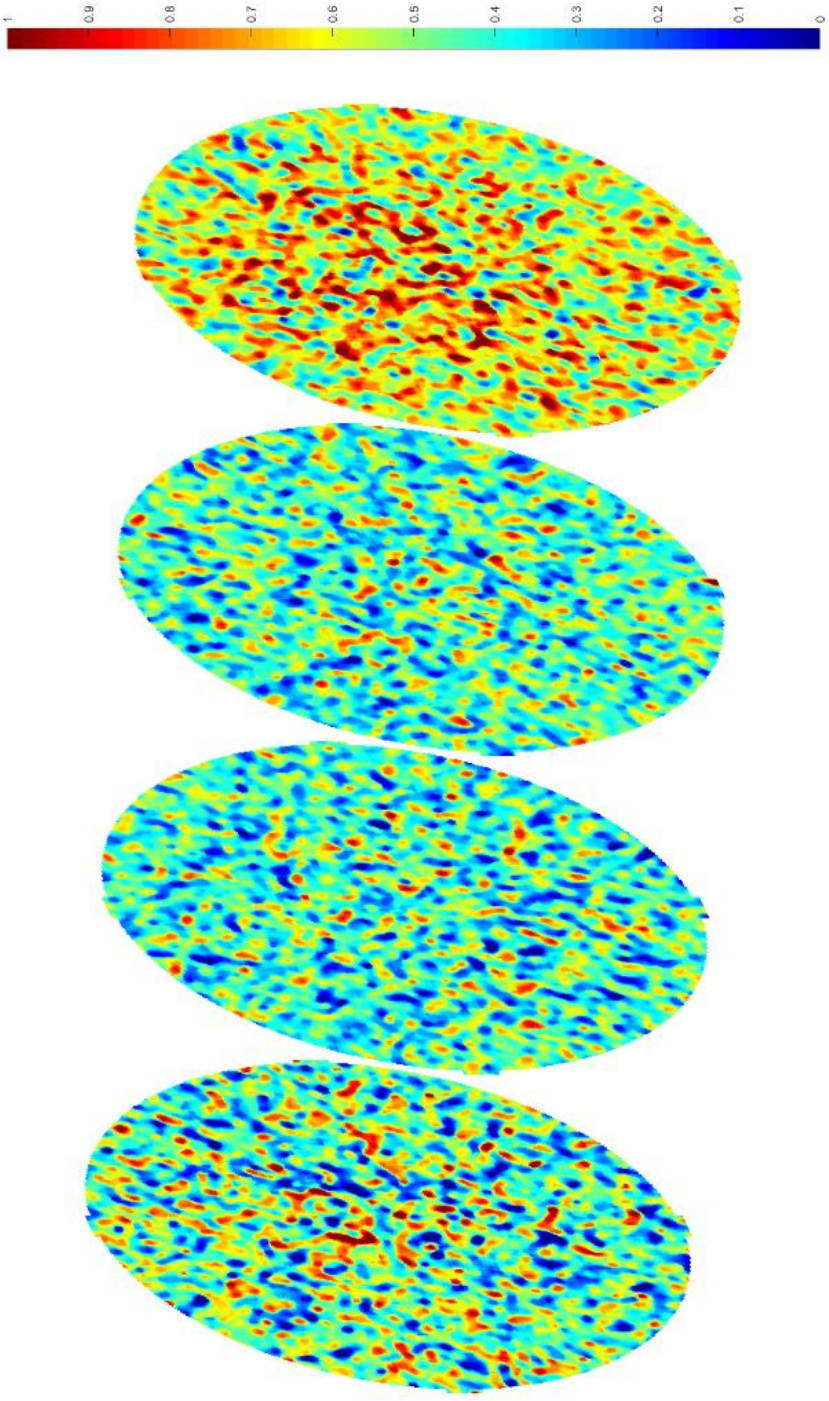

Figure 89: Core #3 flood #2 saturation at 0.56 pore volumes pumped

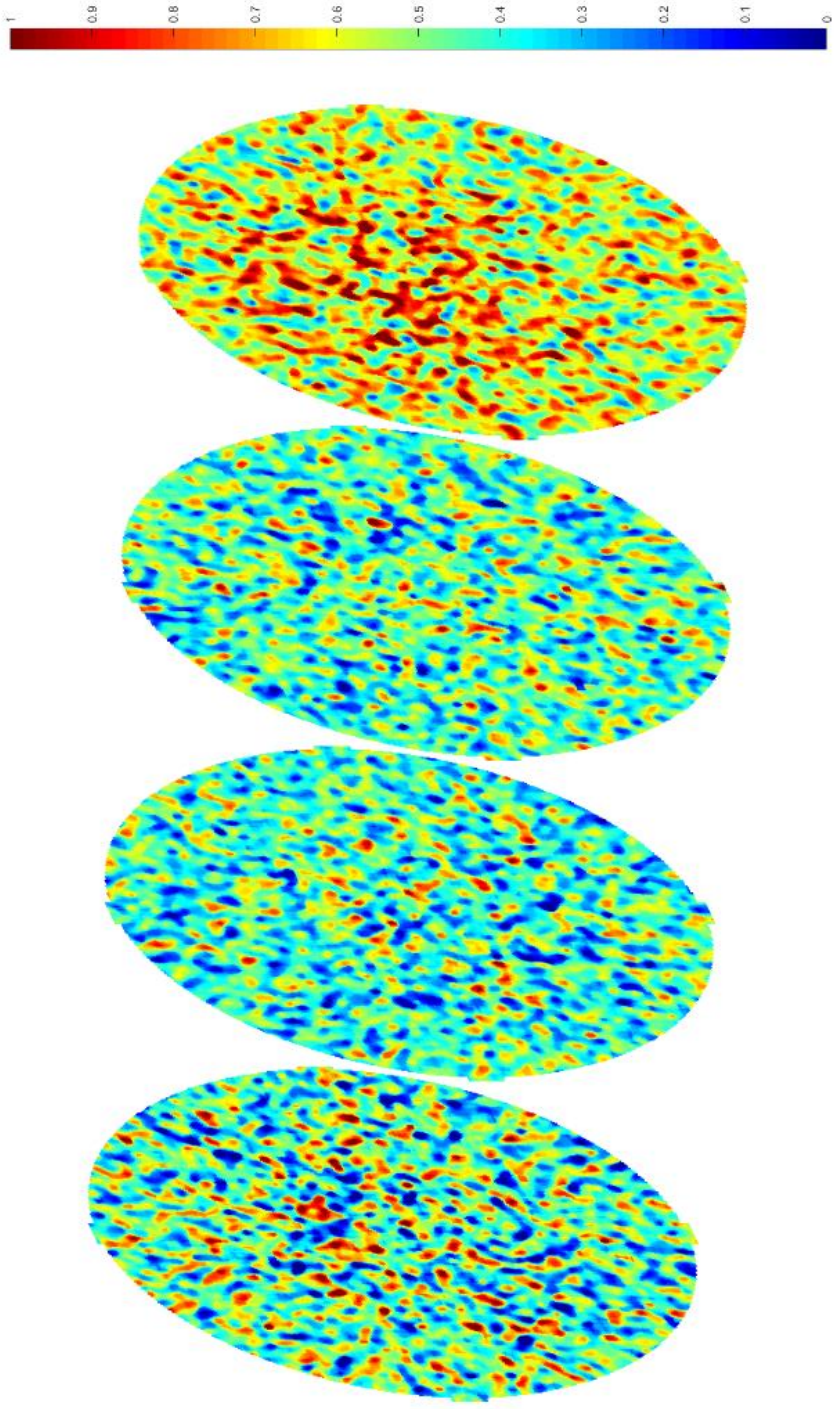

Figure 90: Core #3 flood #2 saturation at 0.67 pore volumes pumped

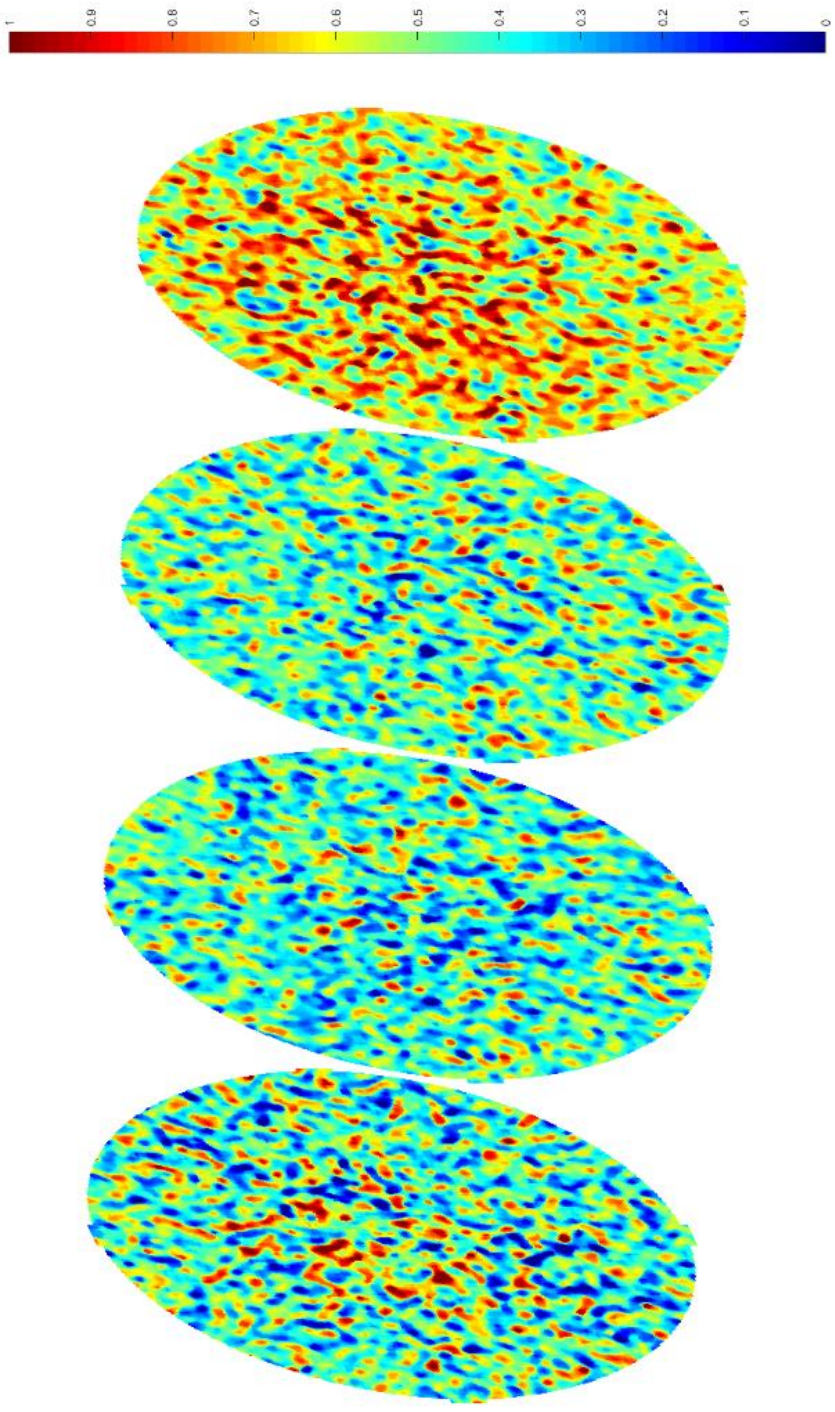

Figure 91: Core #3 flood #2 saturation at 0.77 pore volumes pumped

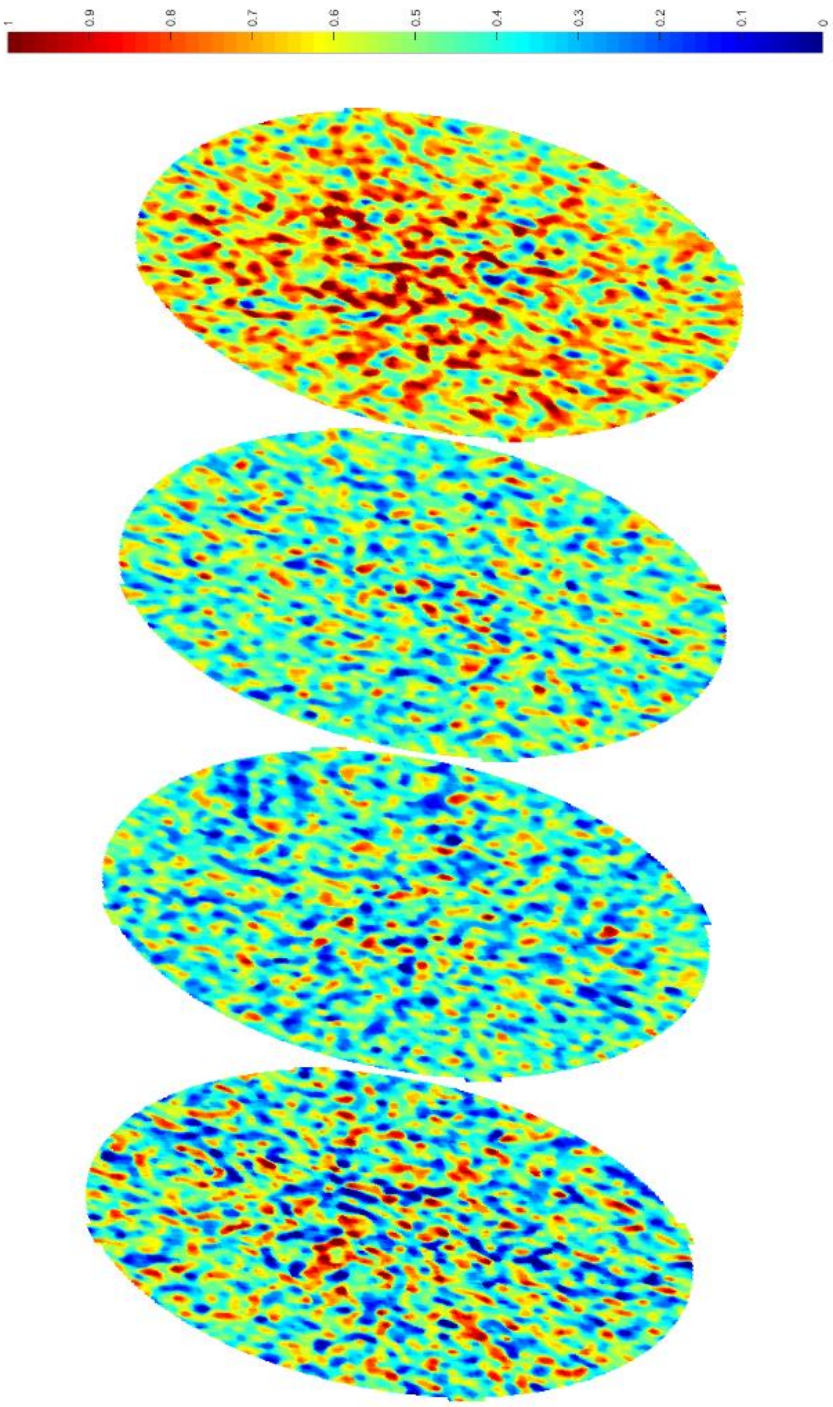

Figure 92: Core #3 flood #2 saturation at 0.87 pore volumes pumped

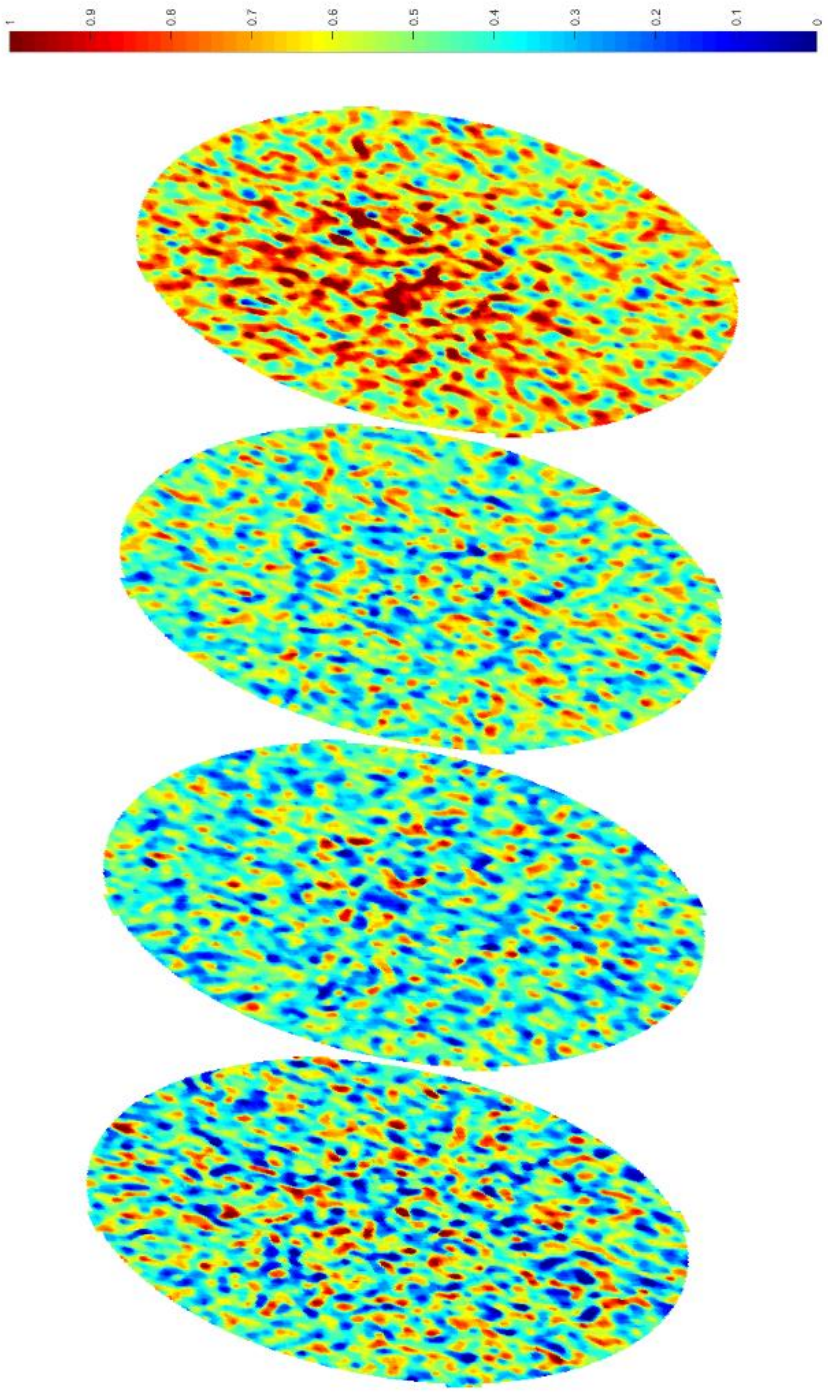

Figure 93: Core #3 flood #2 saturation at 1.03 pore volumes pumped

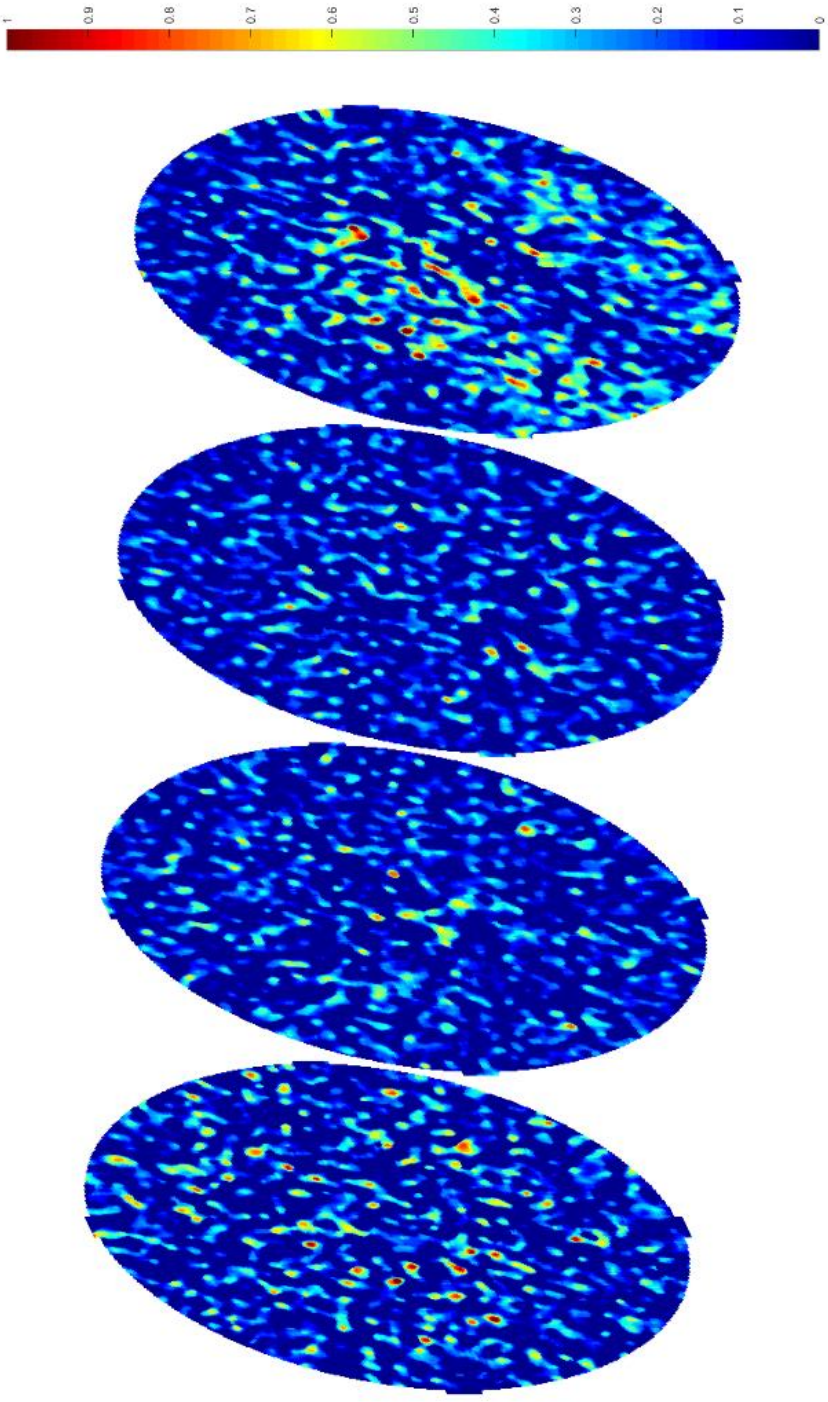

Figure 94: Core #3 flood #3 saturation at 0.03 pore volumes pumped

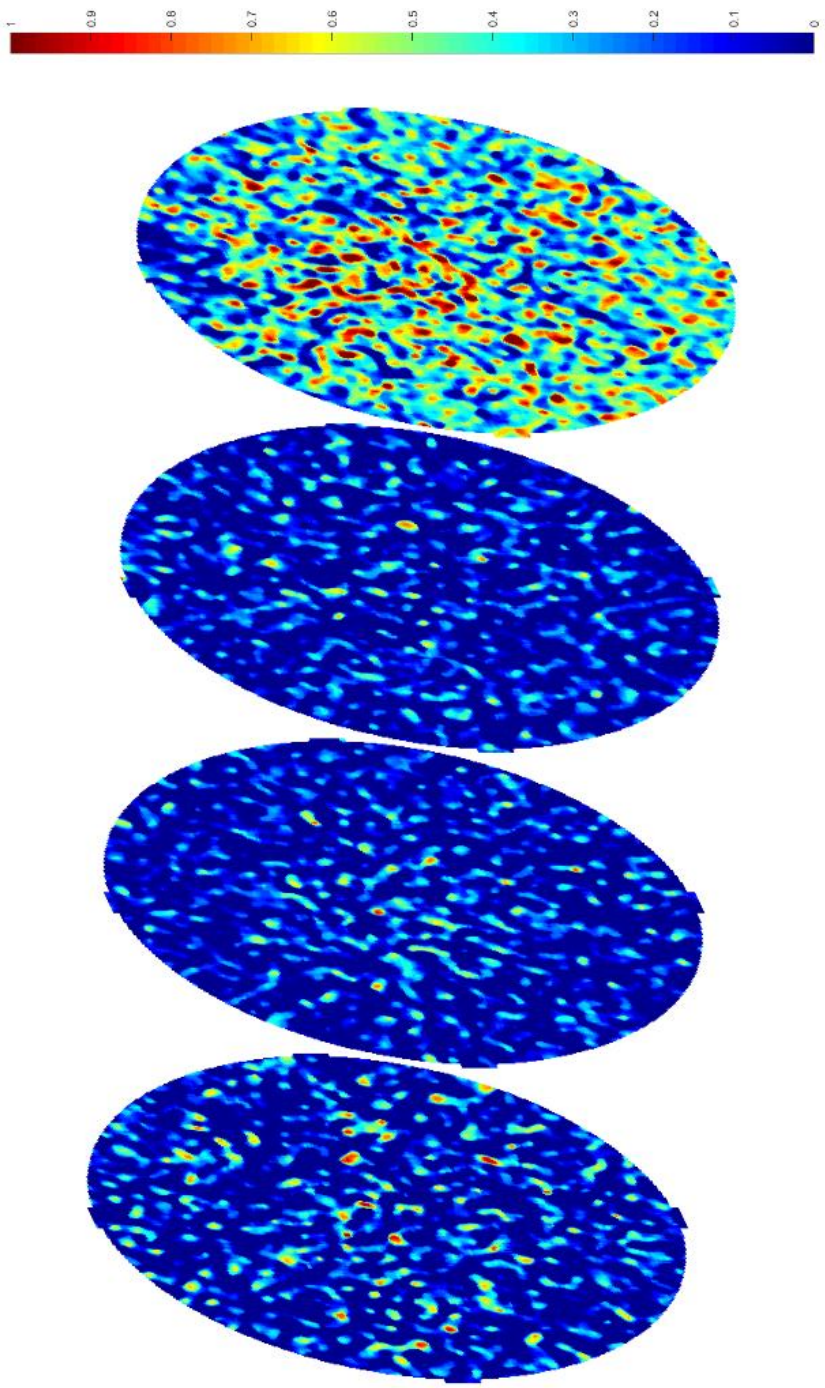

Figure 95: Core #3 flood #3 saturation at 0.06 pore volumes pumped

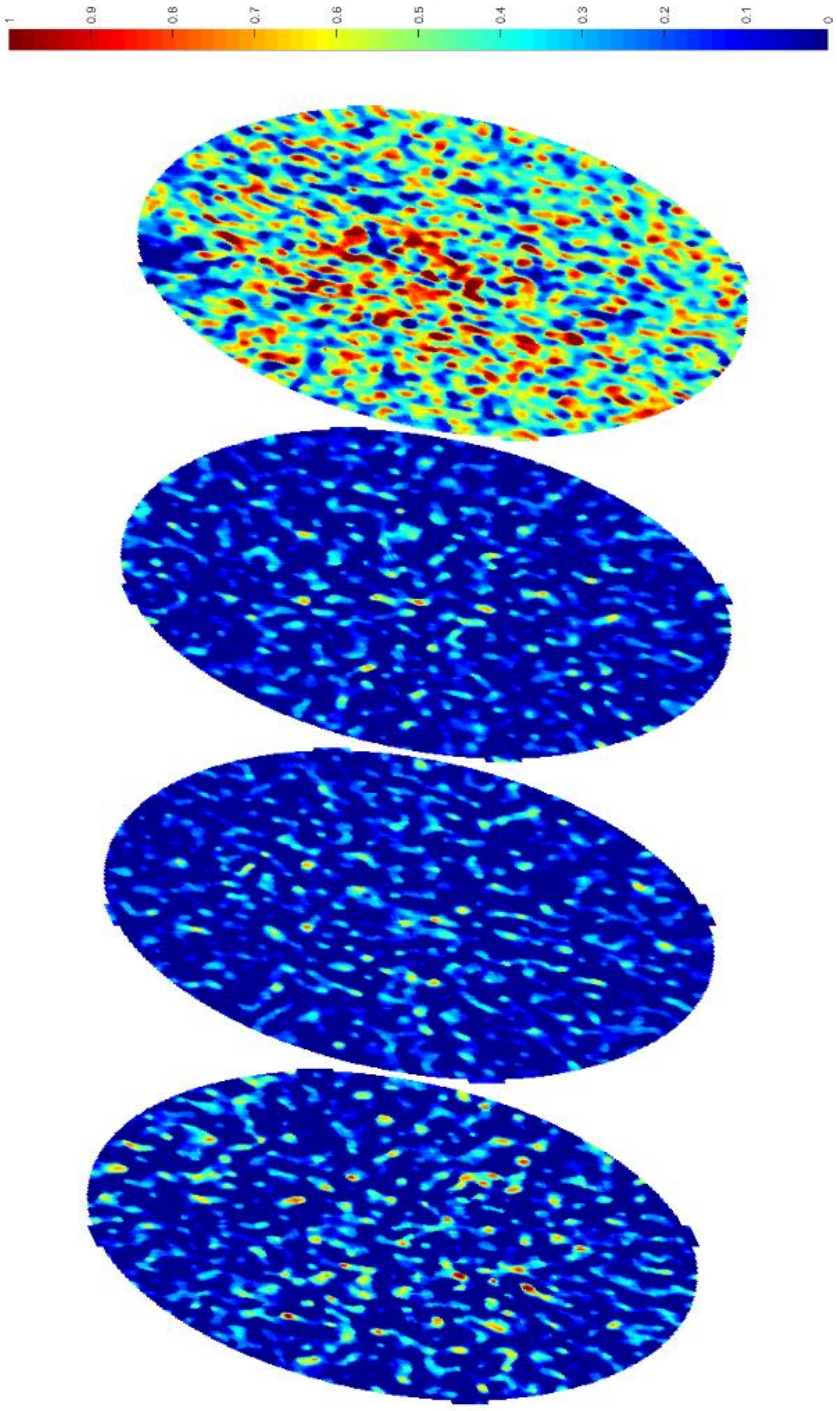

Figure 96: Core #3 flood #3 saturation at 0.10 pore volumes pumped

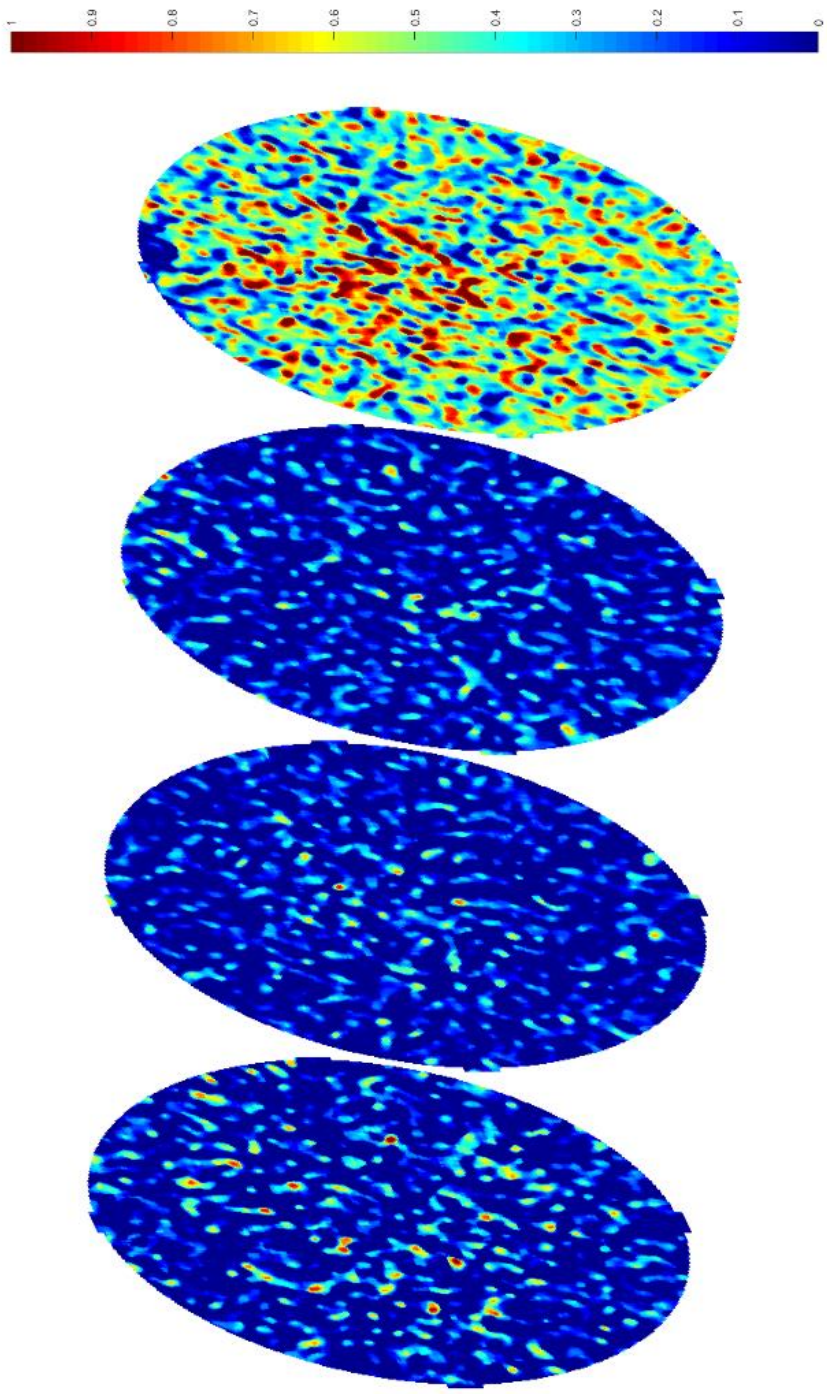

Figure 97: Core #3 flood #3 saturation at 0.13 pore volumes pumped

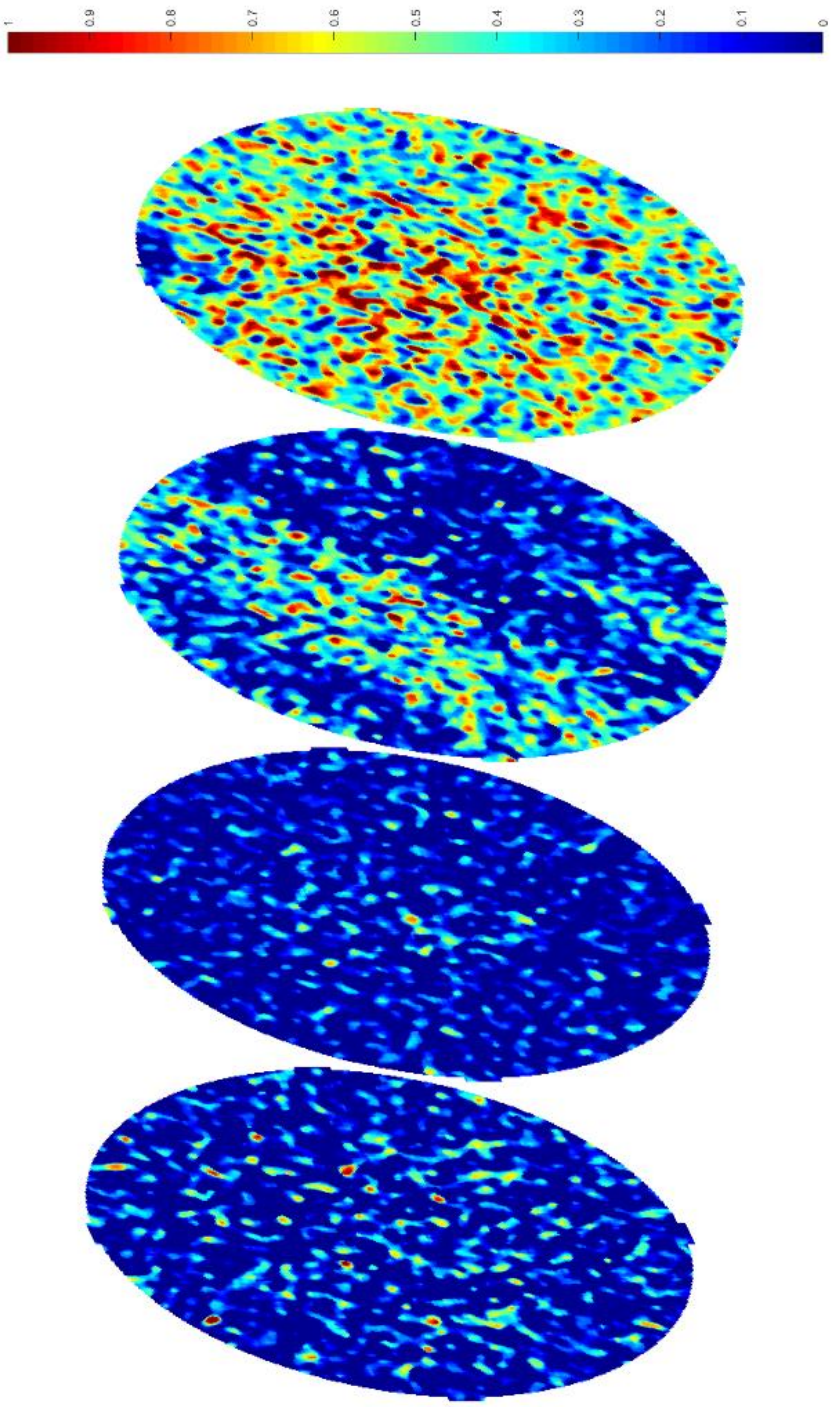

Figure 98: Core #3 flood #3 saturation at 0.17 pore volumes pumped

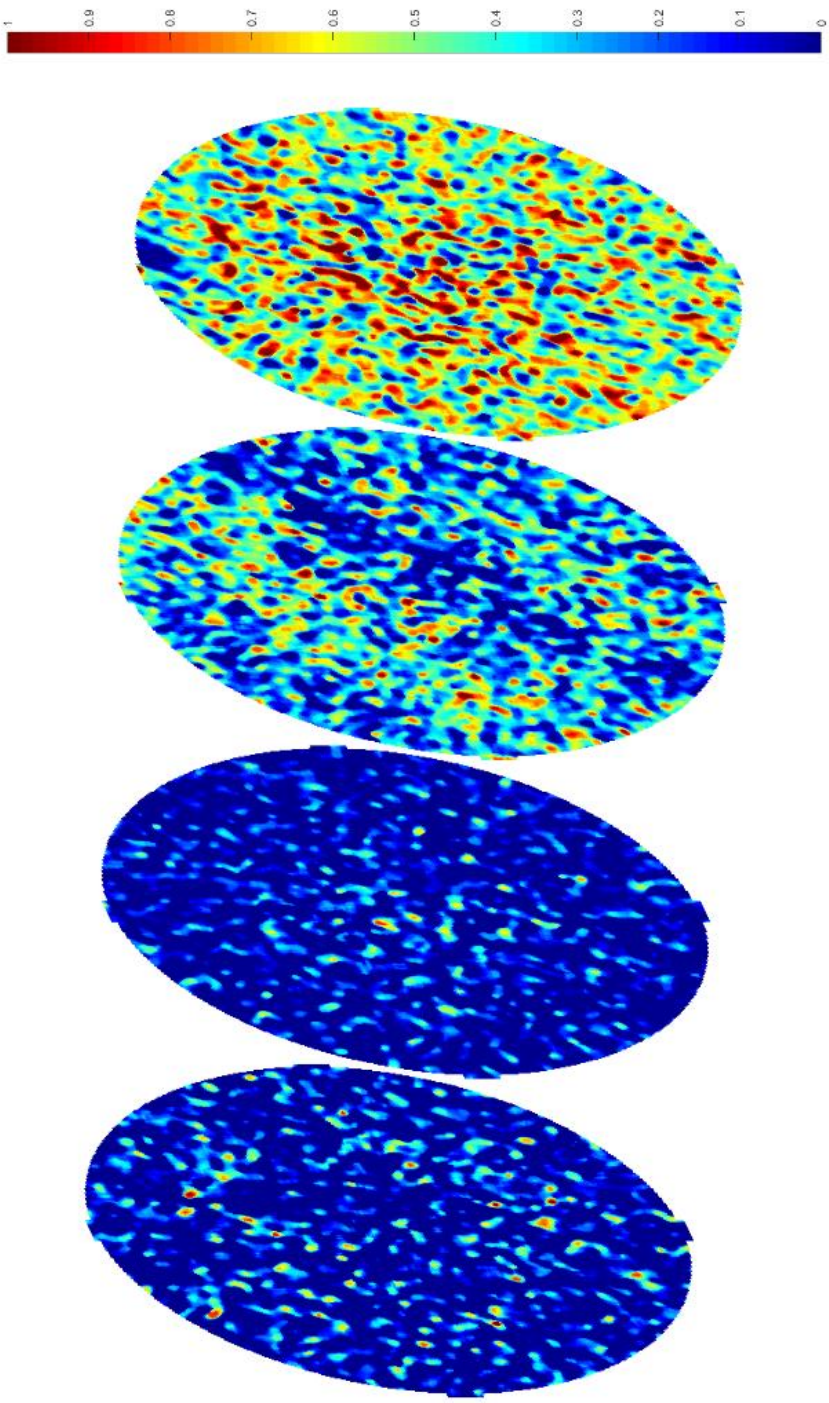

Figure 99: Core #3 flood #3 saturation at 0.20 pore volumes pumped

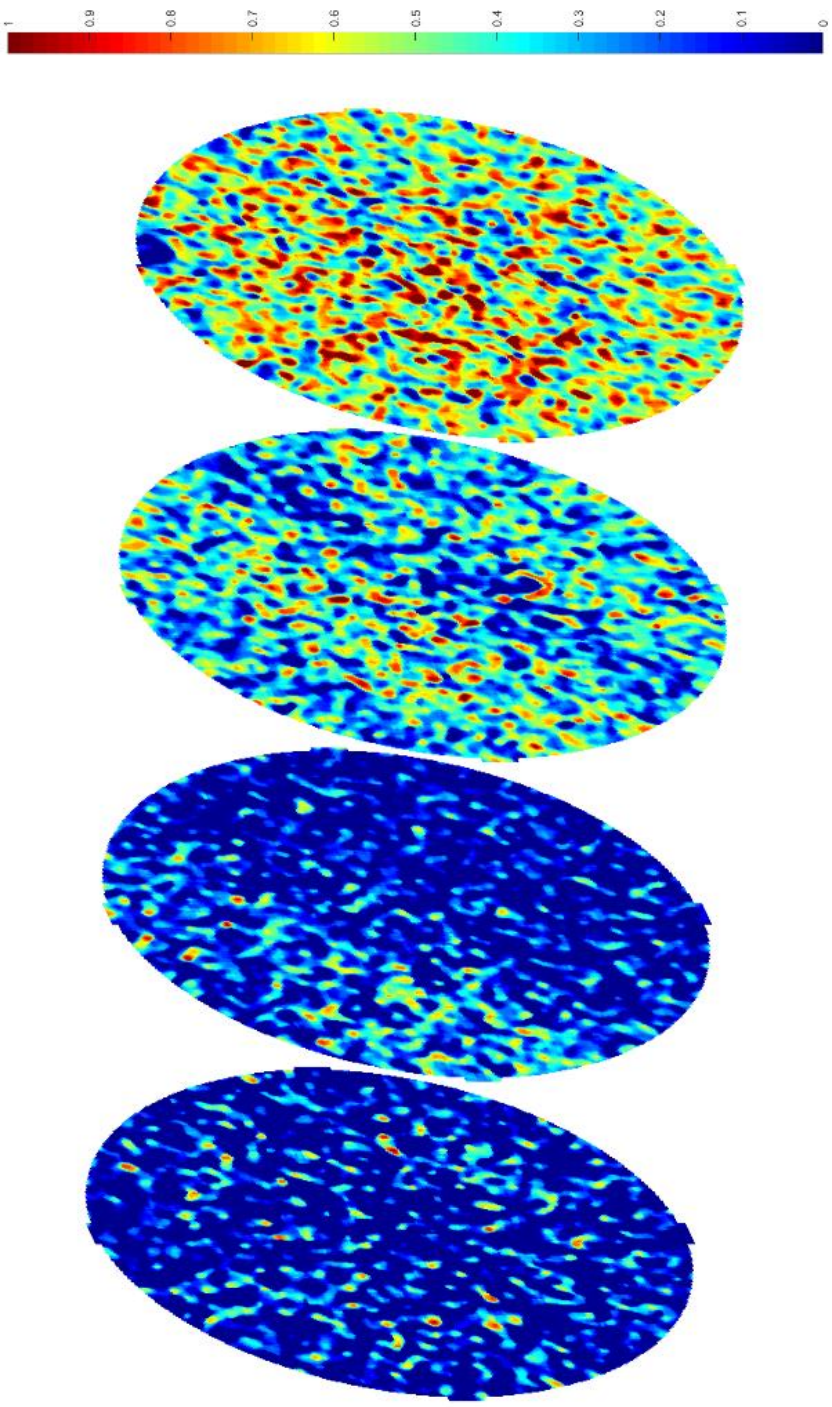

Figure 100: Core #3 flood #3 saturation at 0.25 pore volumes pumped

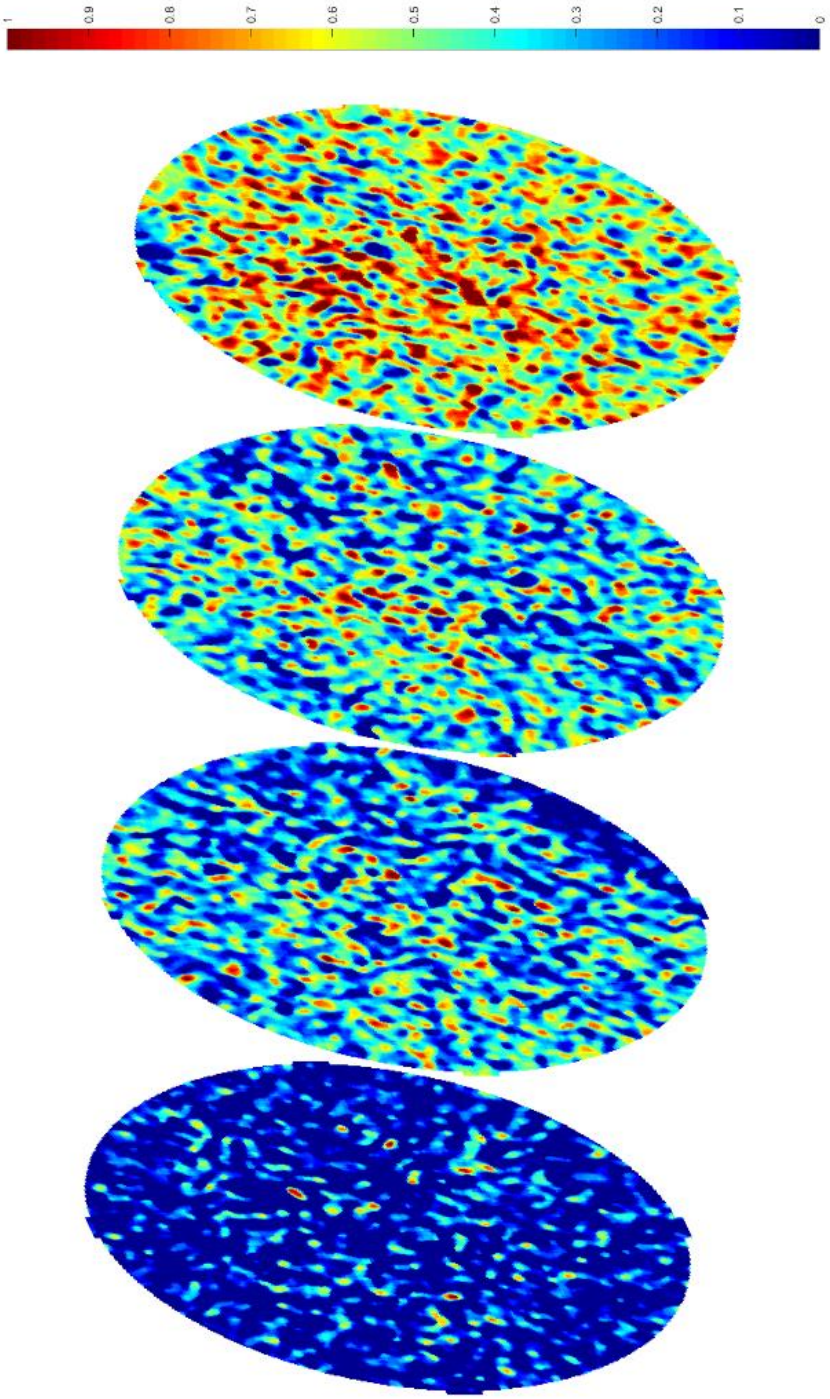

Figure 101: Core #3 flood #3 saturation at 0.31 pore volumes pumped

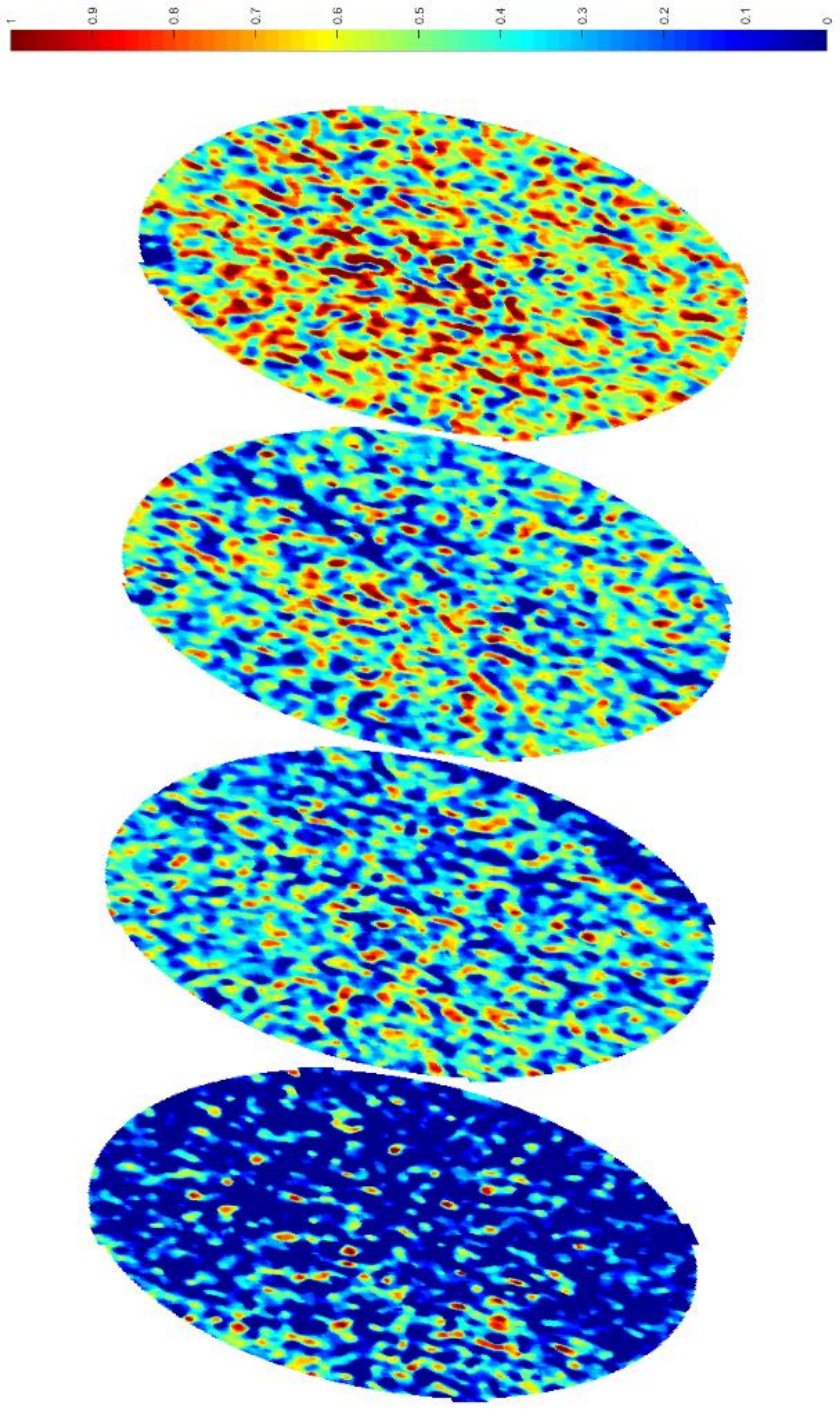

Figure 102: Core #3 flood #3 saturation at 0.36 pore volumes pumped

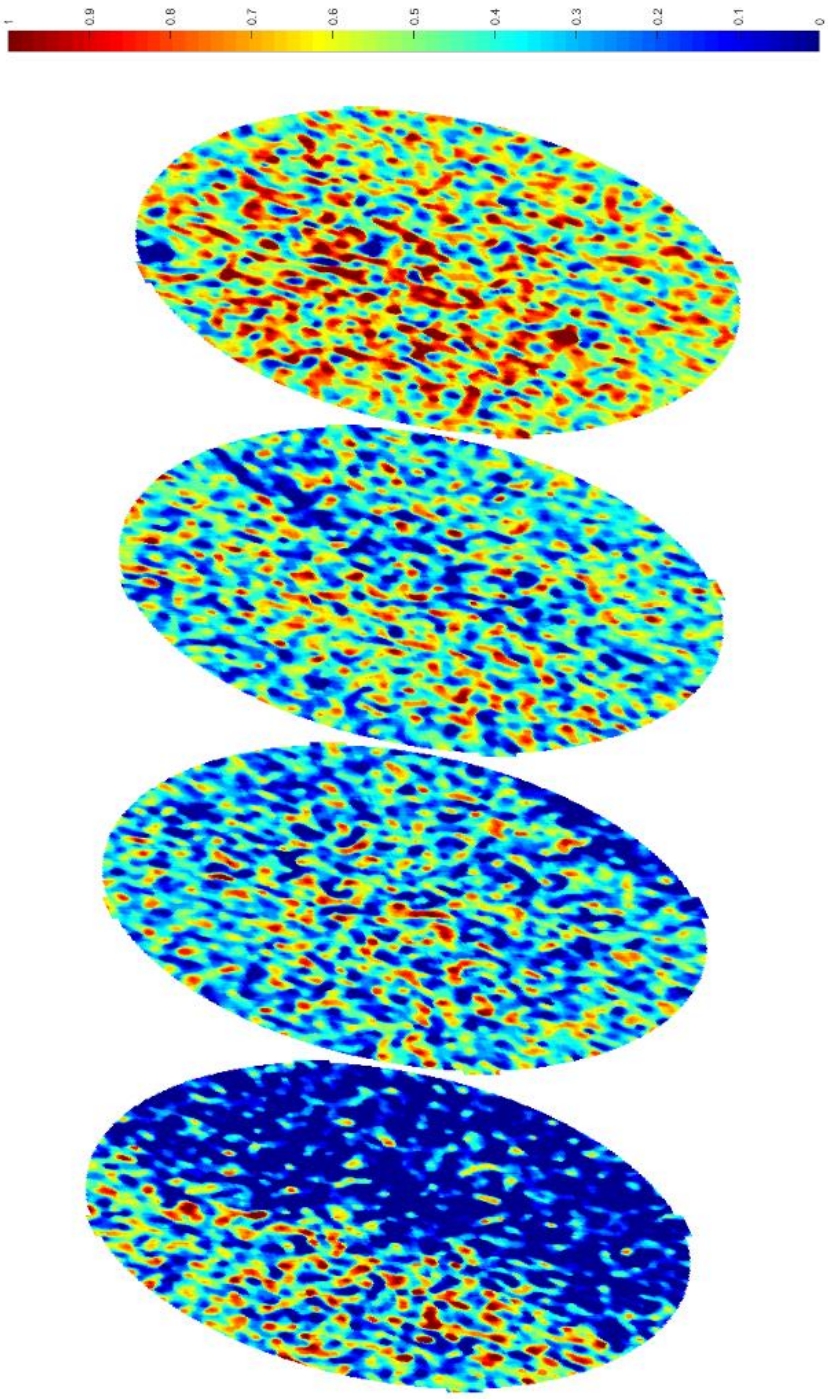

Figure 103: Core #3 flood #3 saturation at 0.41 pore volumes pumped

APPENDIX 3: PICTURES

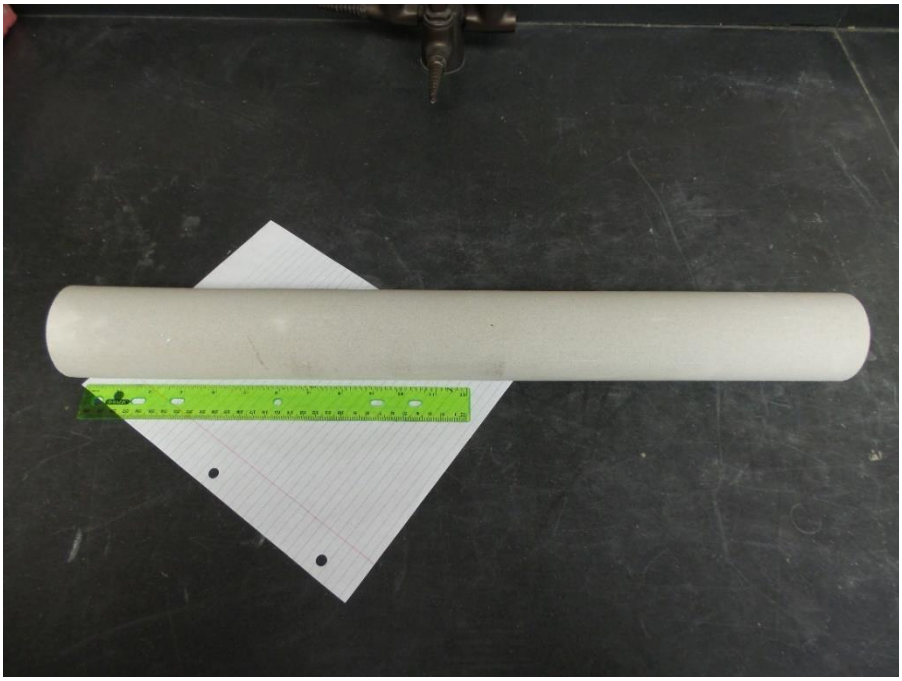

Picture 3: Berea core side view

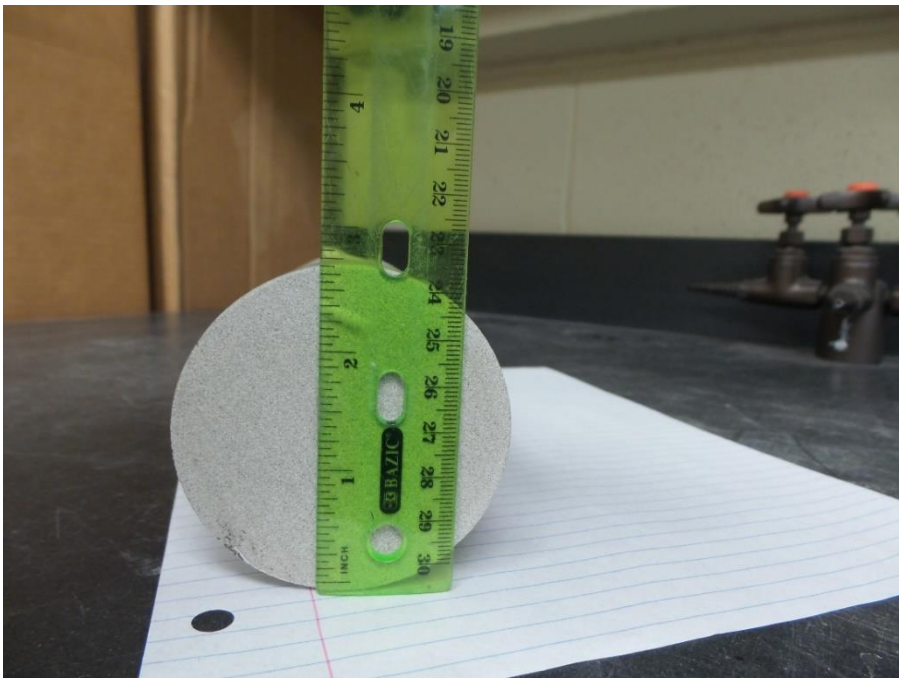

Picture 4: Berea core top view

Picture 5: Core after experiment

Picture 6: Liquid CO_2 tank

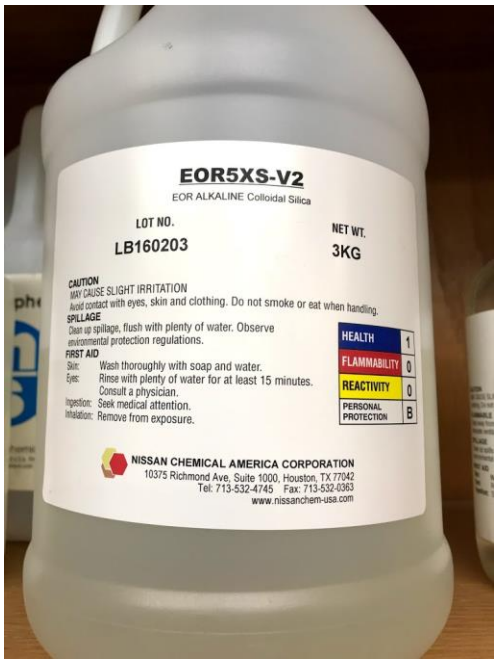

Picture 7: Nissan Chemical EOR5XS-V2 nanoparticles

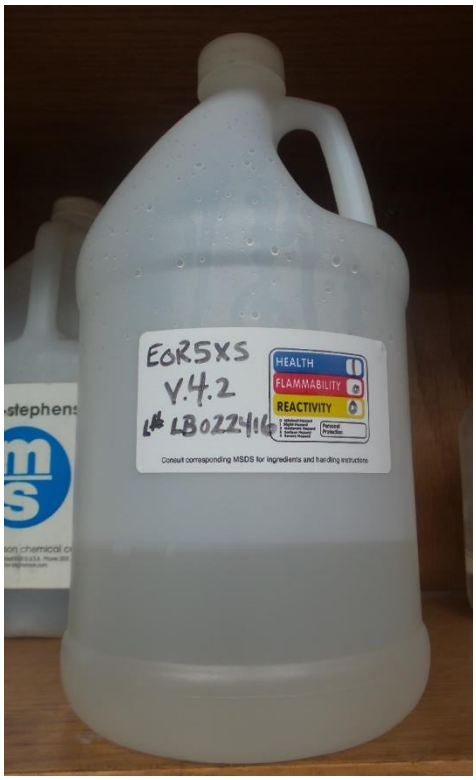

Picture 8: Nissan Chemical EOR5XS-V4.2 nanoparticles

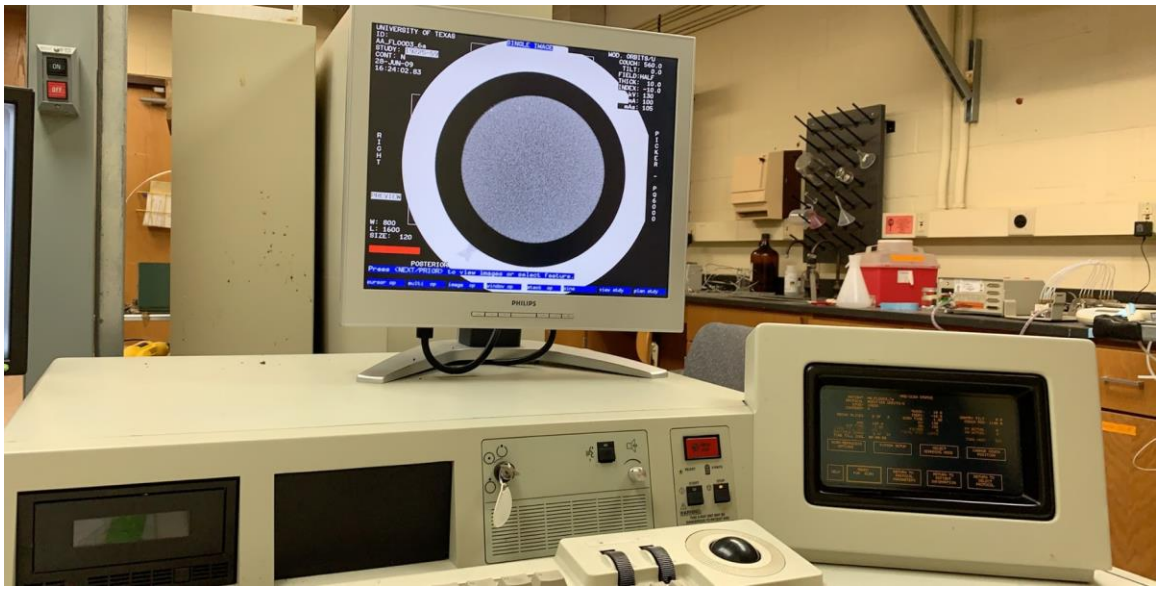

Picture 9: CT scanner console


Picture 10: CT scanner gantry and couch

References

Alghamdi, A. A. (2015, August). Experimental Evaluation of Nanoparticles Impact on Displacement Dynamics for Water-Wet and Oil-Wet Porous Media. *Master's Thesis*. Austin, TX, USA: The University of Texas at Austin.

Aminzadeh, B., DiCarlo, D. A., Chung, D. H., Kianinejad, A., Bryant, S. L., & Huh, C. (2012). Effect of Nanoparticles on Flow Alteration During CO2 Injection. *SPE Annual Technical Conference and Exhibition.* San Antonio: Society of Petroleum Engineers.

Aminzadeh, B., DiCarlo, D. A., Roberts, M., Chung, D. H., Bryant, S. L., & Huh, C. (2012). Effect of Spontaneous Formation of Nanoparticle Stabilized Emulsion on the Stability of a Displacement. *SPE Improved Oil Recovery Symposium.* Tulsa: Society of Petroleum Engineers.

Aveyard, R., Binks, B. P., & Clint, J. H. (2002, July 18). Emulsions Stabilised Solely by Collodial Particles. *Advances in Colloid and Interface Science, 100-102*, 503-546.

Deng, W., Cardenas, M. B., & Bennett, P. C. (2013, December). Extended Roof Snap-Off For a Continuous Nonwetting Fluid and an Eample Case for Supercritical CO2. *Advances in Water Resources, 64*, 34-46.

DiCarlo, D. (2019, June). CT Calibration. DiCarlo Research Group Internal Communication.

Emrani, A. S., & Nasr-El-Din, H. A. (2015). Stabilizing CO2-Foam using Nanoparticles. *SPE European Formation Damage Conference and Exhibition.* Budapest: Society of Petroleum Engineers.

Gauglitz, P. A., Friedmann, F., Kam, S. I., & Rossen, W. R. (2002). Foam Generation in Porous Media. *SPE/DOE Improved Oil Recovery Symposium.* Tulsa: Society of Petroleum Engineers.

Habermann, B. (1960). The Efficiency of Miscible Displacement as a Function of Mobility Ratio. *Petroleum Transactions, 219*, 264-272.

Hill, B., Hovorka, S., & Melzer, S. (2013). Geologica Carbon Storage Through Enhanced Oil Recovery. *Energy Procedia*(37), 6808-6830. doi:10.1016/j.egypro.2013.06.614

IPCC. (2014). *Climate Change 2014: Mitigation of Climate Change. Contribution of Working Group III to the Fifth Assessment Report of the Intergovernmental Panel on Climate Change.* Cambridge, United Kingdom and New York, NY, USA: Cambridge University Press.

Kovscek, A. R., Patzek, T. W., & Radke, C. J. (1993). Simulation of Foam Transport in Porous Media. *SPE Annual Technical Conference and Exhibition* (pp. 309-322). Houston: Society of Petroleum Engineers.

Lake, L. W., Johns, R. T., Rossen, W. R., & Pope, G. A. (2014). *Fundemanetals of Enhanced Oil Recovery.* Richardson, TX: Society of Petroleum Engineers.

Rackley, S. A. (2017). *Carbon Capture and Storage* (Second Edition ed.). Kidlington, Oxford, UK and Cambridge, MA, USA: Elsevier.

Roof, J. G. (1970, March). Snap-Off of Oil Droplets in Water-Wet Pores. *SPE Journal Transactions*, 85-90.

Rossen, W. R. (1996). Foam in Enhanced Oil Recovery. In R. K. Prud'homme, & S. A. Khan, *Foams: Theory, Measurements, and Applications.* New York, NY, USA: Marcel Dekker, Inc.

Rossen, W. R. (1999, December). Foam Generation at Layer Boundaries. *SPE Journal*, 409-412.

Rossen, W. R. (2003, April). A Critical Review of Roof Snap-Off as a Mechanism of Steady-State Foam Generation in Homogeneous Porous Media. *Colloids and Surfaces A: Physiochem. Eng. Aspects, 225*, 1-24.

Senthilnathan, S. (2017, August). Surface-Coated Silica Nanoparticles for Conformance Control of Buoyancy-Driven CO2 Flow. *Master's Thesis*. Austin, TX, USA: The University of Texas at Austin.

Shan, D., & Rossen, W. R. (2004, June). Optimal Injection Strategies for Foam IOR. *SPE Journal*, 132-150.

Tang, G.-Q., & Kovscek, A. R. (2004). Measurement and Theory of Gas Trapping in Porous Media During Steady-State Foam Flow. *SPE Annual Technical Conference and Exhibition.* Houston: Society of Petroleum Engineers.

Wung, R. M. (2015, August). Utilizing Surface Treated Nanoparticles for Enhanced Geologic Carbon Sequestration. *Master's Thesis*. Austin, TX, USA: The Univeristy of Texas at Austin.

Zhang, T., Roberts, M. R., Bryant, S. L., & Huh, C. (2009). Foams and Emulsions Stabilized With Nanoparticles for Potential Conformance Control Applications. *SPE International Symposium on Oilfield Chemistry.* The Woodlands: Society of Petroleum Engineers.

Vita

Ahmad is from the Eastern Province of Saudi Arabia, where he lives with his family. He graduated from the University of Texas at Austin in 2011 with a Bachelor of Science in Petroleum Engineering degree, sponsored by Saudi Aramco. He then worked for Saudi Aramco as a production engineer, reservoir management engineer and workover engineer until 2017, when he was sponsored by the same company for an advanced degree. He started pursuing a Master of Science in Engineering degree at the University of Texas at Austin in 2017 which he completed in 2019. He will go back to work for Saudi Aramco after graduation.

ahmad.alfakher@gmail.com

This thesis was typed by Ahmad Alfakher.